การตรวจสอบกลไกการเกิดแผ่นดินไหวและมิติแฟรกทัลของแผ่นดินไหว
ตามแนวมุดตัวของแผ่นเปลือกโลกสุมาตรา-อันดามัน

นายต.ติณ เกตุทอง

จุฬาลงกรณ์มหาวิทยาลัย
Chulalongkorn University

บทคัดย่อและแฟ้มข้อมูลฉบับเต็มของวิทยานิพนธ์ตั้งแต่ปีการศึกษา 2554 ที่ให้บริการในคลังปัญญาจุฬาฯ (CUIR)
เป็นแฟ้มข้อมูลของนิสิตเจ้าของวิทยานิพนธ์ ที่ส่งผ่านทางบัณฑิตวิทยาลัย
The abstract and full text of theses from the academic year 2011 in Chulalongkorn University Intellectual Repository (CUIR)
are the thesis authors' files submitted through the University Graduate School.

วิทยานิพนธ์นี้เป็นส่วนหนึ่งของการศึกษาตามหลักสูตรปริญญาวิทยาศาสตรมหาบัณฑิต
สาขาวิชาโลกศาสตร์ ภาควิชาธรณีวิทยา
คณะวิทยาศาสตร์ จุฬาลงกรณ์มหาวิทยาลัย
ปีการศึกษา 2559
ลิขสิทธิ์ของจุฬาลงกรณ์มหาวิทยาลัย

INVESTIGATION OF FOCAL MECHANISM AND FRACTAL DIMENSION ALONG THE SUMATRA-ANDAMAN SUBDUCTION ZONE

Mr. Toatin Ketthong

จุฬาลงกรณ์มหาวิทยาลัย
Chulalongkorn University

A Thesis Submitted in Partial Fulfillment of the Requirements
for the Degree of Master of Science Program in Earth Sciences
Department of Geology
Faculty of Science
Chulalongkorn University
Academic Year 2016

Copyright of Chulalongkorn University

Thesis Title	INVESTIGATION OF FOCAL MECHANISM AND FRACTAL DIMENSIONALONG THE SUMATRA-ANDAMAN SUBDUCTION ZONE
By	Mr. Toatin Ketthong
Field of Study	Earth Sciences
Thesis Advisor	Associate Professor Santi Pailoplee, Ph.D.

Accepted by the Faculty of Science, Chulalongkorn University in Partial Fulfillment of the Requirements for the Master's Degree

.....Dean of the Faculty of Science
(Associate Professor Polkit Sangvanich, Ph.D.)

THESIS COMMITTEE

.....Chairman
(Assistant Professor Sombat Yumuang, Ph.D.)

.....Thesis Advisor
(Associate Professor Santi Pailoplee, Ph.D.)

.....Examiner
(Professor Montri Choowong, Ph.D.)

.....External Examiner
(Assistant Professor Krit Won-in, Ph.D.)

ต.ติณ เกตุทอง : การตรวจสอบกลไกการเกิดแผ่นดินไหวและมิติแฟรกทัลของแผ่นดินไหวตามแนวมุดตัวของแผ่นเปลือกโลกสุมาตรา-อันดามัน (INVESTIGATION OF FOCAL MECHANISM AND FRACTAL DIMENSIONALONG THE SUMATRA- ANDAMAN SUBDUCTION ZONE) อ.ที่ปรึกษาวิทยานิพนธ์หลัก: รศ. ดร.สันติ ภัยหลบลี้, 129 หน้า.

แนวมุดตัวของแผ่นเปลือกโลกสุมาตรา-อันดามัน เป็นแนวมุดตัวที่มีการเกิดแผ่นดินไหวมากมาย ซึ่งในการศึกษานี้มีวัตถุประสงค์ในการตรวจสอบกลไกการเกิดแผ่นดินไหว (focal mechanism) และมิติแฟรคทัล (fractal dimension) ในส่วนของการตรวจสอบกลไกการเกิดแผ่นดินไหว ได้แบ่งการศึกษาออกเป็นแผ่นดินไหวระดับตื้น (0-50 กิโลเมตร) กับแผ่นดินไหวระดับลึก (50-1,000 กิโลเมตร) ทั้งสองระดับมีกลไกการเกิดเป็นแบบเลื่อนเอียง (oblique) กับเลื่อนวนกลับ (reverse) และมีมุมเอียงในการเลื่อนตัวประมาน 45 องศา ในส่วนของมิติแฟรคทัล ได้ศึกษาในเชิงพื้นที่และเชิงเวลา โดยได้แบ่งข้อมูลการศึกษาเป็นก่อนคัดเลือกข้อมูลกับหลังคัดเลือกข้อมูลซึ่งผลของมิติแฟรคทัลในเชิงพื้นที่กับเชิงเวลา มีค่าประมาณ 2 ซึ่งมีรูปแบบการเกิดแผ่นดินไหวเป็นแบบระนาบ นอกจากนั้นยังได้มีการศึกษาค่า b ในเชิงพื้นที่ พบว่ามีค่า b ต่ำที่บริเวณเมืองย่างกุ้งกับเมืองซิตตเวประเทศพม่าและนอกชายฝั่งของเกาะสุมาตรา ซึ่งมีค่า b อยู่ระหว่าง 0.91-0.36 และ 0.79-0.56 ตามลำดับ นอกจากนั้นบริเวณแนวมุดตัวของแผ่นเปลือกโลกสุมาตรา-อันดามันมีความสัมพันธ์ระหว่างค่า Dc กับ b เป็นแบบแปรผกผัน (negative)

จุฬาลงกรณ์มหาวิทยาลัย
Chulalongkorn University

ภาควิชา ธรณีวิทยา ลายมือชื่อนิสิต .....

สาขาวิชา โลกศาสตร์ ลายมือชื่อ อ.ที่ปรึกษาหลัก .....

ปีการศึกษา 2559

5672162823 : MAJOR EARTH SCIENCES

KEYWORDS: EARTHQUAKE CATALOGUE / EARTHQUAKE DECLUSTERING / FOCAL MECHANISM / FRACTAL DIMENSION

TOATIN KETTHONG: INVESTIGATION OF FOCAL MECHANISM AND FRACTAL DIMENSIONALONG THE SUMATRA-ANDAMAN SUBDUCTION ZONE. ADVISOR: ASSOC. PROF. SANTI PAILOPLEE, Ph.D., 129 pp.

The Sumatra–Andaman Subduction Zone (SASZ) is one of the most seismically active subduction zone which have generated continuously many great earthquakes. The main aim of this research is to investigate focal mechanism and fractal dimension including b value of the frequency-magnitude distribution model. Regarding to focal mechanism, this research focused on two seismotectonic setting which are (i) interplate, 0-50 km-depth and (ii) intraslab, 50-1,000 km-depth. Both settings reveal the mechanisms of fault as oblique and reverse faulting. The average dip angle of the thrust fault is around 45°. In case of fractal dimension and b value, we analyzed both of spatial and temporal terms and divided two groups of seismicity data which are (i) before and (ii) after earthquake declustering process. The result of Dc in spatial and temporal term was estimated reached 2.0. It means that the seismic pattern is a plane source. . For the spatial distribution of b value, the lowest values are in the vicinity of Yangon and Sittwe, Myanmar and the offshore of Sumatra Island. In the temporal investigation at 6 locations of hazardous earthquakes, the b values are in the range of 0.91 – 0.36 and 0.79 – 0.56, respectively. In addition, all the Dc/b relationship of six specific events along the SASZ was defined as negative relationship.

จุฬาลงกรณ์มหาวิทยาลัย
Chulalongkorn University

Department:	Geology	Student's Signature	.....
Field of Study:	Earth Sciences	Advisor's Signature	.....
Academic Year:	2016		

ACKNOWLEDGEMENTS

I sincerely thank my Advisor, Assistant Professor Dr. Santi Pailoplee, Department of Geology, Faculty of Science, Chulalongkorn University for his supports, encouragements, critically advises and reviews of thesis. I thank to Miss Kanokkarn Vajchakom, Mr. Santawat Sukrungsri and all of my friends for their kindly help throughout my study at the university. I am grateful to Thai Meteorological Department who gave me opportunity to this study.

Finally, I express my deep respectfulness and gratitude to my family for their inspiration on scientific thinking is greatly appreciated.

จุฬาลงกรณ์มหาวิทยาลัย
Chulalongkorn University

CONTENTS

Page

จุฬาลงกรณ์มหาวิทยาลัย
Chulalongkorn University

Page

จุฬาลงกรณ์มหาวิทยาลัย
CHULALONGKORN UNIVERSITY

Page

Page

Page

จุฬาลงกรณ์มหาวิทยาลัย
Chulalongkorn University

LIST OF TABLES

จุฬาลงกรณ์มหาวิทยาลัย
Chulalongkorn University

LIST OF FIGURES

Chulalongkorn University

จุฬาลงกรณ์มหาวิทยาลัย
Chulalongkorn University

CHAPTER I

INTRODUCTION

1.1. Background

In the Mainland Southeast Asia (MLSEA), there are a number of seismic source zones that had a tremendous impact on the ASEAN member states, especially in Thailand. Among these earthquake sources, the Sumatra-Andaman Subduction Zone (SASZ), strike north-south in the Indian Ocean, is one of the most hazardous zones. The SASZ is a subduction zone that has generated many devastating earthquakes in history, i.e., Mw 8.6 in 1861, Mw 7.6 in 1907, Mw 7.7 in 1935, Mw 7.9 in 2000, Mw 7.3 in 2002, Mw 8.6 in 2005, including the severe Mw 9.2 earthquake in past decade which have a significant effect on Southern Thailand (Waldhauser et al., 2012). The earthquake occurred at 07:58 local time in Indonesia (00:58 UTC) (Figure 1.1).

The 2004 Indian Ocean tsunami on December 26th was generated by a large earthquake (Mw = 9.2) which caused widespread devastation and heavy loss of life throughout the Indian Ocean basin and beyond. The rupture of a section of the megathrust extended 1,200-1,300 kilometres from the offshore northern Sumatra to the Andaman Islands and subsequent reaction of Mw 8.2 and Mw 8.6 earthquake on April 11th, 2012.

As stated in the past study, the tsunami arrived in northern Sumatra, the hardest-hit region, within 15–20 minutes after the earthquake. Indonesia was the worst hit that 128,645 people were killed, followed by 35,322 of Sri Lanka, 12,405 of India and 5,395 of Thailand. In addition, more than 2,817 people still listed as missing, and 7,000 displaced (USAID, 2005). These potential disasters led to heavy loss of life, injury and damage to properties. Thus, the country must rehabilitate the tsunami affected areas for several years (Jaffe et al., 2006) (Figure 1.2).

จุฬาลงกรณ์มหาวิทยาลัย
Chulalongkorn University

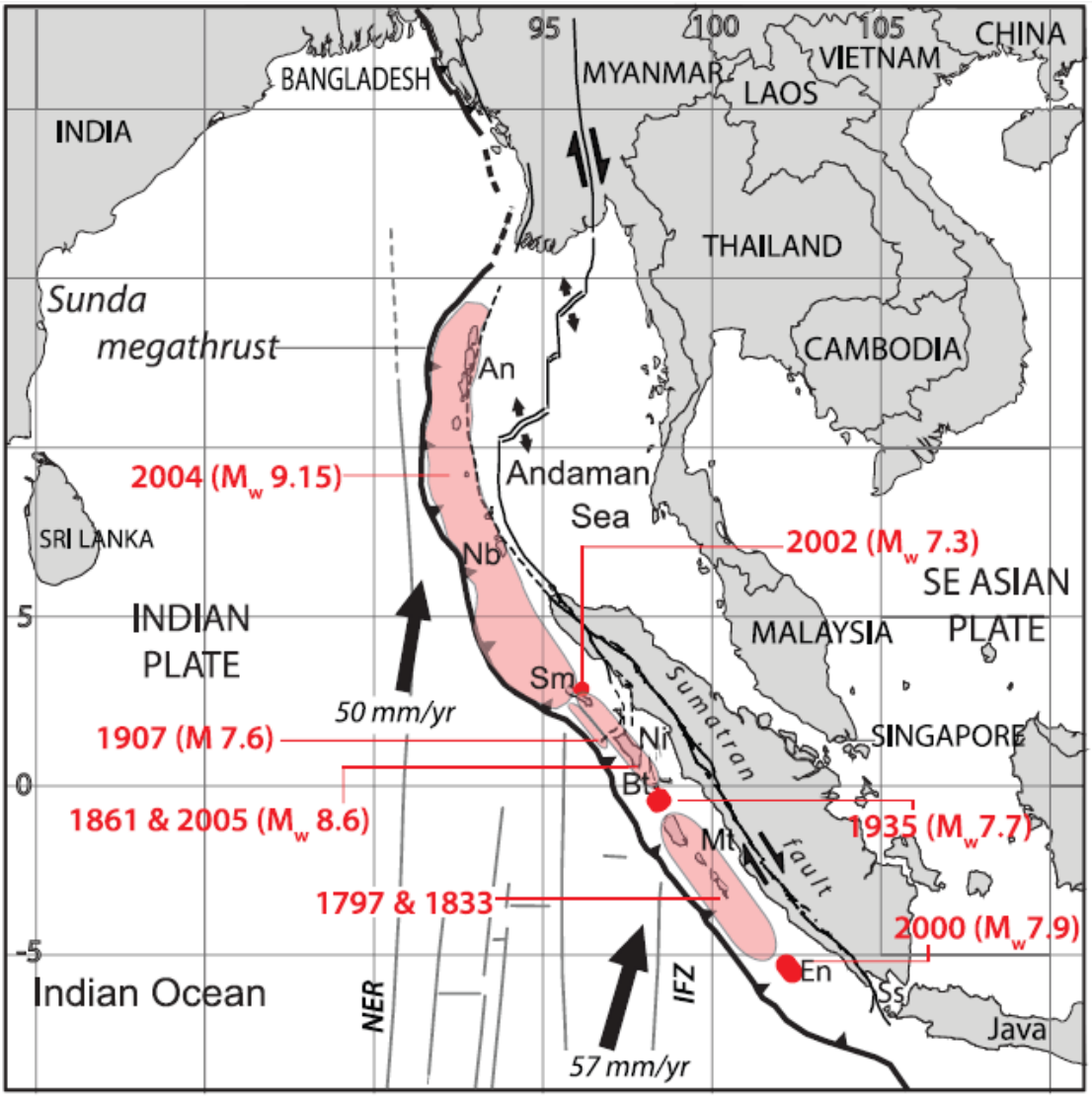

Figure1. 1 Map of Mainland Southeast Asia showing the SASZ in the thick black line. Black arrows show the direction and the rate of Indian plate movement and subduction underneath the Eurasian plate. Red polygons indicate the risk of earthquake zones. Ss, Sunda; En, Enggano Island; Ni, Nias island; Sm, Simeulue island; Nb, Nicoba island; An, Andaman island; Mt, Mentawai island; Bt, Batu island; NER, Ninety-East Ridge and IFZ, Investigation Fracture Zone (Natawidjaja et al., 2006).

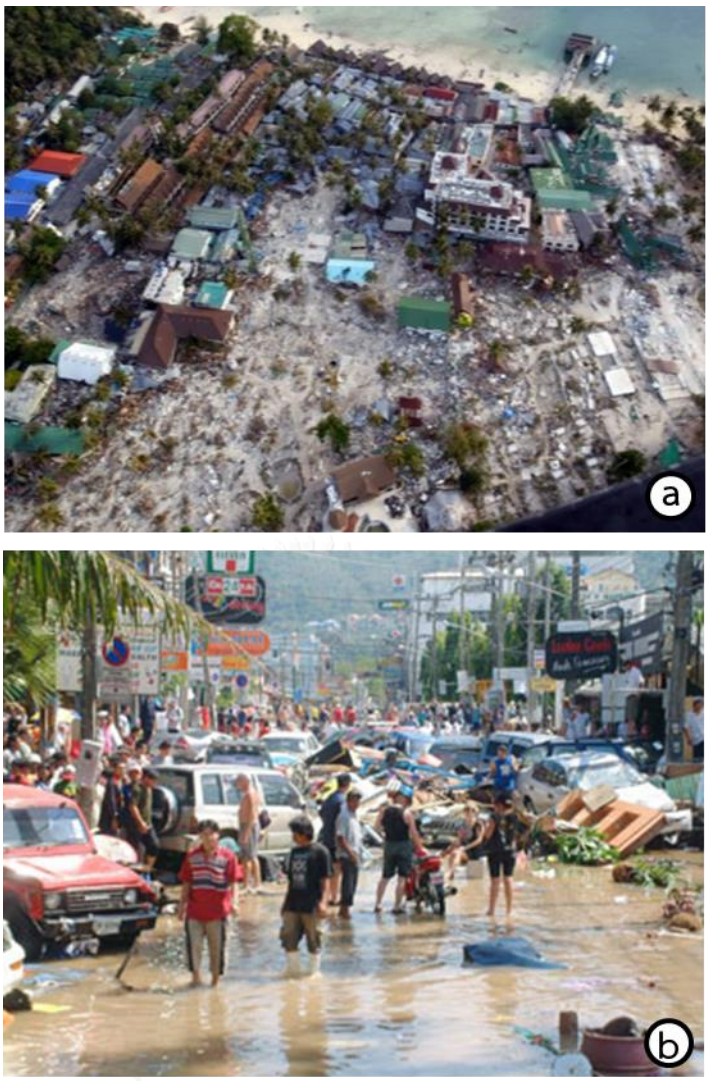

Chulalongkorn University

Figure1.2 (a) Koh Phi Phi, Krabi, the resorts and houses were savagely attacked by the tsunami in 2004. The several hundred people were being buried alive, blown and drowned into the sea. (b) Patong, Phuket, many people were affected by the 2004 tsunami. As a number of assets were damaged and left on the road (Sarapee Pittayakom School, http://www.sarapee.ac.th/ [Online]. Nov. 10, 2015).

According to geological records, the SASZ has been indicated natural disasters from earthquakes and tsunami. Furthermore, there was significant evidence from coral microatolls for the great earthquakes. As reported by the study of Natawidjaja et al. (2006), they investigated evidences for the emergence of coral microatolls from the

great Sumatran megathrust earthquakes of 1797 and 1833. The example of coral in this research was Sibelua Site (Sbl) which represents zone along the northeastern coasts of the Mentawai islands. They studied modern microatoll, Sbl02A2 and fossil microatolls, Sbl02A1 (Figur 1.3). The HLS that recorded by the fossil and modern microatoll slab in 1797 and 1833 were approximately 0.5 and 1.1 m, respectively. The lack of 1797 coral heads implied that the HLS was about 0.5 m because they must extrapolate the older record to 1797. The result revealed that pre-earthquake HLS was about 0.3 m above the 2002 HLS and post-earthquake HLS was about 0.2 m below the 2002 HLS. They estimated that evidence of 1833 microatolls emerged about 1.1 m. The study also found that the pre-1833 HLS was a few centimeters above the 2002 HLS and post-1833 HLS was a little more than 1.0 m below the 2002 level (Figure 1.4).

From the mentioned above, it can be described that the SASZ is one of the most high-risk potential hazard zones which can cause the severe earthquake from both of geological and disaster evidences. These devastating disasters had a remarkable effect and caused a great destruction in Thailand. Therefore, this research concentrated on the SASZ as the study area.

1.2. Tectonic Setting

Convergent plate boundaries are located where lithospheric plates are moving towards one another. The plate collisions that occur in these areas can produce earthquakes, tsunami, volcanic activity and crustal deformation. Convergent plate boundary can happen in 3 patterns which are (i) continental and continental plates, (ii) continental and oceanic plates and (iii) oceanic and oceanic plates. This research focused on the SASZ which is oceanic and continental convergent plate boundary.

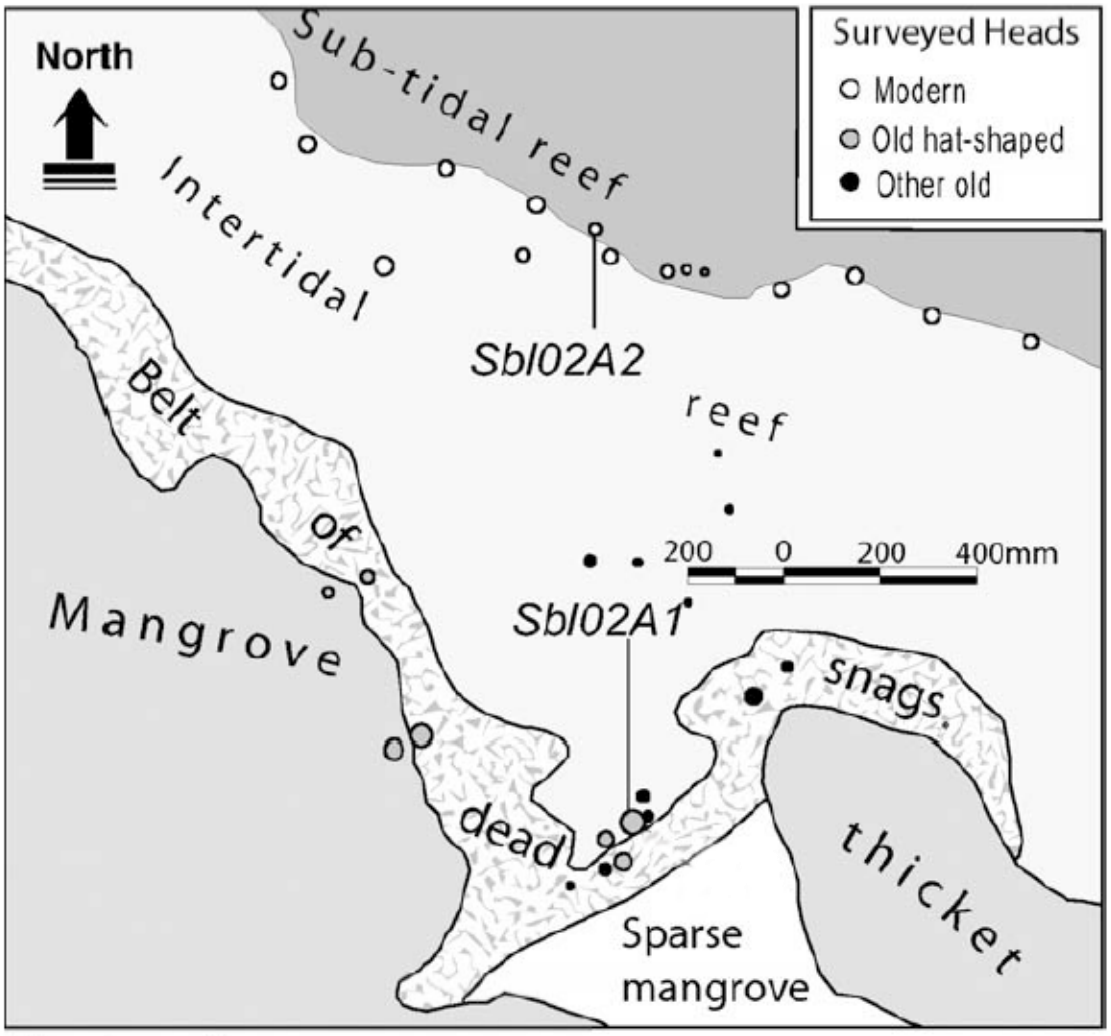

Figure1. 3 Map of the Sibelua site on the north east coast of South Pagai island showing the fossil microatoll Sbl02A1 and modern microatoll Sbl02A2 (Natawidjaja et al., 2006).

The SASZ is formed by the collision of Indo-Australian and Eurasian plate which had distance around 1,300 km-long. It has been shown that the Indian plate converges obliquely towards the Asian plate at the average rate of 50 mm/year. (DeMets et al., 1994). While the average dip angle of subduction that estimated from the cross-section of the earthquakes distribution is around 20° and the earthquakes were observed down to the depths of 700 km.

The Sumatran megathrust has a long history of large destructive earthquakes. As the geodetic survey data suggested that strain accumulation on the megathrust was

being locked and led to varying degrees of tectonic and volcanic activity along the subduction margin. For this reason, the SASZ is risk area of great earthquake. If the SASZ generates them, it can bring about a large number of effects of seismic disaster, tsunami, etc. Hence, we interested in studying focal mechanism along the study area to identify what is mechanism of fault of the SASZ.

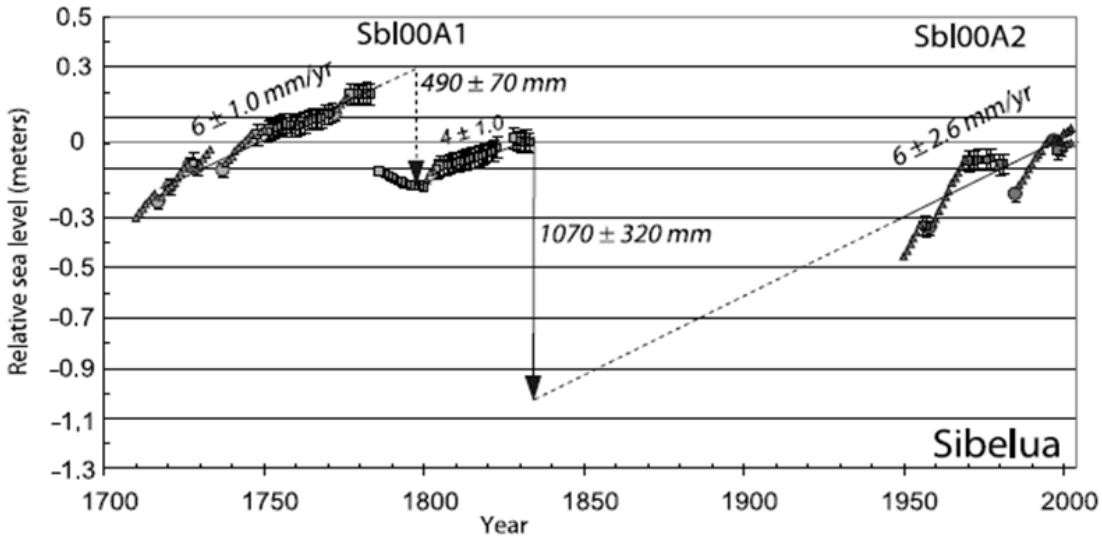

Figure1.4 HLS time series from modern and fossil microatolls at Sibelua showing 0.5-m uplift in 1797 followed by 1.1-m uplift in 1833 (Natawidjaja et al., 2006) .

จุฬาลงกรณ์มหาวิทยาลัย
Chulalongkorn University

Up to the present, the methods of the earthquake study have been developed which can be divided into 3 terms, i.e., short-term (day-month), intermediate-term (month-year) and long-term (years) (Shebalin, 2006) (Table 1.1). Firstly, a short-term is an earthquake prediction in the days to months. It can be observed from animal perception, characteristics of cloud or earthquake lights (Figure 1.5). Then, a long-term is the ways to predict earthquake in the 10-10,000 years. These procedures come from the study of the paleo-seismological, seismic hazard analysis or historical study (Figure 1.6). Lastly, an intermediate-term is the methods for statistical analysis to use for earthquake prediction. From the previous works, it has been accepted that the intermediate-term is the most successful technique which provides many ways such as b-value (Nuannin et al., 2005), Z-value (Wiemer and Wyss, 1994), RTL algorithm

(Huang, 2004) , Pattern Information (Nanjo et al., 2006), Fractal Dimension (Bhattacharya and Kayal, 2003), etc. These methods are called statistical seismology which is all important and reliable in different ways.

Table1.1 State of the art of the earthquake prediction (Shebalin, 2006).

Method	Reference
A. Short-term (day-month)	
A.1 Animal perception	Kirschvink, 2000
A.2 Characteristic of cloud	Simons, 2008
A.3 Light earthquake	Yasui, 1968
B. Intermediate-term (months-year)	
B.1 b-value	Nuannin et al., 2005
B.2 Z-value	Wiemer and Wyss, 1994
B.3 RTL algorithm	Huang et al., 2004
B.4 Pattern Information	Nanjo et al., 2006
B.5 Fractal Dimension	Bhattacharya and kayal., 2003
C. Long-term (years)	
C.1 Paleo-seismological study	McCalpin. 1996; Pailoplee et al., 2009a
C.2 Seismic hazard analysis	Kramer, 1996; Pailoplee et al., 2009b
C.3 Historical study	McCue, 2004; Stirling and Petersen, 2006

The first one is b value analysis which is estimated from the frequency-magnitude distribution (Gutenberg and Richter, 1944). The parameter is strongly related to the seismotectonic stress accumulation and led to the risk of earthquake zones in the future. While the Z values identify the precursory seismic quiescence, that is a significant decrease of the mean seismicity rate as compared to the background rate in the same crustal volume ((Wiemer and Wyss, 1994) and Wyss, 1994). Then, the RTL algorithms are consideration of the influence weight of each prior event, in the main

event under investigation, depends on all three parameters (time, place and magnitude) of earthquakes (Sukrungsri and Pailoplee, 2017).

Figure1.5 (a) Before the 1999 Chi-Chi earthquake in Taiwan occurred M_w 7.6, the earthworms were migrating due to seismic vibrations [http://www.e-pisco.jp]. (b) Before the earthquake in Japan occurred, the people found earthquake lights appeared in the sky (Yasui, 1968).

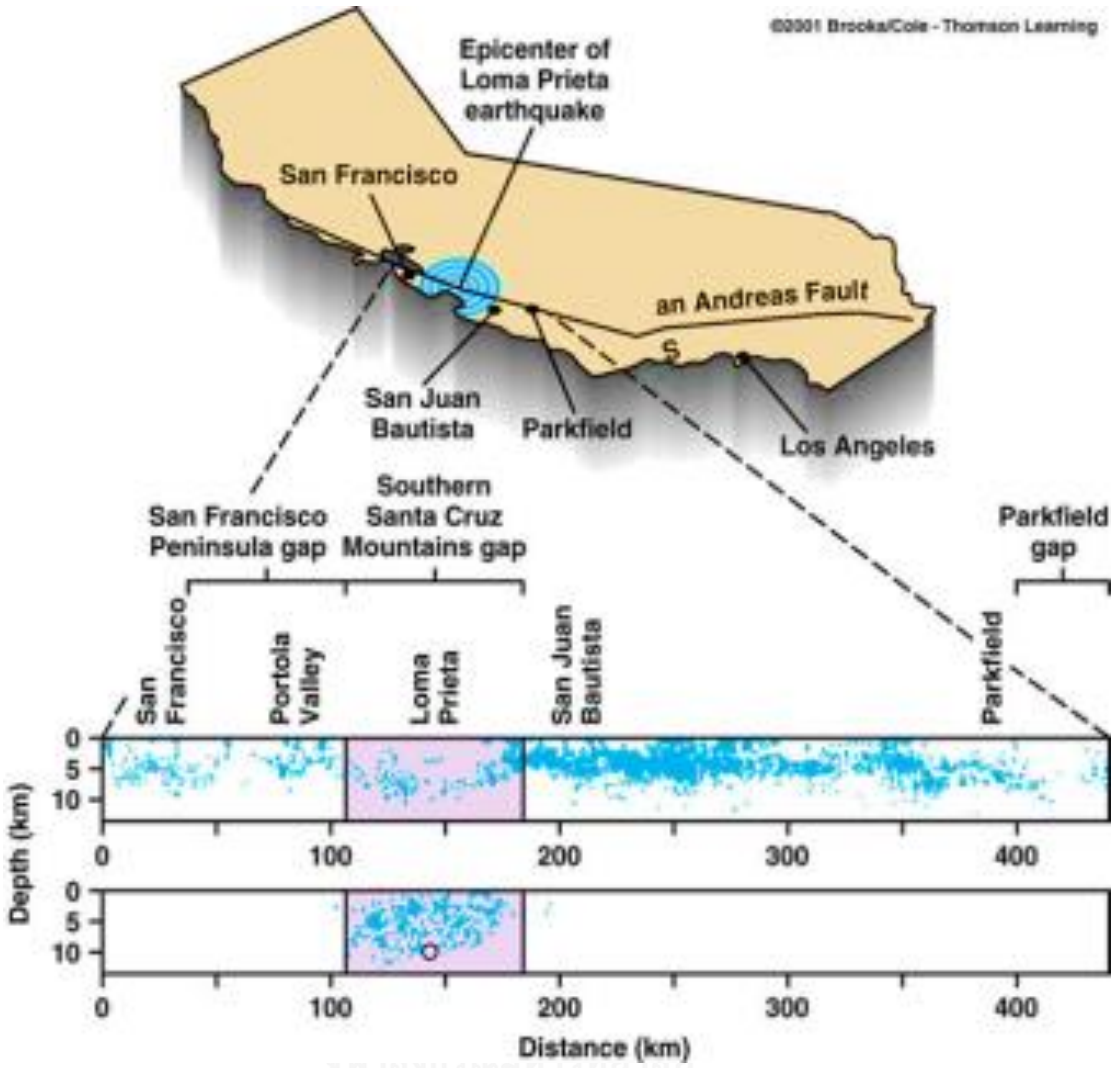

Figure1. 6 Statistics earthquakes in the past along the San Andreas Fault Andreas showing the gap earthquake before 2532 (USGS, 1989).

Next, the pattern informatics can be used to detect the precursory seismic activation or quiescence and also analyse the space– time patterns of the past earthquakes to find the possibility of locations where the future large earthquakes are expected (Nanjo et al., 2006). Finally, the fractal dimension is a mathematical method that relies on a similar classification of information in the study area, the distance between the point of the earthquake origin and nature (Bayrak and Bayrak, 2012). It can give the result of seismic pattern of study area.

For these reasons, it is able to be seen that the intermediate term earthquake predictions apply scientific principles to investigate that provide both of accurate and precise results due to statistical data analysis. Thus, we gave the consideration to the intermediate-term predictions by using statistical seismology in this study.

1.3. Previous Work

The SASZ is one of the large seismic active zone. So, a number of worldwide seismologists interested in studying this area. For this case, we reviewed two research papers that related to our selected area of work. There are Pailoplee et al. (2013) who studied b-value and Sukrungsri and Pailoplee (2014) who studied z-value and RTL algorithm.

In a research article by Pailoplee et al. (2013) who applied b value analysis, the most subsequent earthquakes were located in the areas showing low b value anomalies along the northern segment of the SASZ. The earthquake data were divided into three groups of (a) 1980–1994, (b) 1980–2003, and (c) 1980–2010. They selected 50 numbers of events which showed significant result for 0.25 x 0.25 grid nodes covering the study area. (Nuannin et al., 2005). Then, they used ZMAP developed by Wiemer (2001) to calculate b value for selected cross section and displayed the spatial distribution of b value maps in Figure 1.7. The results, analysed from the seismicity data during 1980–1994, implied the two regions of low b value, namely, the South and North of the Nicobar Islands (Figure 1.7a). In Figure 1.7b, rechecking with the extended dataset recorded during 1980–2003, revealed one more prospective zone from the last Figure 1.7a that is the West coast of Myanmar. Then in the present-day dataset (1980–2010), it showed the three obvious anomalous low b value areas which are (i) the southward offshore region of the Nicobar Islands (ii) the offshore area north of the Nicobar Islands and (iii) the West coast of Myanmar. The results in this research supported the hypothesis that a smaller b value probably means the stress is high and may cause an earthquake, when the southward offshore region of the Nicobar Islands produced earthquake with magnitude 7.5 Mb on June 12th, 2010. However, after that they are still quiescent up to the present day (2013) (Figure 1.7c).

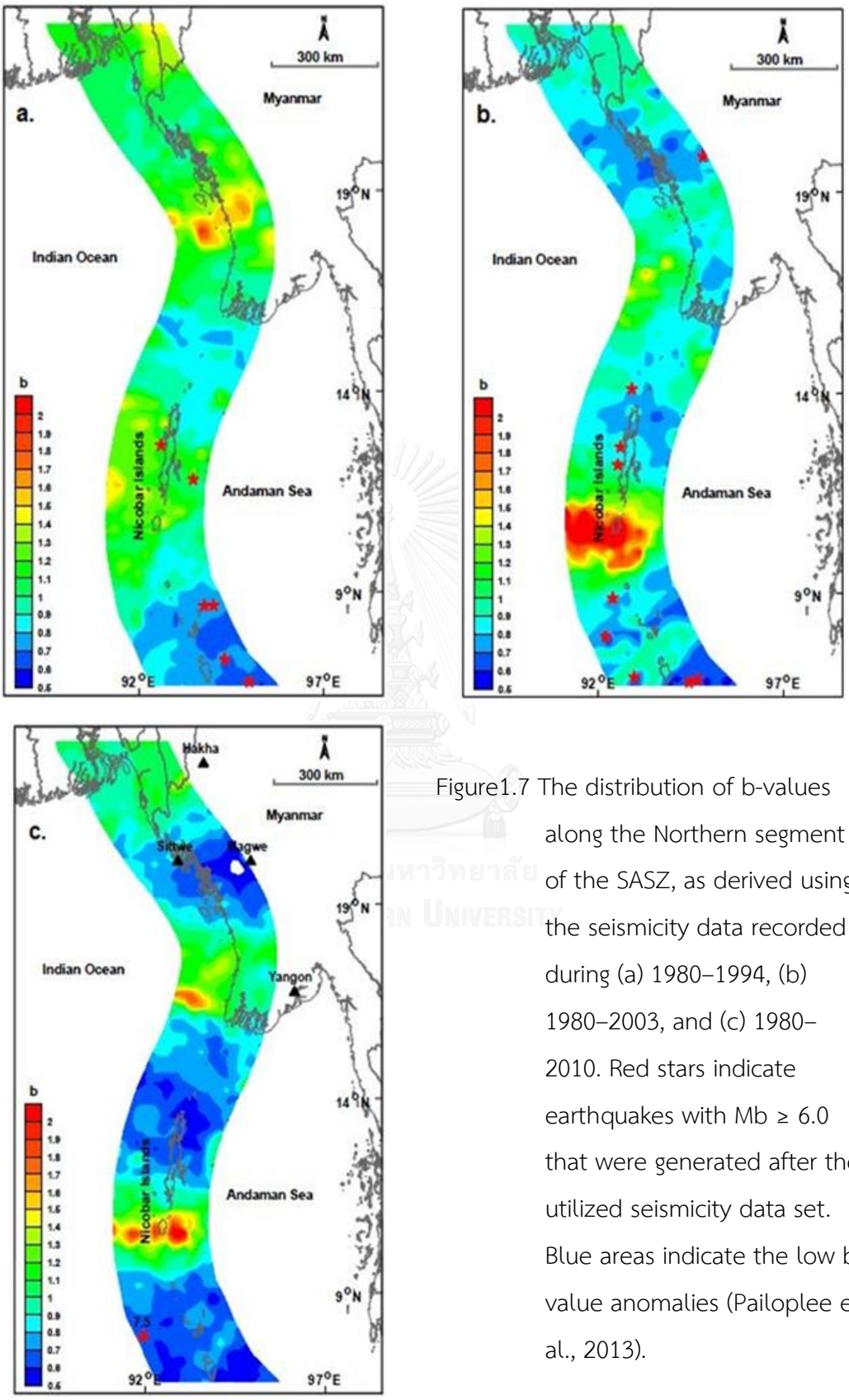

Figure1.7 The distribution of b-values along the Northern segment of the SASZ, as derived using the seismicity data recorded during (a) 1980–1994, (b) 1980–2003, and (c) 1980–2010. Red stars indicate earthquakes with Mb ≥ 6.0 that were generated after the utilized seismicity data set. Blue areas indicate the low b-value anomalies (Pailoplee et al., 2013).

Sukrungsri and Pailoplee (2014) conducted a study to examine Z value in the SASZ. The study areas were divided by a grid of latitude 2°S- 24°N and longitude 88-100°E, with an interval of 0.25° gridded spacing. Thus, the total number of nodes is 4,992. In order to compute Z values, they fixed the 50 events of earthquake in any radius. However, in this study the limit of radius r = 250 km was fixed. He did retrospective test to investigate Z values at the starting time of seismicity quiescence. For example, in Figure 1.8a, the Z value maps showed the obvious area of quiescence after 1999.68, near the epicenters of the Mw 9.0 and Mw 8.6 in 2004 and 2005, with range of Z value between +6.4 and +7.0, respectively, covered 1.25-4.5°N latitude and 95.35-96.6°E longitude (red areas). Next, in Figure 1.8b, it can be described that the quiescence mentioned was also followed by the major earthquakes with Mw 6.8 and 6.9, respectively. Lastly, the distribution of Z values in Figure 1.8c, before the June 12nd, 2010 Mw 7.5, displayed the anomalous decreasing of seismicity rate covered 182 km far from the epicenter before the major earthquake produced about 2.1 years. The study provided Z value between +5.6 and +6.7, covered 8.75– 11.25°N latitude and 92.01-94.01°E longitude in 2008.31. All of these results combined gave conclusion to a present-day map of the anomalous Z values which can be defined by the maximum of Z = 6.5, i.e., Nicobar Islands (Figures 1.8d).

He also studied the RTL algorithm in this study area. The area of SASZ was separated into a grid of 0.25° x 0.25° to present a high resolution and the temporal variations of RTL scores that were evaluated at each grid node. The study area was divided into 4,992 nodes for each time slice. Since, there were more than 900 time slices, the total number of effective grid nodes, where RTL values were calculated, are more than 4,555,200.

He found parameter of the RTL algorithm by retrospective test. According to Figure 1.9a, showed the anomalous RTL score prior to the Mw 9.0 of December 26th, 2004 on the western offshore of Sumatra Island between -0.05 and -0.3, which was evident 0.15 during 2001.41-2002.06. While the following analysis indicated the anomalies in the west coast of Sumatra Island during 2007.39-2008.12 (Figure 1.9b) with range of -0.05 to -0.4. After approximately 0.3-2.4 years, the M_w 7.3 earthquake actually happened in the anomalous area.

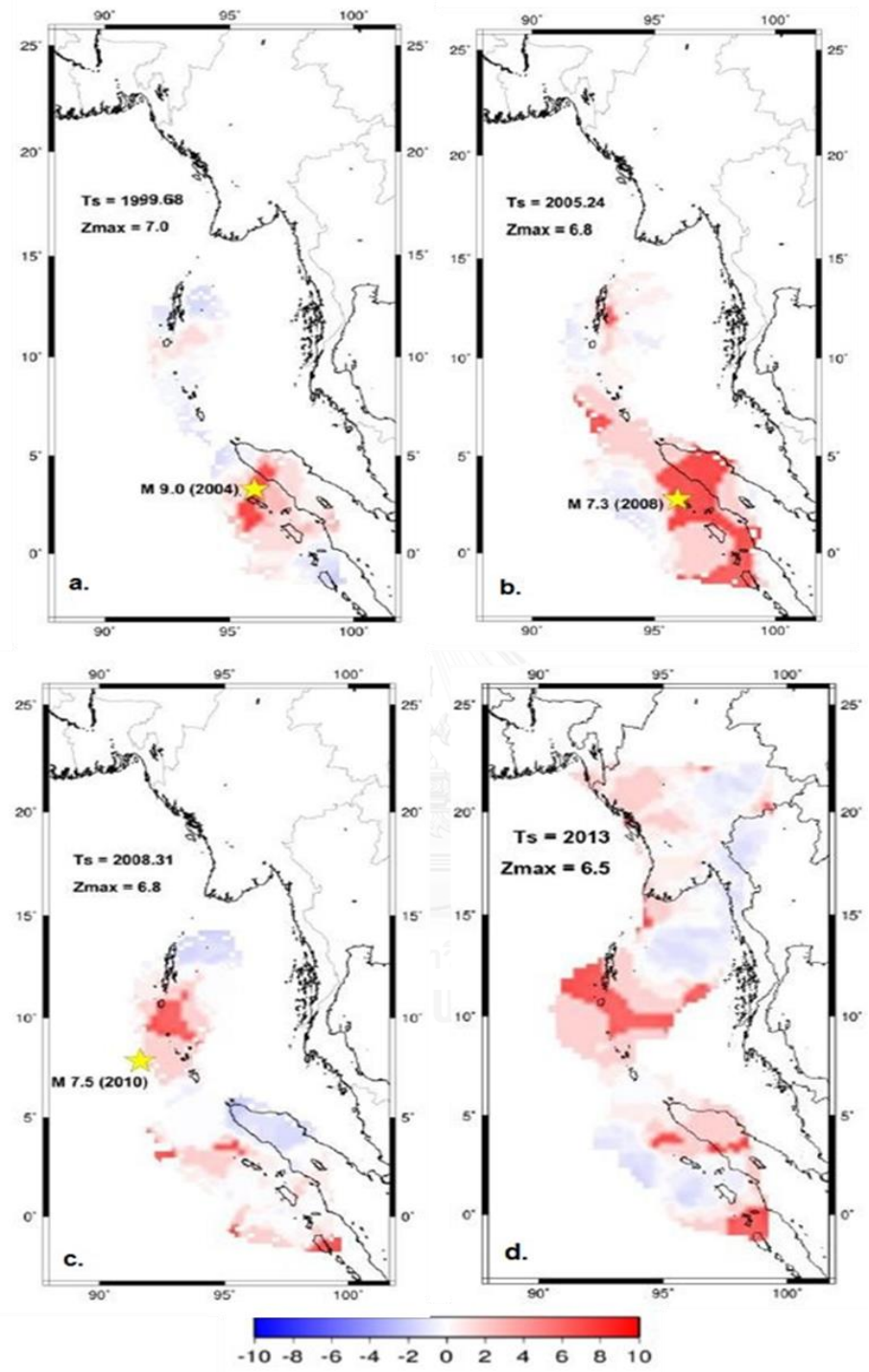

Figure1.8 Map showing the spatial distribution of Z values at the starting time of quiescence of the earthquake (a) December 26th, 2004 Mw 9.0 (95.6°E, 1.75°N), (b) February 20th, 2008 Mw 7.3 (97.26°E, 2.25°N), (c) June 12nd, 2010 Mw 7.5 (92.26°E, 9.5°N) and (d) present map. The anomalous zones are

indicated as shaded areas and the epicenters are shown as yellow stars (Sukrungsri and Pailoplee, 2017).

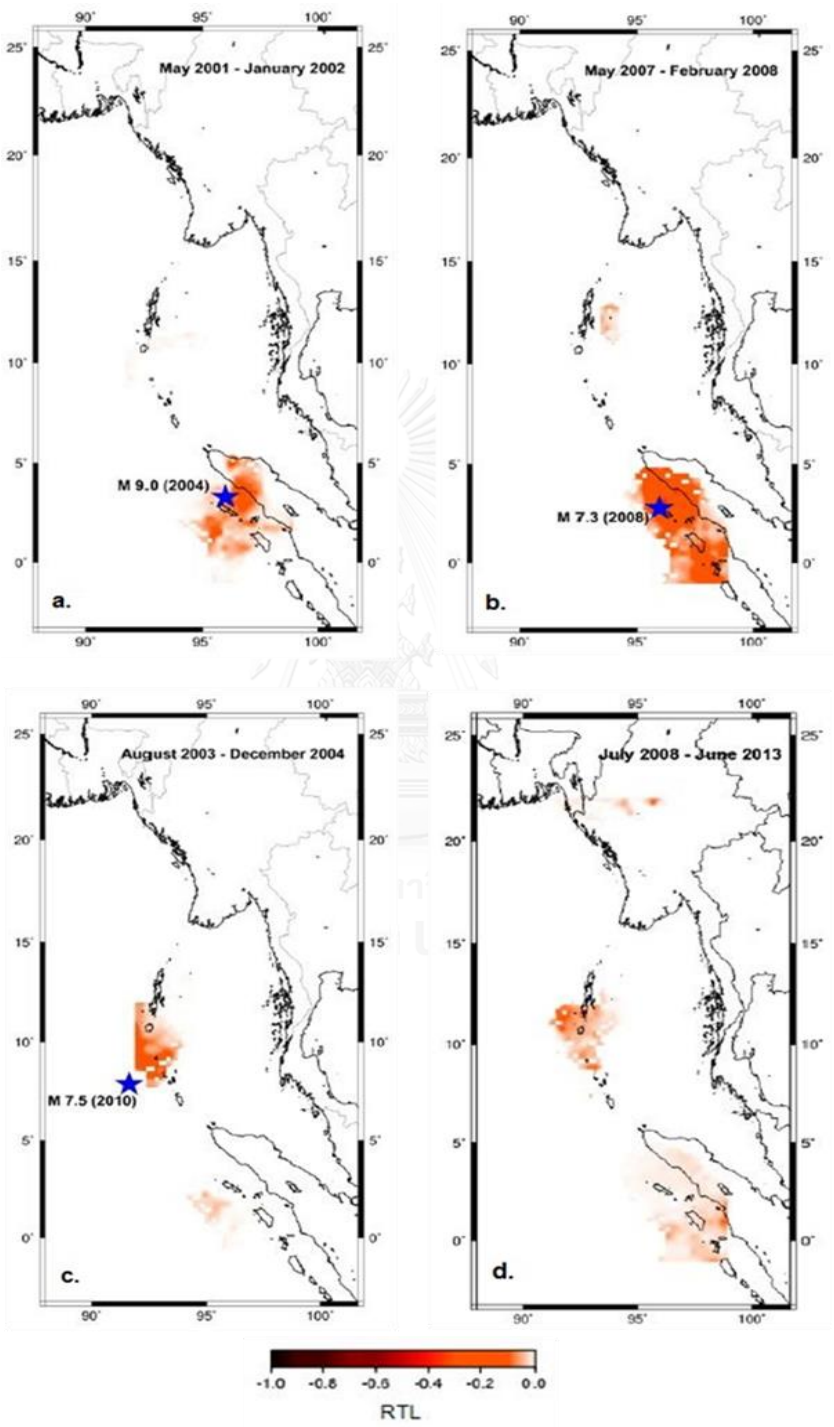

Figure1.9 Map of the SASZ showing the spatial distribution of RTL score at the starting time of quiescence of the earthquakes (a) December 26th, 2004 Mw 9.0

(95.6°E, 1.75°N), (b) February 20th, 2008 Mw 7.3 (97.26°E, 2.25°N), (c) June 12nd, 2010 Mw 7.5 (92.26°E, 9.5°N), (d) present map during 2008–2013 (Sukrungsri and Pailoplee, 2017).

1.4. Study Area

The study area is located on the SASZ, 2°S to 24°N latitude and 88°E to 100°E longitude, which can happen the potential hazards of both ground shaking and local tsunami in Indonesia, Myanmar, India, including Thailand. The both of focal mechanism and fractal dimension were used to analyse to detect the mechanism of fault rupture and seismic pattern of the area (Figure 1.10).

1.5. Objective

In this thesis, the development of focal mechanism and fractal dimension methodology which are able to integrate all available information of mechanism of fault and seismic pattern performed in the SASZ, are presented. The main detailed purposes are these following.

- To investigate the mechanism of fault along the SASZ by focal mechanism.
- To investigate the seismic pattern along the SASZ by fractal dimension.

จุฬาลงกรณ์มหาวิทยาลัย
Chulalongkorn University

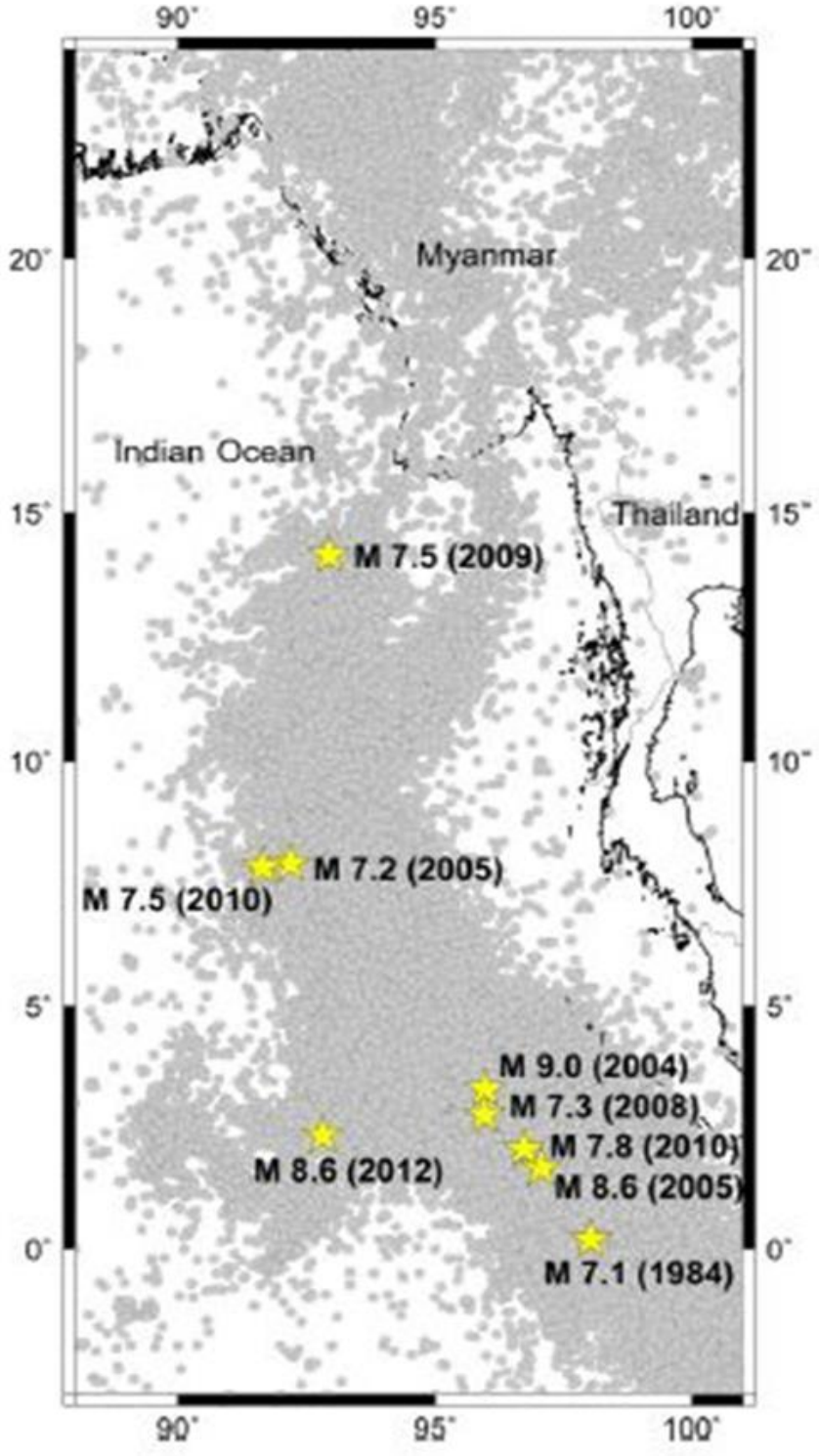

Figure1.10 Map of SASZ showing earthquake distributions in the area indicate by grey circles. Yellow stars indicate the epicenters of $M_W \geq 7.0$(Sukrungsri and Pailoplee, 2017).

CHAPTER II
THEORY AND METHODOLOGY

2.1. Focal Mechanism

2.1.1. Theory of focal mechanism

Focal mechanism is fault plane solutions for earthquakes which is meaning that they tell us the orientation in 3-D space of two potential fault planes. They have generated the seismic wave associated with the earthquake. The focal mechanism can be derived the first arriving P waves break up or down or no apparent signal. The first onset of the P-wave on a seismogram of the seismometer is used to distinguish between a compressional and dilatational. When all data are plotted the axes which are two orthogonal nodal planes separating compressional and dilatational. The axes of maximum shortening and maximum lengthening bisecting the quadrants are known as the P and the T axes, respectively. The P axis lies within the quadrant of dilatational initial motions, whereas the T axis lies within the quadrant of compressional initial motions (Figure 2.1).

In this schematic, The P axis lies within the white quadrant of compressional initial motions, whereas the T axis lies within the gray quadrant of dilatational initial motions. Both are perpendicular to the intersection of the two nodal planes. The computed focal mechanisms show only the P and T axes and do not use shading. Whether the responsible fault was normal, reverse, strike-slip, or oblique reverse (Figure 2.2).

The focal mechanism can also provide the information of strike, dip angle and rake angle for the individual event (Figure 2.3).

- strike: strike is the direction of a line created by the intersection of a fault plane and a horizontal surface, relative to North. The strike orientations must be measured in degree (0°-360°).

- dip: dip angle is the angle between the fault and a horizontal plane. The dip of a vertical fault is 90°, while a horizontal fault is 0°.

- rake: rake angle is the moving direction of a hanging wall during rupture, as measured on the plane of the fault. It is measured relative to fault strike, ±180°.

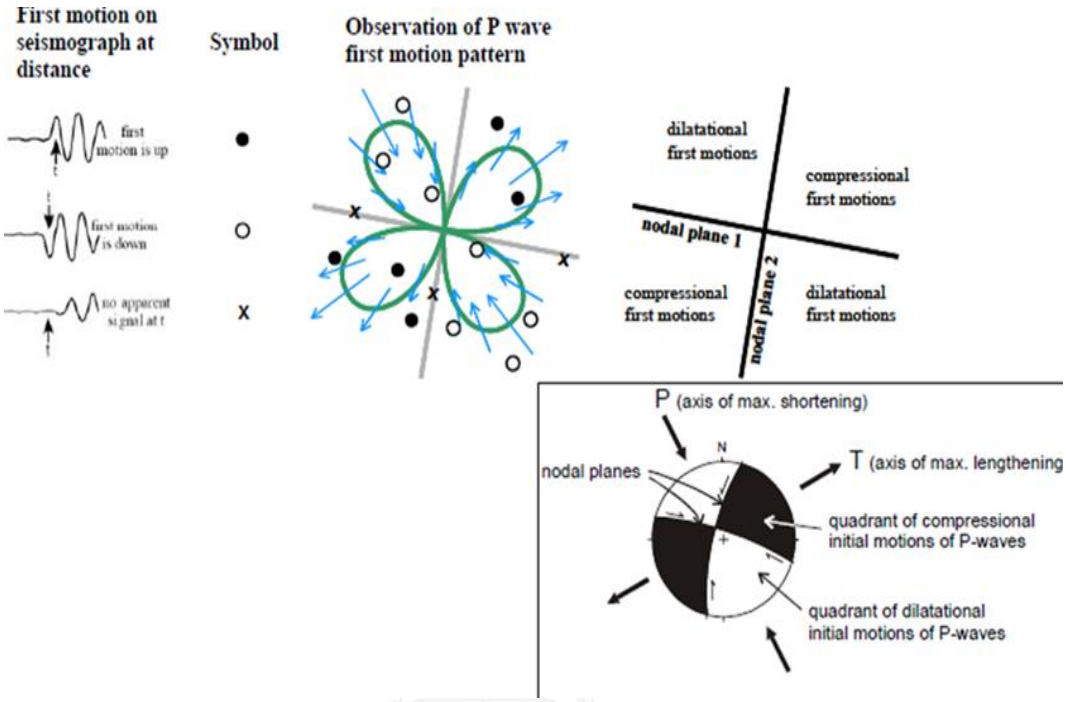

Figure2.1 Elements of a fault plane solution (Barth et al., 2008).

2.1.2. Literature review

Rao et al. (2006), they studied in the Muzaffarabad region in western Himalaya. The case study was the 2005 earthquake on October 8 occurred at 03:50:40 UTC, located at 34.493° N latitude and 73.629° E longitude with 26 km depth, as stated by United States Geological Survey. This is one of the strongest earthquake with a magnitude of 7.6 followed by a number of aftershocks with magnitude greater than 5.0 which were roughly 50 km NW of the main shock. This potential disaster destroyed several parts of Pakistan, Jammu and Kashmir.

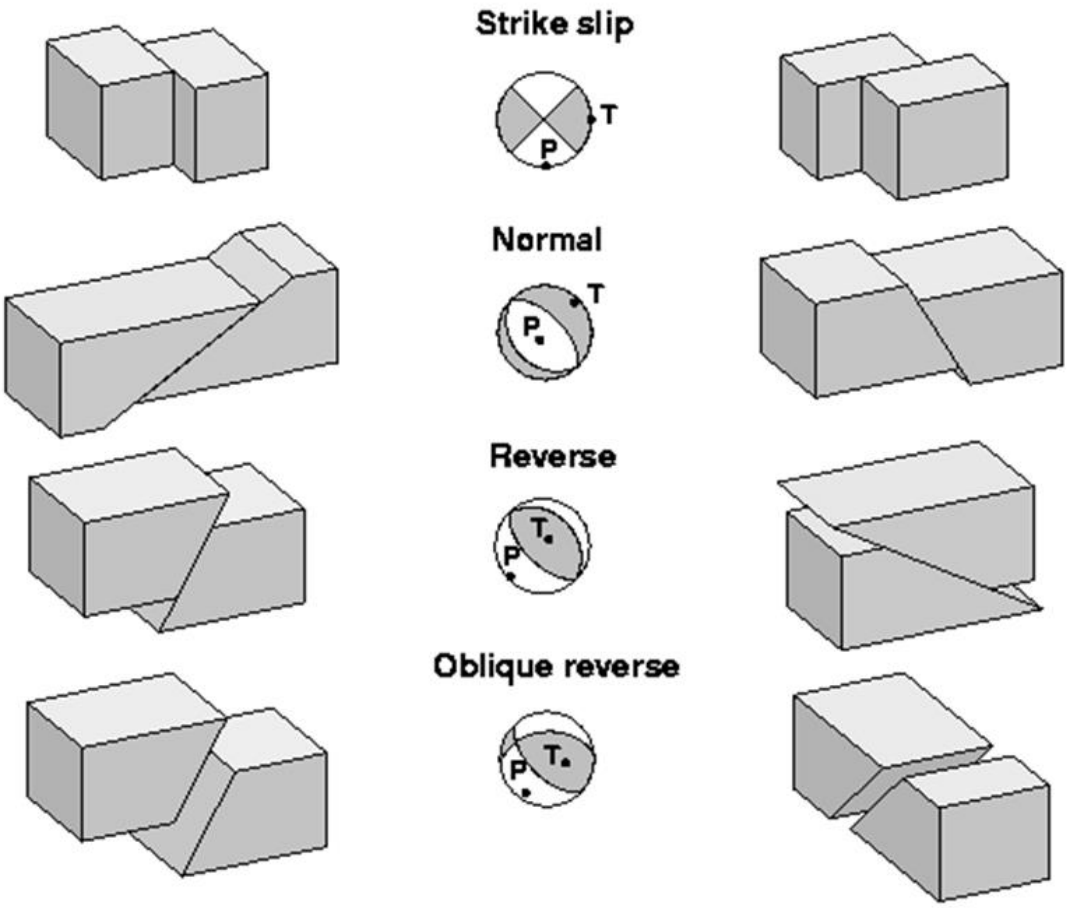

Figure2.2 Schematic diagram of a focal mechanism. P is shortening which is axis of max. T is lengthening which is axis of max (USGS, 1996).

Chulalongkorn University

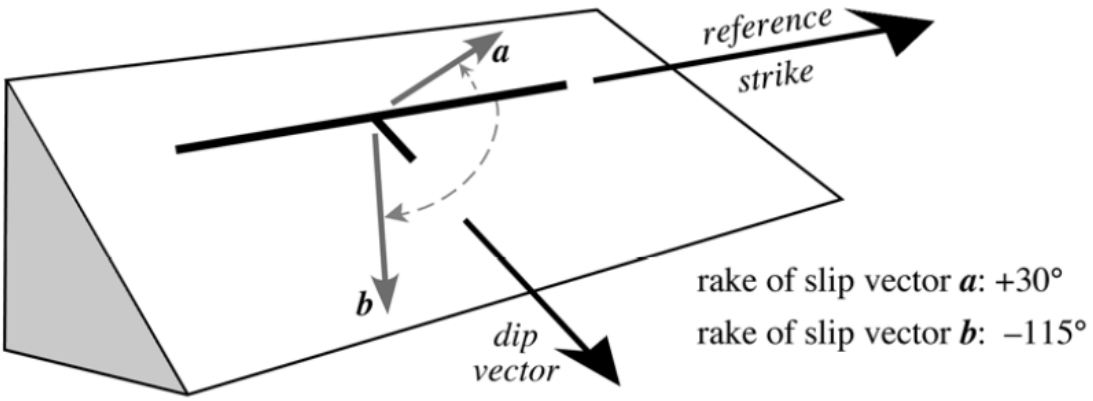

Figure2.3 Strike, Dip and Rake of Focal Mechanism (Cronin et al., 2010).

According to the focal mechanism study, the result in Himalaya was the shallow (5–10°) north dipping thrust faults with a shallow distribution of focal depth. While the Tibetan Plateau's north side was the normal fault along the NS trending fault plane and strike-slip motion along the EW plane. In the event of Pamir–Hindukush, the mechanisms mostly were thrust and strike-slip type with the principal compressive stress axis oriented NNW. Finally, the Burmese arc was the strike-slip type in the upper of 90 km and the thrust type below 90 km, along the eastward dipping Indian lithospheric slab (Figure 2.4).

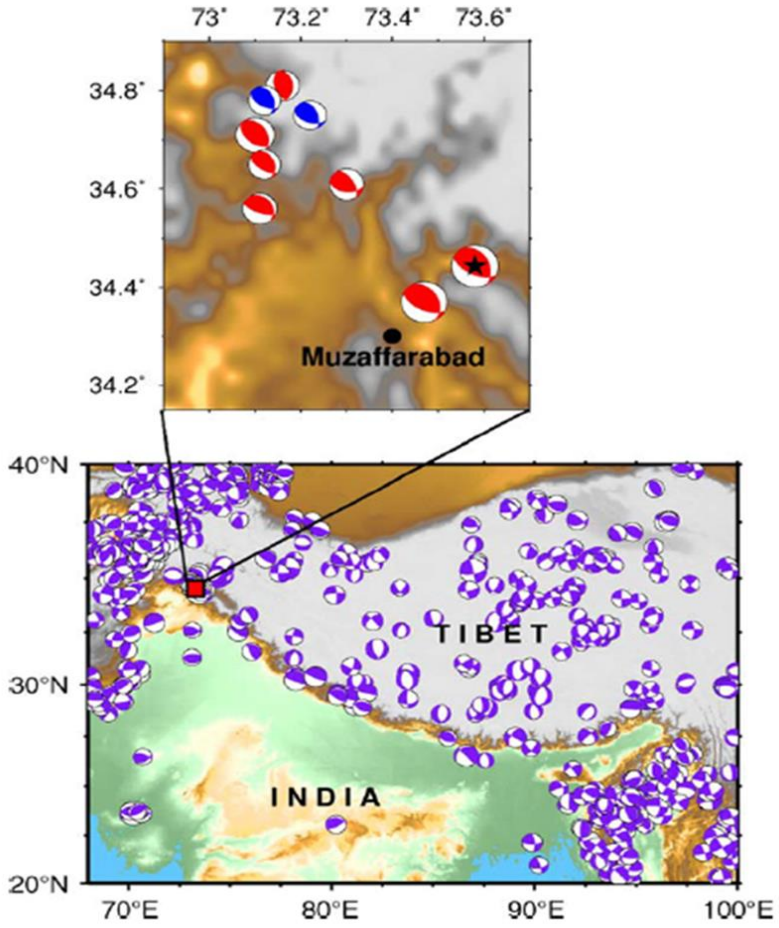

Figure2.4 Focal mechanism solution of the earthquakes happened in Himalaya, Tibet, Pamir and Hindukush regions from the Harvard CMT catalogue. Inset: a close up of the Muzaffarabad region indicates the focal mechanisms of the 2005 Himalayan earthquake and aftershocks. The blue beach balls correspond to the earthquakes prior to this event (Rao et al., 2006).

In summary, the focal mechanism of the Muzaffarabad earthquake, which occurred in the westernmost part of the Himalayan arc, presented the thrust fault along the NNW orientation. The fault planes appeared to be dipped as much as 45° (Figure 2.5).

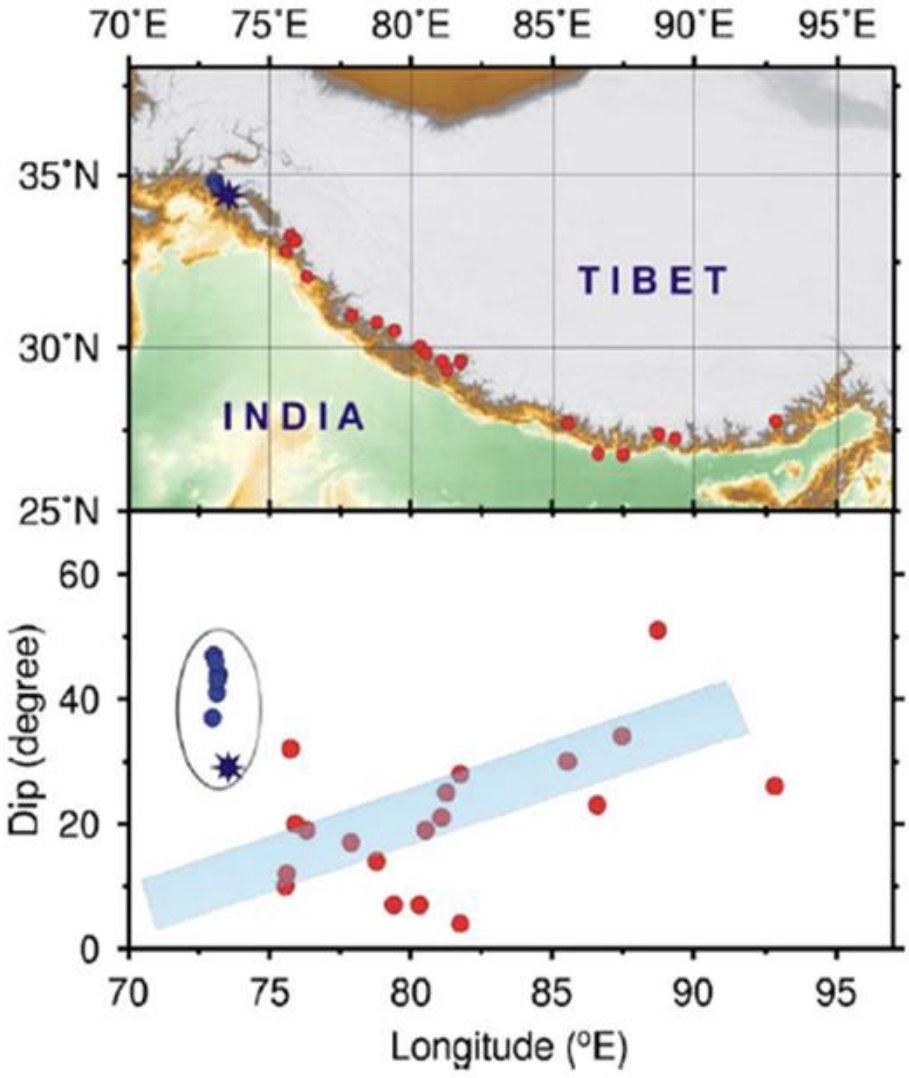

Figure2.5 Variation of the dip angles of the shallow northward dipping fault planes of Himalayan earthquakes, from west to east (Rao et al., 2006).

The following review is reported by Asano et al. (2012). They conducted a study to investigate the foreshocks and aftershocks in the Pacific coast of Tohoku

Earthquake which occurred at 5:46 (UTC) on March 11st, 2011 along the boundary between the subduction of Pacific Plate and the overriding plate, 9.0 Mw (Figure 2.6).

First, they could estimate the CMTs of 942 foreshocks. The focal mechanism of interplate earthquakes was thrust-type (Figures 2.6a and c). For examples, the Mw 7.3 seismic activity that occurred on March 9th, 2011 can be considered to be the foreshocks of the event which provide the thrust-type mechanism.

While the 1,028 aftershocks produced in a wide area close to Iwate, Miyagi, Fukushima, Ibaraki, and Chiba (Figure 2b). The focal mechanisms were various types down to locations of occurrence. For instances, (i) both of the Mw 7.4 and 7.6 on March 11 occurred at 6:08 and 6:15 respectively, were thrust-type earthquakes along the plate boundary. (ii) The Mw 7.6, occurred in the outer-rise of the Pacific plate at 6:26 on March 9, was normal fault. (iii) The Mw 7.1 was thrust type, occurred in the subducting slab at 14:32 on April 7. Lastly, (iiii) The Mw 6.7 was normal fault type that occurred in the eastern Fukushima at 8:16 on April 11 (Figures 2.6b and d).

The next related work is a report released by Myhill, 2013 who examined the focal mechanisms of deep-focus earthquakes in the Marianas slab. It represents a subducting Pacific plate, being overridden by the Philippines Plate between the Volcano Islands and Guam. The deep-focus earthquakes are limited from 16°N to 20°N. The cross-section was projected along the line A-A˜. Most of the focal plane solution was reverse faulting (red beach ball). While the other focal models distributed around plane. The blue, cyan and green models indicated oblique reverse at 400-600 km depth (Figure 2.7a and b).

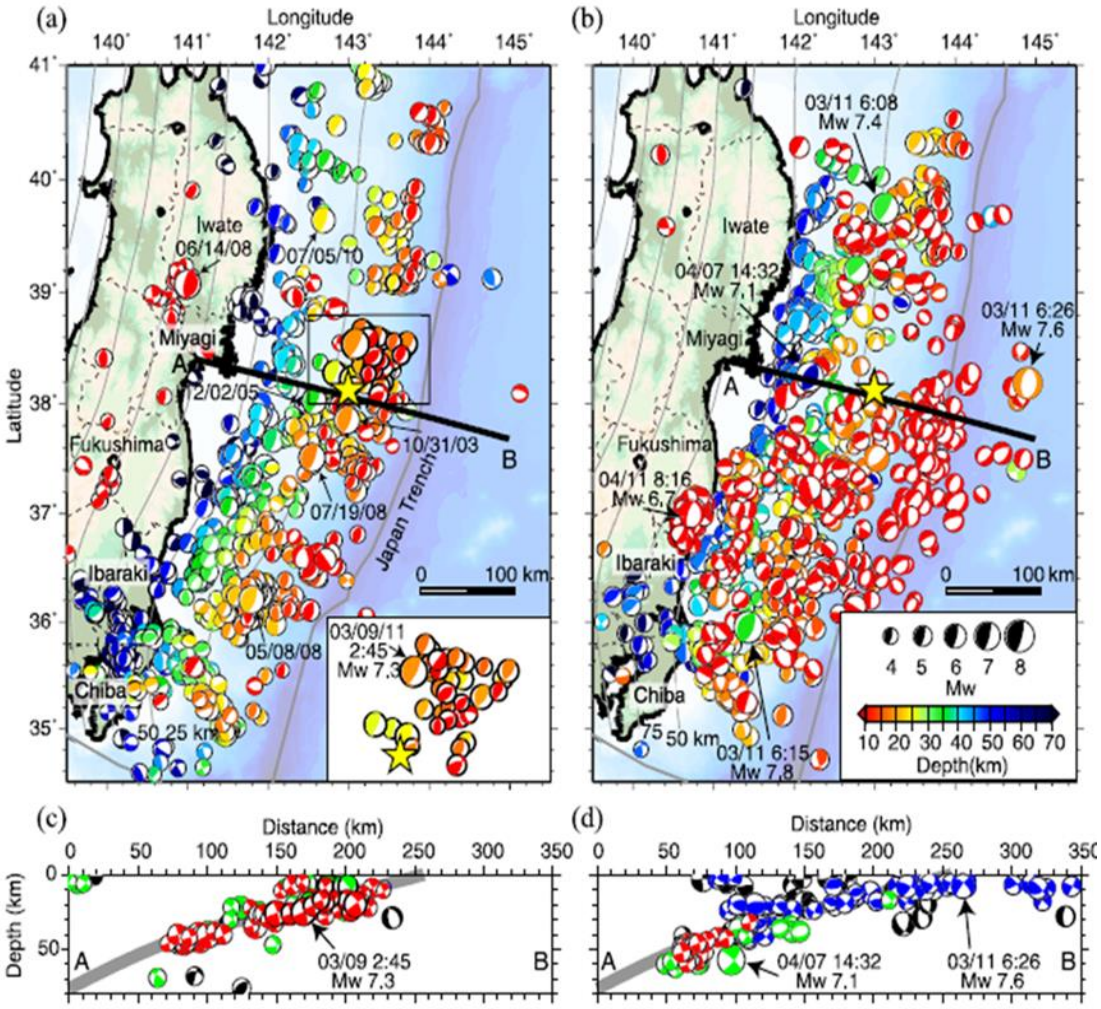

จุฬาลงกรณ์มหาวิทยาลัย
CHULALONGKORN UNIVERSITY

Figure2. 6 Map showing the focal mechanism map of foreshock and aftershock from the Mw 9.0 main shock which (a) and (b) reveal the horizontal distributions; (c) and (d) show the depth distributions along the thick black line AB (Asano et al., 2011).

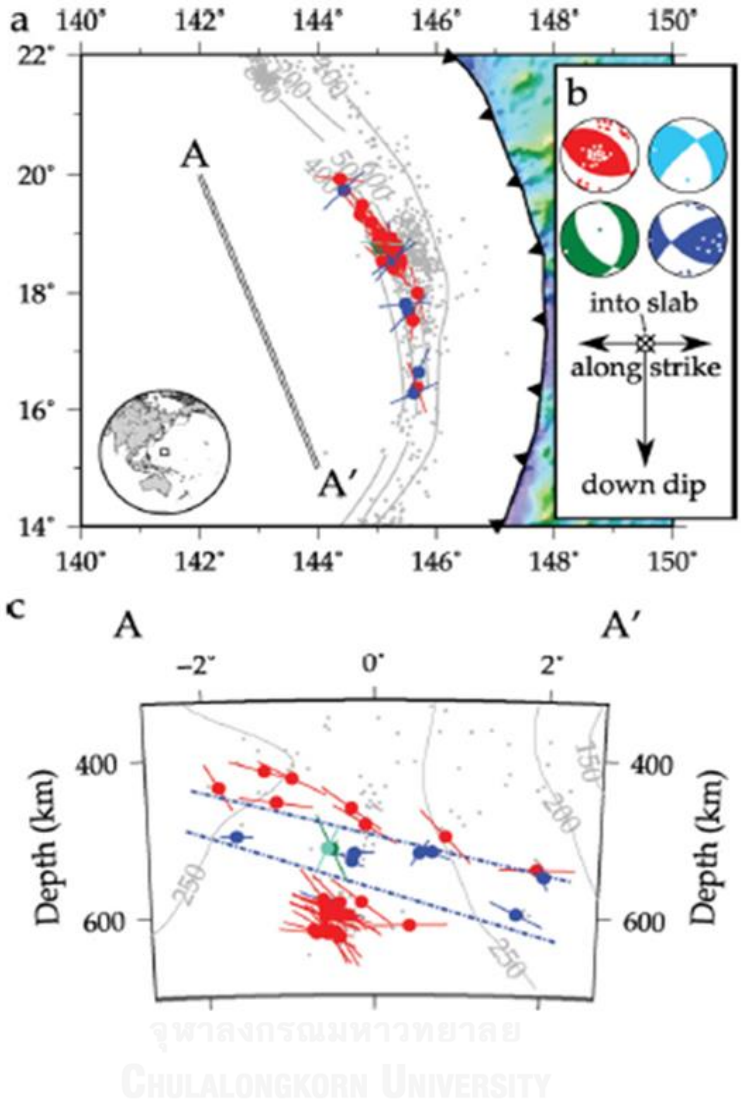

จุฬาลงกรณ์มหาวิทยาลัย
Chulalongkorn University

Figure2. 7 The diagrams show the earthquakes analysis in the Marianas slab which the cross-section was projected along the line A-A˙. (a) Map view of the slab and earthquakes. (b) The focal mechanism types (Asano et al., 2011).

2.2. Fractal Dimension

2.2.1. Theory of fractal dimension

The fractal dimension, Dc value, is a mathematical method that relies on a similar classification of information in the study area from an earthquake, the distances between the points of origin to the nature of earthquakes. The correlation dimension defined by Grassberger and Procaccia (1983) measures the spacing of a set of points,

which in this case are the earthquake epicenters. Dc values indicate the seismic pattern of area. The study used this following formula to estimate the correlation dimension:

$$C_r = \frac{2}{N(N-1)} N_{(R<r)} \qquad \text{equation (2.1)}$$

where N is the number of earthquakes

$N(R\langle r)$ is the number of earthquakes at distance R<r

r is the distance between the two events

The following relationship demonstrates the fractal dimension(Bayrak and Bayrak, 2012):

$$C_r \approx r^{D_c} \qquad \text{equation (2.2)}$$

where C_r is the correlation function

Dc is the fractal dimension which can practically obtain from the slope of the graph.

จุฬาลงกรณ์มหาวิทยาลัย
Chulalongkorn University

The distance (r) between the two earthquakes which provide θ_1, ϕ_1 and θ_2, ϕ_2 respectively is calculated by using a spherical triangle, as is given by Hirata (1989) (Hirata, 1989):

$$r = \cos^{-1}[\cos\theta_1 \cos\theta_2 + \sin\theta_1 \sin\theta_2 \cos(\phi_1 - \phi_2) \qquad \text{equation (2.3)}$$

where θ_1 and θ_2 are the latitudes of event 1 and 2.

ϕ_1 and ϕ_2 are the longitudes of event 1 and 2.

The Dc value has been observed to characterize a fault system by Aki (1981) (Aki, 1981). It can be assumed that the Dc value close to 3 signifies that earthquake fractures are filling up a volume of the crust. If a value close to 2, implies that a plane

is being filled up and a value close to 1 means that its predominant feature is line sources.

2.2.2. Literature review

In a research article by Kumar (2012), he studied the NW Himalaya region. (Kumar, 2012) The earthquake data collected from 10-19 WIHG stations (2004-2010) and USGS catalogue (1995-2003). The total amount of earthquake data recorded in the study area was 5544 data, in the 74° to 82° longitude and 28° to 32° latitude. Lastly, the 1300 earthquakes with magnitude ≥3 were selected in Figure 2.8. The area was divided at 1° x 1° spacing and separated into 47 grid nodes.

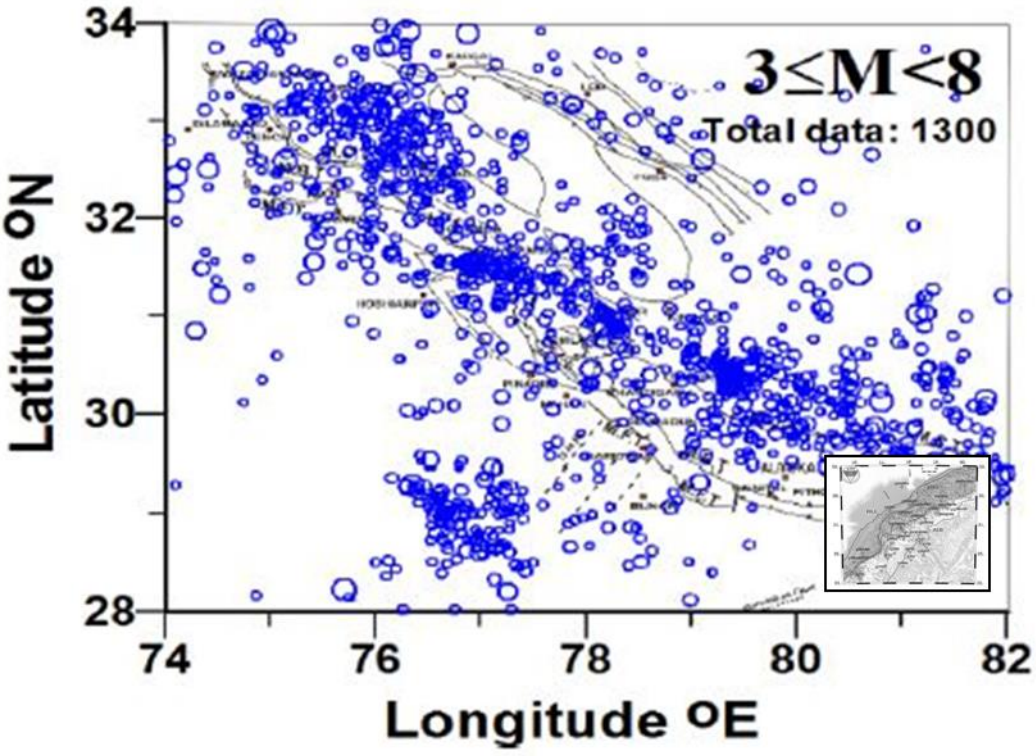

Figure2.8 Epicentral plot which are shown with the circles (Kumar, 2012).

In the NW Himalayan region, the fractal correlation dimension (Dc) varied from 0.18 to 0.75, which showed that this zone had low D_c value in Figure 2.9. Since the value of Dc was close to 1, the characteristics of a faulty system were the line source.

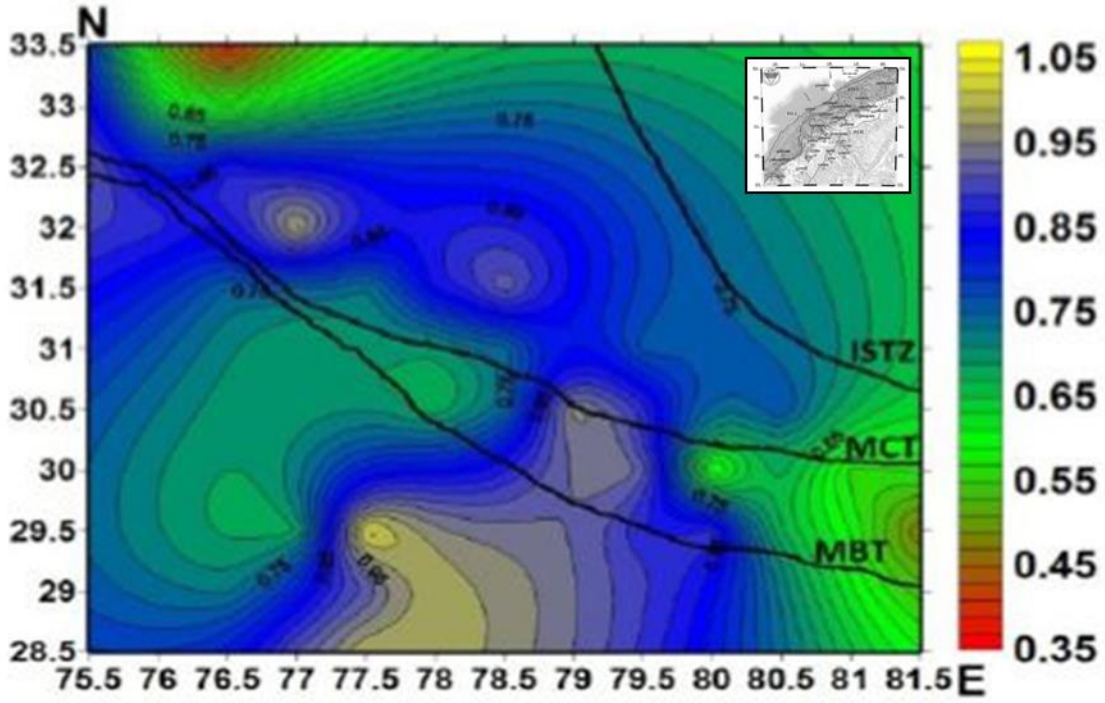

Figure2.9 Dc value contour map of total 1300 earthquakes (M≥3.0). Blue area indicates the low b value (Kumar, 2012) .

Bhattacharya et al. (2002) conducted a research to analyze the fractal dimension and b-value map in the NE India (24° to 28° N latitude, 89° to 98° E longitudes) by using permanent micro-earthquake network data and teleseismic data. The teleseismic data came from the International Seismological Catalogue (ISC) and the teleseismic micro-earthquake network data derived from the National Geophysical Research Institute (NGRI) and Regional Research Laboratory, Jorhat (RRL(J)).

The Dc value contours suggested the higher trend in the NW-SE direction along the Kopili lineament (Dc varies from 1.65 to 1.85) and along the Indo-Burma ranges (Dc varies from 1.70 to 1.80) indicated clustering of epicenters in Figure 2.10. (a-c).

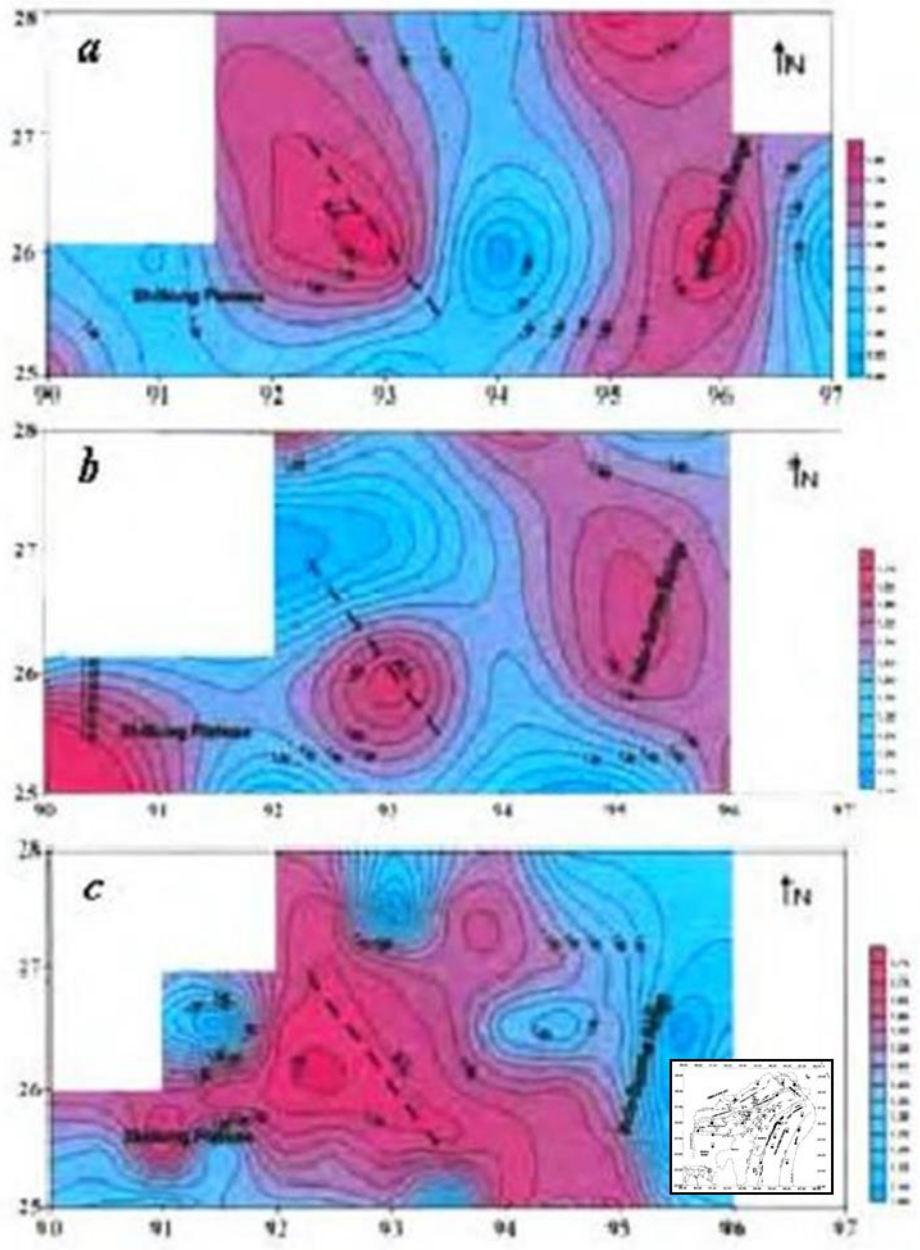

Figure2.10 The map shows the contours of fractal dimension (Dc) for the earthquake in the NE India: (a) ISC data with 2° grid, (b) NGRI/RRI(J) data with 2° grid and (c) RRL(J) data with 1° grid (Bhattacharya et al., 2002).

Roy and Mondal (2012) used the USGS PDE data (Mb >3.5) for the period 1973-2008 study in the Himalayan region. The Wadia Institute of Himalayan Geology which provided local network data for the period of 2004 to 2006 was also included in the analysis. The analysis area was extending of latitude 28°N to 33°N and longitude 76°E

to 82°E. The total of 16 windows, of fifty events was formed with the total of 783 events in the region. The result revealed the low Dc value, varied from 0.28 to 0.96.

2.3. B value

2.3.1. Theory of b value

Many researchers have found the relation between the fractal dimension (Dc) and b value. The b value is inversely related to tectonic stress that means, the low b value can suggest that the stress is high which can be the risk area of earthquake in the future (Mogi, 1967; Scholz, 1968). In order to analyse the b value, we can determine from the frequency-magnitude distribution (FMD) equation (Gutenberg and Richter, 1944):

$$LogN = a - bM \qquad \text{equation (2.4)}$$

where N is the cumulative number

a is the total number of earthquake, referred to a values, practically obtain from y-intercept

b describe the relative size distribution, referred to b value, practically obtain from slope

M is the magnitude

จุฬาลงกรณ์มหาวิทยาลัย
Chulalongkorn University

While the relation between Dc and b-values which is concordant with Hirata, 1989's relationship shows a negative or positive correlation Thus, we applied this relationship between Dc and b value to predict the upcoming high-risk potential earthquake zones.

2.3.2. Literature review

The literature reviews of b value that we studied were related with fractal dimension. In case study of Kumar (2012), which we mentioned his work of fractal dimension before, the study area was the NW Himalayan region. The result indicated

the b value varied from 0.18 to 0.36, showed the low b-value anomalous zone in Figure 2.11. The relationship between b-value and Dc value are positive correlation.

The following research is in the NE India. According to Bhattacharya et al. (2002) we reviewed before, the b-value maps in Figure 2.12. (a-c) showed higher b-value contour in the Indo-Burma ranges, i.e., in the Kopili Fault and the Shillong Plateau. However, the Assam valley was lower b-value contour. The relationship between b-value and Dc value are positive correlation.

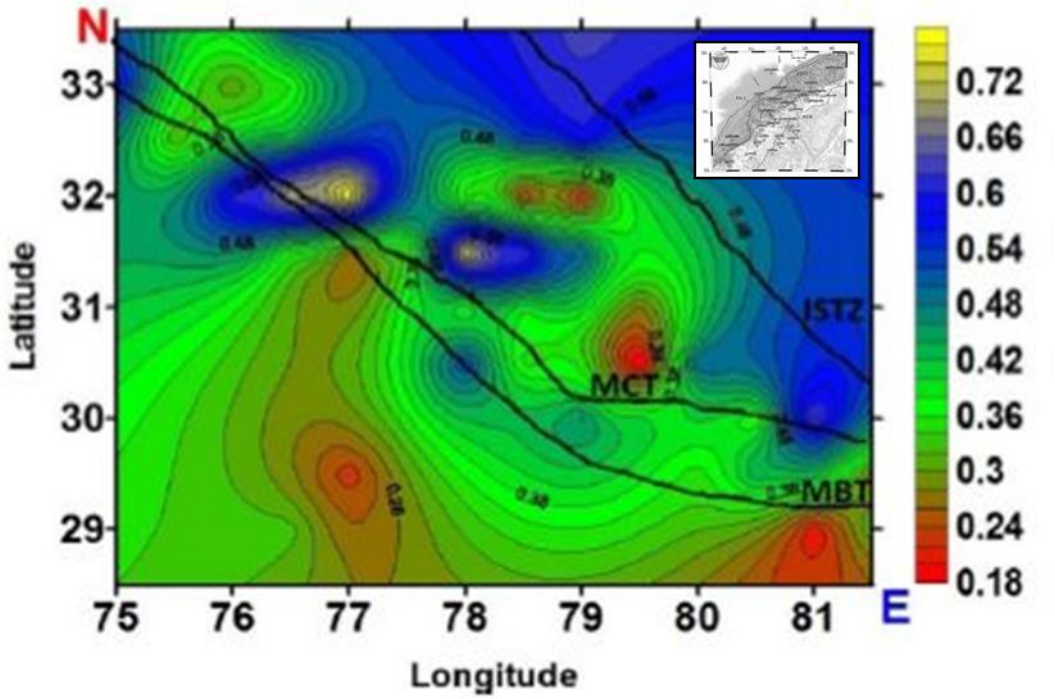

Figure2.11 The b-value contour map of total 1300 earthquakes, M≥3.0 (Kumar, 2012).

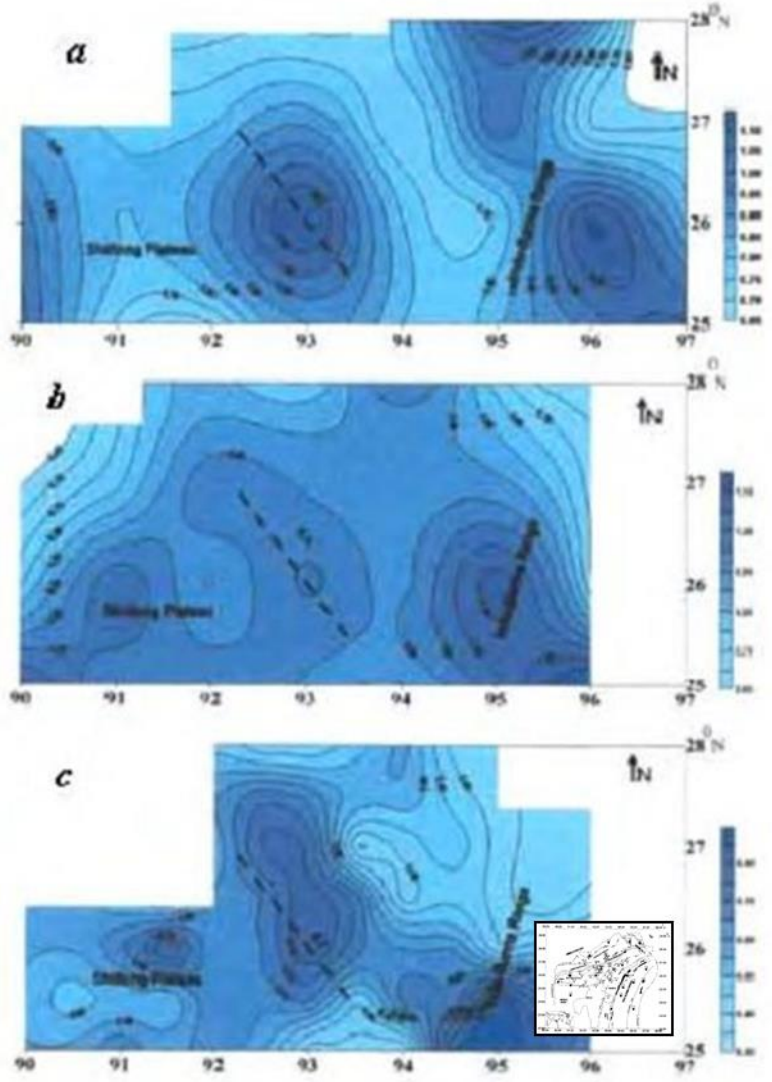

Figure2.12 The map shows the contours of b-value for the earthquake in the NE India: (a) ISC data with 2° grid, (b) NGRI/RRI(J) data with 2° grid and (c) RRL(J) data with 1° grid (Bhattacharya et al., 2002).

Roy and Mondal (2012) who investigated the fractal dimension in the Himalayan region. The study showed the frequency-magnitude relation is 0.87 (Figure 2.13) which provided positive correlation between b-value and Dc value (Figure 2.14).

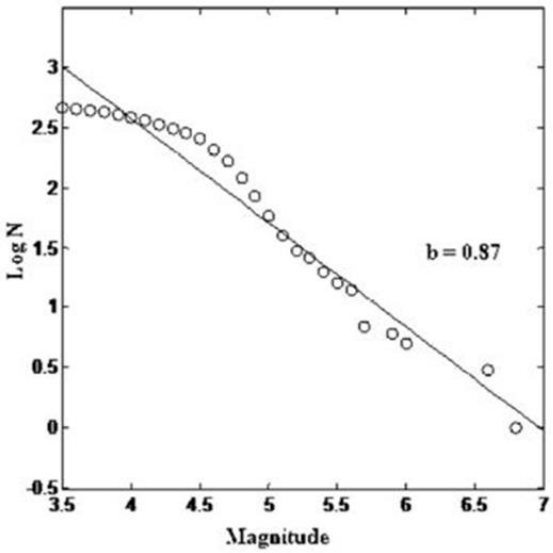

Figure2.13 The frequency-magnitude distribution of events occurred in the study region (Roy and Mondal, 2012).

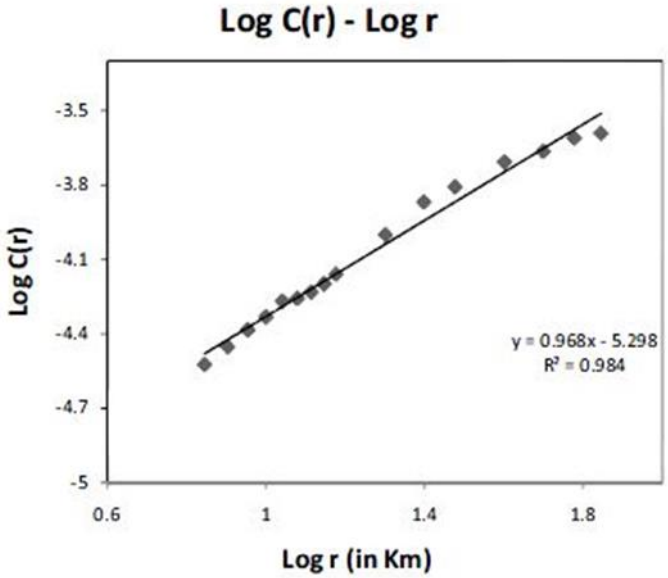

Figure2. 14 Log C(r) versus Log r is shown for ninth time windows for the Himalayan region with latitude (28°N–33°N) and longitude (76°E–82°E), the slope gives Dc (Roy and Mondal, 2012) .

2.3. Methodology

In this study, the methodology for investigating both focal mechanism and fractal dimension are described consecutively as shown in Figure 2.15.

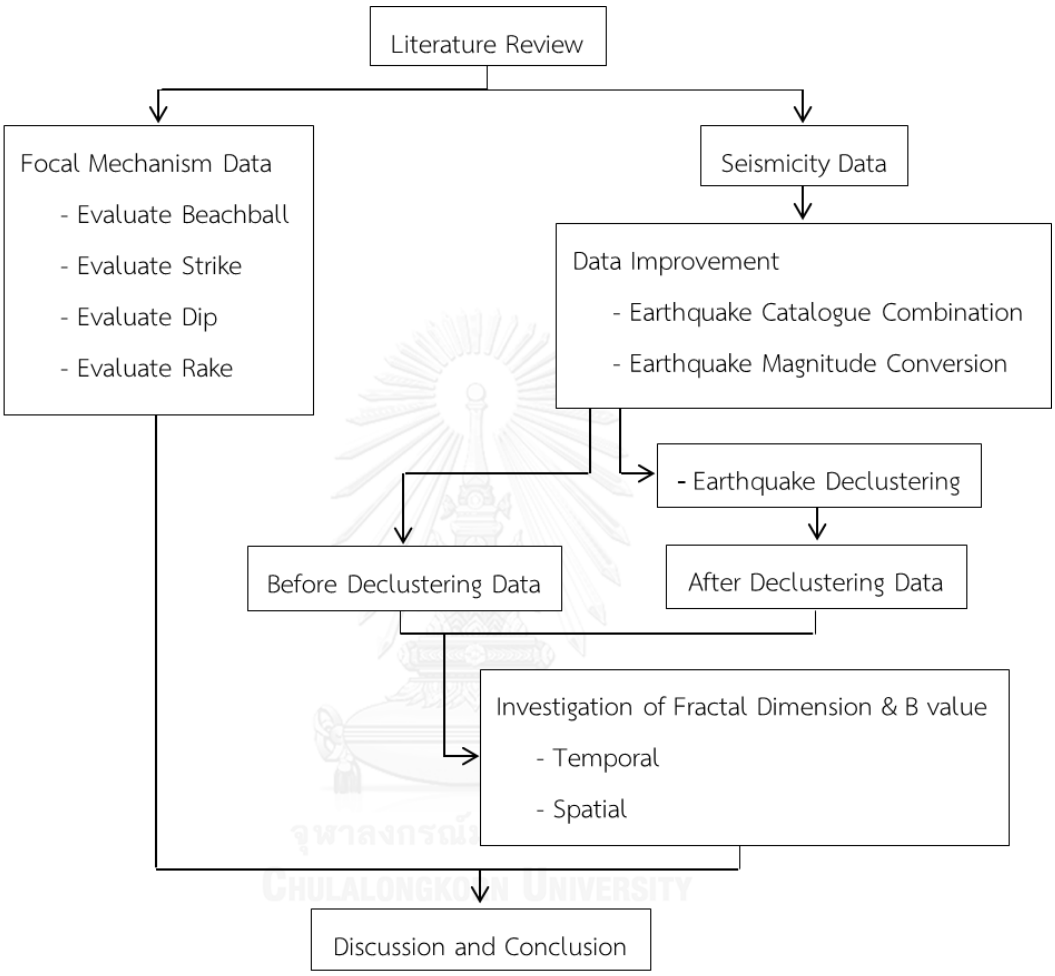

Figure2.15 Simplified flow chart showing the methodology applied in this study.

2.3.1. Literature review

In the first part of the study, we considered the previous works, the related theories in particular. The main objective of this procedure is to summarize the methodology, including complied the variables, i.e., the radius and time for focal mechanism investigation and the number of earthquakes for fractal dimension investigation, used in various areas. The output obtained from this section was the

useful guideline for finding out the most suitable factors for the study area, that is, SASZ.

2.3.2. Earthquake compile data

The second step was the seismic data accumulation that occurred in the study area. The recorded dataset came from various sources worldwide. The examples of catalogues we used were Incorporated Research Institutions for Seismology (IRIS) and Thai Meteorological Department (TMD). As the catalogues date back to the beginning of seismic activity record, they contain abundant events that we can analyze and get statistically significant result.

2.3.3. Catalogue improvements

The original earthquake catalogues have been recorded non-systematically in practice. It means that the unrevised data may not significantly represent the result. Therefore, they must be refined before analysis in the next methods to get the best possible accuracy and precision. The improvement consists of 3 stages which are earthquake magnitude conversion (Kagan and Knopoff, 1980b) , earthquake declustering (Gardner and Knopoff, 1974) , man-made seismicity (Habermann, 1987) .

2.3.4. Estimation of characteristic parameters in focal mechanism and fractal dimension

Based on literature reviews, we must consider the most appropriate parameters in focal mechanism and fractal dimension, such as the number of earthquakes, the radius, the time and others, to obtain the best possible values from the analysis that has been done successfully for the SASZ.

2.3.5. Focal mechanism investigation

The following method, we examined the focal mechanism by using the characteristic parameters obtained from the previous step and analyzed them by using the most recent data. The result demonstrated the focal mechanism which showed the characteristic of tectonic setting map, implying the prospective areas for the upcoming earthquakes.

2.3.6. Fractal dimension investigation

Next, we conducted a study to investigate fractal dimension by analysis the previous step and using the characteristic parameters. The result gave the fractal dimension map showing anomalies which led to the prospective areas for the upcoming earthquakes.

2.3.7. Interpretation of focal mechanism and fractal dimension

Ultimately, according to both of focal mechanism and fractal dimension, the map allowed the characteristic of tectonic of SASZ and the distribution of the seismic anomalies which implied the prospective areas might be posed by the upcoming earthquakes.

2.4. Scope of Study

The study area is located on the SASZ, covers 2°S to 24°N latitudes and 88°E to 100°E longitudes. Geographically, if the segment ruptures of SASZ happen, especially in vertical movement, the earthquake generates the potential hazards of both grounds shaking and local tsunami for Myanmar and India, including neighbouring countries like Thailand. This study used both of focal mechanism and fractal dimension, related with b value method to analyse the mechanism of fault rupture, seismic pattern and anomalous areas in SASZ. The data came from the instrumental earthquake record. Eventually, the obtained results should be useful for preparing long-term mitigation plans for both seismic and tsunami hazards.

CHAPTER III
SEISMICITY DATA AND COMPLETENESS

The earthquake catalogues can be separated into three types by timeline and completeness of the data. The first two classifications are the geological record and the historical record, which are both recording data for a very long time (10,000-100,000 years) Nevertheless, the seismic data is less reliable because data recording is descriptive stylistic. Another one is the instrumental earthquake record which could last for a much shorter time period than those claimed before and comprises data on numerical analysis of processes, mathematics and science. The recorded details for the earthquake catalogues consist of location (longitude, latitude and depth), time (year, month, day) and magnitude. Nowadays, the instrumental record is the most accepted worldwide, known as the earthquake catalogues. There are several global institutes recording this seismic information viz., the National Earthquake Information (NEIC), the International Seismological Center (ISC), the Global CMT Catalogue (GCMT) and the Thai Methodological Department (TMD). However, the raw data that come from these different sources are invalid to analyze yet due to various problems, such as undesired data like foreshock and aftershock (Gardner and Knopoff, 1974), man-made seismic activity (Habermann, 1987), etc. These obstacles can greatly influence accuracy and precision of result. Therefore, we have to improve earthquake catalogue before analysis.

In this chapter III, the earthquake catalogue is clarified in order to improve the completeness of data to bring to investigate for both focal mechanism and fractal dimension in the next chapter. The methodology for seismicity data analysis followed as Figure 2.15 in Chapter II.

3.1. Focal Mechanism data

The first stage in the study is data acquisition of the earthquake catalogue by downloading the focal mechanism data from the public instrument recording station, covered the study area. The recorded data contain of location (longitude, latitude),

mechanism of fault rupture (strike, dip, rake) (Table 3.1) Since the SASZ has distance around 1,300 km-long. This research can be divided the study area into 11 segment determined by segment space about 1° or 110 km-long along the zone for high resolution and accuracy of mechanism of fault rupture analysis. The data of interplate are 999 data. The data of intraslab are 253 data. The both of data use to analysis in 1976-2016 year. As reported by Table 3.1., we can analyze these data to focal mechanism diagram (beach ball) by Faultkin program and can detect strike, dip angle and rake angle by Grapher 10 program.

Table3.1 Examples of focal mechanism data.

long	lat	str1	dip1	rake1	str2	dip2	rake2
98.65	24.39	323	80	-172	232	82	-10
98.58	24.29	242	88	0	152	90	178
98.60	24.26	342	72	-169	249	80	-18
96.24	3.18	338	28	99	147	62	85
98.57	24.74	338	88	-178	248	88	-2
99.50	1.08	92	46	132	220	58	56
100.04	0.50	312	80	179	42	89	10
92.77	21.60	216	72	3	125	87	162
98.43	0.70	332	11	112	130	80	86
95.58	4.26	78	19	-140	310	78	-76

3.2. Seismicity data

There are several instrumental earthquake recording stations that have different strengths and weaknesses. For examples, the three global networks operated by NEIC, ISC and GCMT can detect the most accurate and precise data but mostly give precedence to the size larger than 3 Mw. While local station like TMD can record more correct data that smaller than 3 Mw. Thus, we needed to combine an earthquake catalogue from various stations to get the best possible data, which in terms of quality and quantity (Figure 3.2). The present-day earthquake record, covered the study area,

have been developed. The result in this method gave the better data validation that provided longer duration of the measurement and wider distribution of earthquakes, including location (longitude, latitude and depth), time (year, month, day, hour, minute) and various kinds of magnitude like the body wave magnitude (Mb), the surface wave magnitude (Ms), the moment magnitude (Mw) and some local magnitudes (Ml) (Table 3.2).

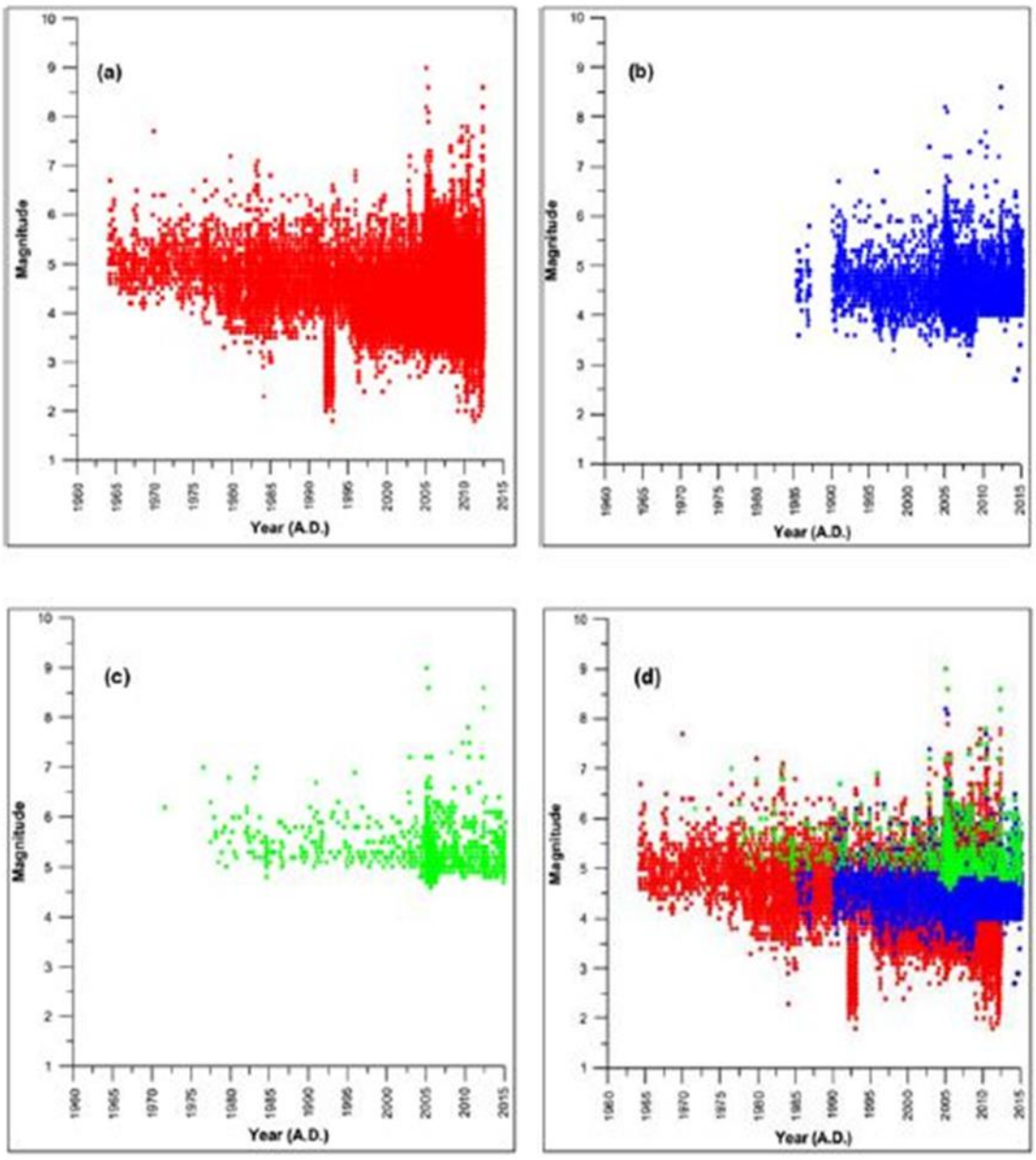

Figure3.1 The relationships between the magnitude and date of earthquakes recorded in individual earthquake catalogues, (a) ISC (b) NEIC (c) GCMT, and (d) Composite (Sukrungsri and Pailoplee, 2014).

Table3.2 Examples of earthquake catalogue.

Long	Lat	Year	Month	Day	Depth	Hour	Min	Sec	Mw	Mb	Ms	Ml
95.34	2.48	2011	1	22	35	7	34	17	5.2	-	-	-
95.52	2.88	2011	1	22	28.	7	34	17	5.2	5.4	-	-
95.55	2.79	2011	1	22	10	7	34	16	5.9	5.3	-	5.4
95.34	2.48	2011	1	22	35	7	34	15	5.2	-	-	-
96.17	2.38	2011	1	18	15	11	33	46	5.9	-	-	-
96.40	2.63	2011	1	18	21	11	33	45	5.9	5.7	5.9	-
96.40	2.63	2011	1	18	21	11	33	45	5.9	5.7	5.9	-
96.41	2.50	2011	1	18	10	11	33	44	5.7	5.6	-	5.8
96.17	2.38	2011	1	18	15	11	33	44	6	-	-	-
102.64	-5.03	2011	1	17	36	19	20	57	6	6.1	5.9	-

The instrumental seismic networks, all existing earthquake catalogues (i.e., ISC, NEIC, and GCMT) were merged in this study. As a result, the composite earthquake catalogue contained 65,535 total numbers of data in 1960-2016, ranged between Mw 2.0-9.0.

3.3. Earthquake Magnitude Conversion

The first main problem is the instrumental earthquake recording station measures the size of earthquakes in different forms of magnitudes, which are in control by a seismic wave, mostly are local magnitude (Ml), body-wave magnitude (Mb) and surface-wave magnitude (Ms). The M_b is obtained from the first arrival P-wave from a seismogram while the Ms and Ml are quantifications from the surface wave and S-wave, respectively. Both of body-wave and surface wave magnitude could be affected by the amplitudes of seismic wave which they have their own limit of detection or called "saturation of earthquake magnitude" (Figure 3.2). As stated by Kagan and

Knopoff, 1980b, there is an upper limit on size determined by the measurement scales (Figure 3.3).

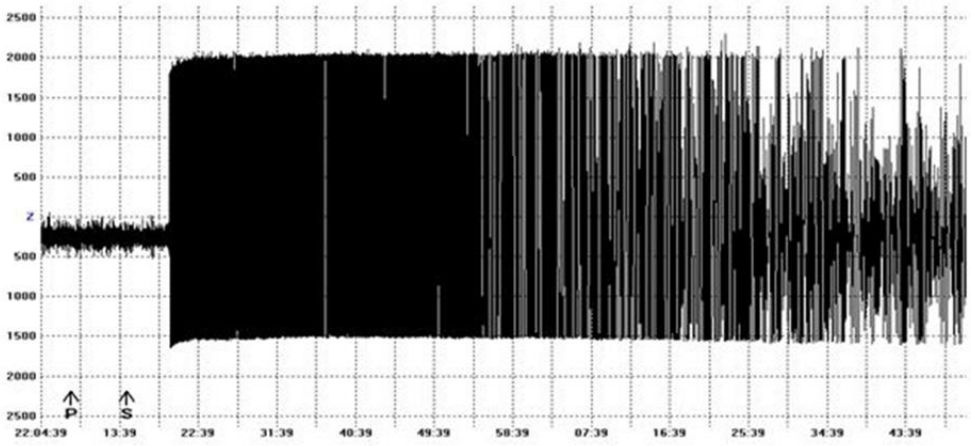

Figure3. 2 The examples of seismic waves are detected by the instrumental record which present the waves are over their limit. Especially, the surface wave is higher in amplitude than the body-wave (Kagan and Knopoff, 1980b).

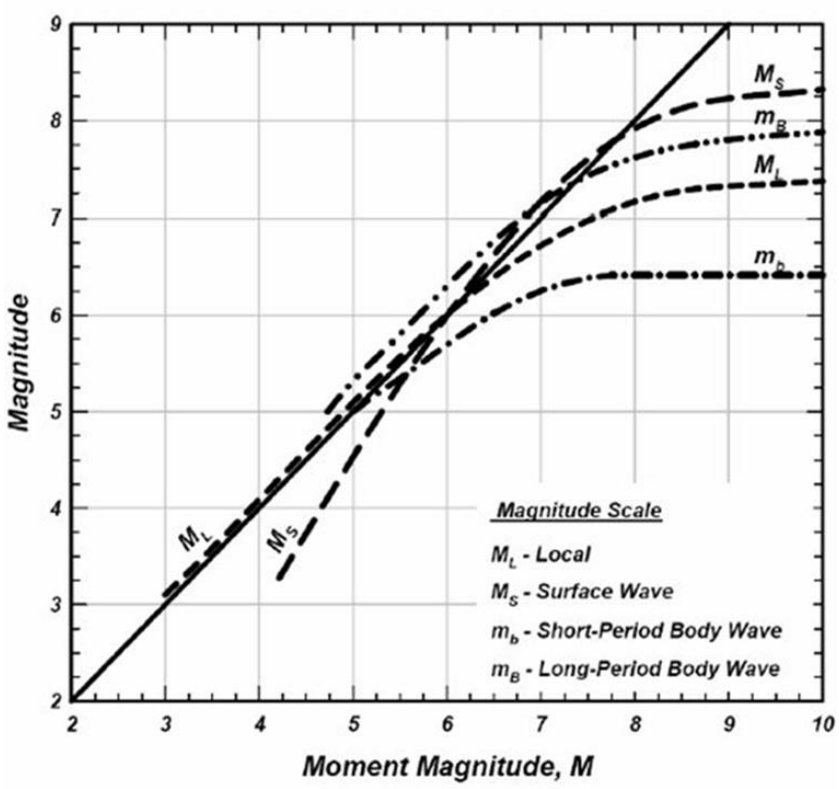

Figure3.3 The graph shows the saturation of the various magnitude scales by Kagan and Knopoff (1980b) (Campbell, 1985).

In order to analyze this accuracy, it needed to convert these earthquake data to have the same form. The process began with the development of relationships between these different magnitude scales and converted them to the standard M_w which is the most reliable because it does not depend on a recording instrument. The most appropriate relations were considered by the coefficient of determination (R^2) in the regressive equations between each pair of different scales (Figure 3.4).

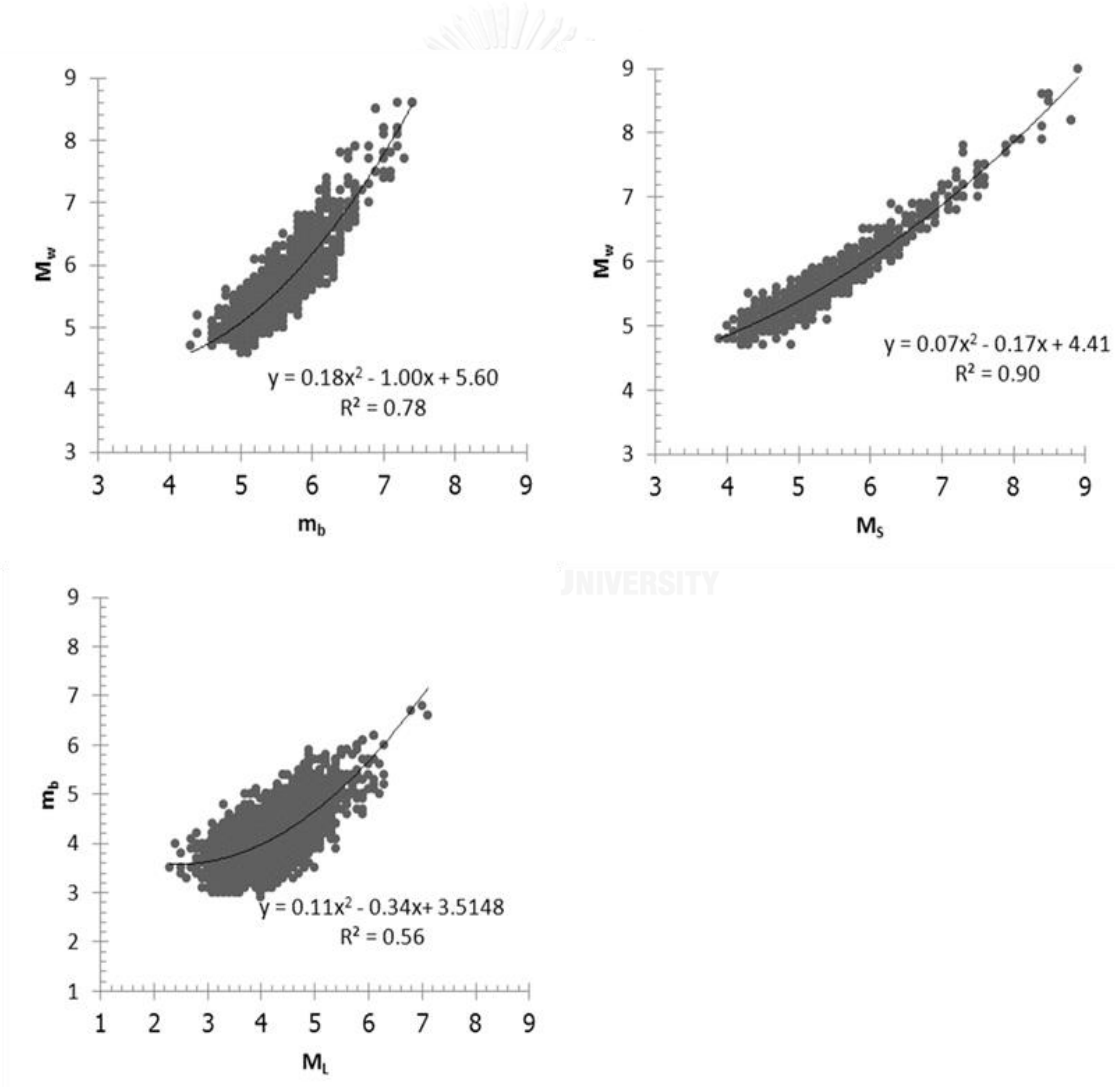

Figure3.4 The empirical relationships between (a) body wave magnitude (Mb) and moment magnitude (Mw), (b) surface wave magnitude (Ms) and moment

magnitude (Mw), and (c) local magnitude (Ml) and body wave magnitude (Mb).

3.4. Earthquake Declustering

In general, the seismic measurements provide three types of earthquakes; foreshock, main shock, and aftershock, relatively. The main shocks refer directly to the released tectonic stress. Meanwhile, the foreshocks are generated before main shocks. The aftershocks are co-seismic stress change of the individual mainshocks (Felzer et al., 2004). The main purpose of this stage was to remove foreshocks and aftershocks, to get the best possible estimate for the rate of mainshocks that directly indicate the released energy from tectonic stress.

As claimed by the past studies, the SASZ generated the great severe earthquake, on December 26th, 2004 (Mw = 9.2) that led to tsunami and large series of aftershocks. Therefore, the data obtained from the previous procedures needed to be decluttered by filtering only main shocks from an enormous number of foreshocks and aftershocks, in order to acquire complete independent earthquake data (Figure 3.5).

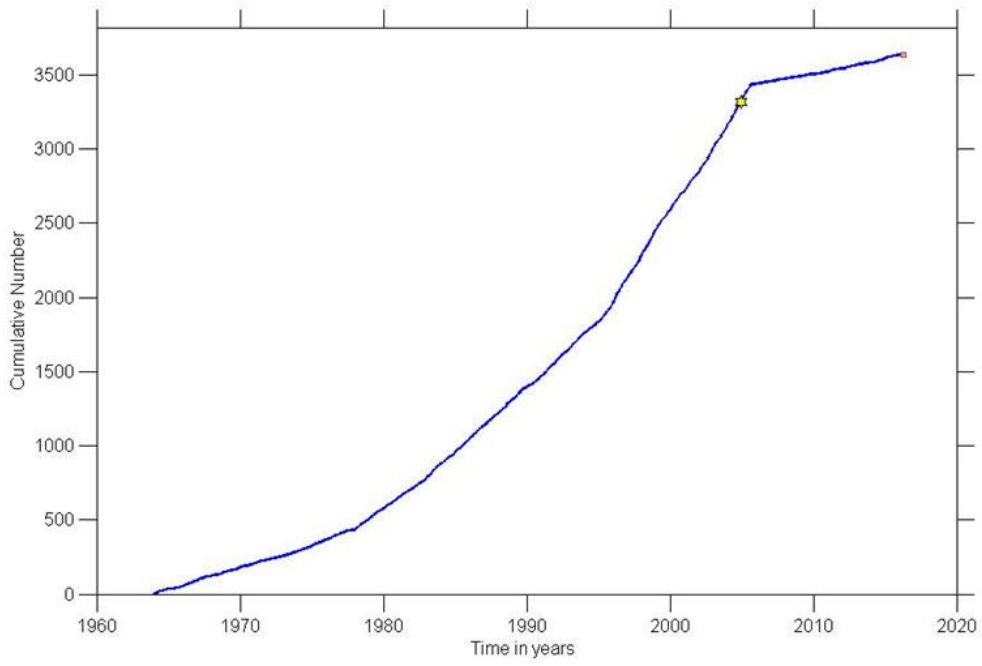

Figure3. 5 The cumulative number of events as a function of time followed the earthquake declustering. The blue line indicates the completeness of the catalogue.

In this step, the study accepted the model by Gardner and Knopoff (1974) to eliminate foreshocks and aftershocks. The main idea is related to magnitude, distance and time of earthquake events. It can be described that if it occurs a great earthquake, a distance and time are wider and longer, respectively. Moreover, the seismic data from several databases showed the repeated record or called "Identical earthquake" which these undesired data can be erased by Gardner and Knopoff, 1974 (Figure 3.6).

In summary, the unrevised catalogue displayed 111,323 total events. After finishing the magnitude conversion, the data remained 65,535 events. Then, the decluttering process removed foreshocks and aftershocks which gave the result 3,632 main shocks. After the earthquake catalogues were revised through all the mentioned above, the seismotectonic activities were defined and then used in all further analysis (Figure 3.7).

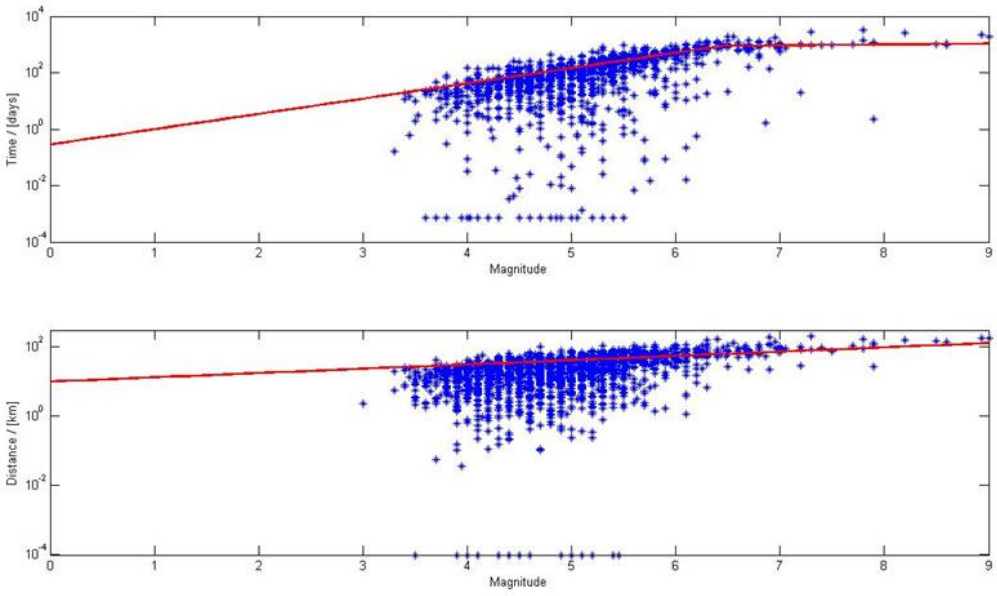

Figure3. 6 The parameters were used to declutter and remove foreshocks and aftershocks according to the model of Gardner and Knopoff, 1974. (a) time

window and (b) space window. The earthquake data (blue stars) above the red lines of both time and space windows are identified as main-shock events.

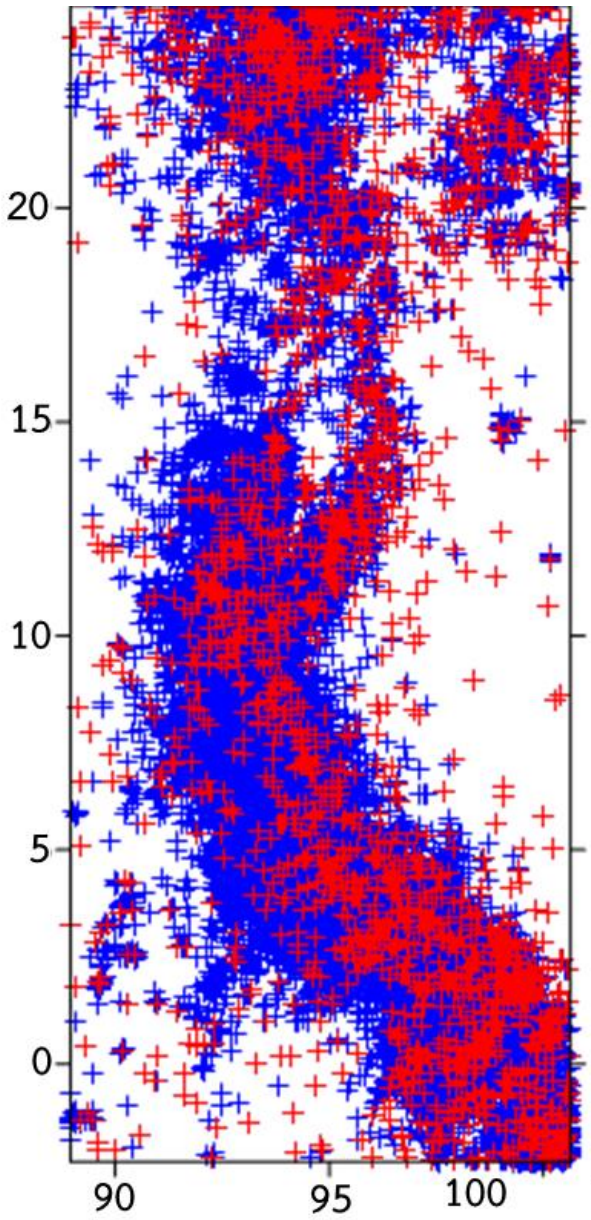

Figure3.7 Map of SASZ presents the distribution data (a) before declustering and (b) after declustering with the algorithm according to Gardner and Knopoff (1974). The blue plus indicates before declustering earthquake. The red plus indicates after declustering earthquake.

3.5. Cross Section of Earthquake Distribution

Seismotectonically active zones were caused by a subduction zone of the SASZ, was occupied by the two different seismotectonic settings, i.e., i) shallow crust and ii) deep intraslab earthquakes. There are three lines of cross-section were established perpendicular the strike of SASZ, as shown in Figure 3.9. These diagrams have been characterized that (a) the northern area along the Andaman subduction zone produces the crustal earthquakes which ranges from the earth's surface to 0–45 km depth and northward-dipping slab with 40°–45°. Next, the line (b) is located along the Nicobar-Andaman. The zone can generate earthquake in the depth of 300 km and the dip angle of slab is about 45° down to depths of 180 km. And the line (c), the northern area along the Sumatra, Indonesia can generate in the beginning at 450 km depth down to 650 km with the 30° of slab dip angle (Figure 3.8).

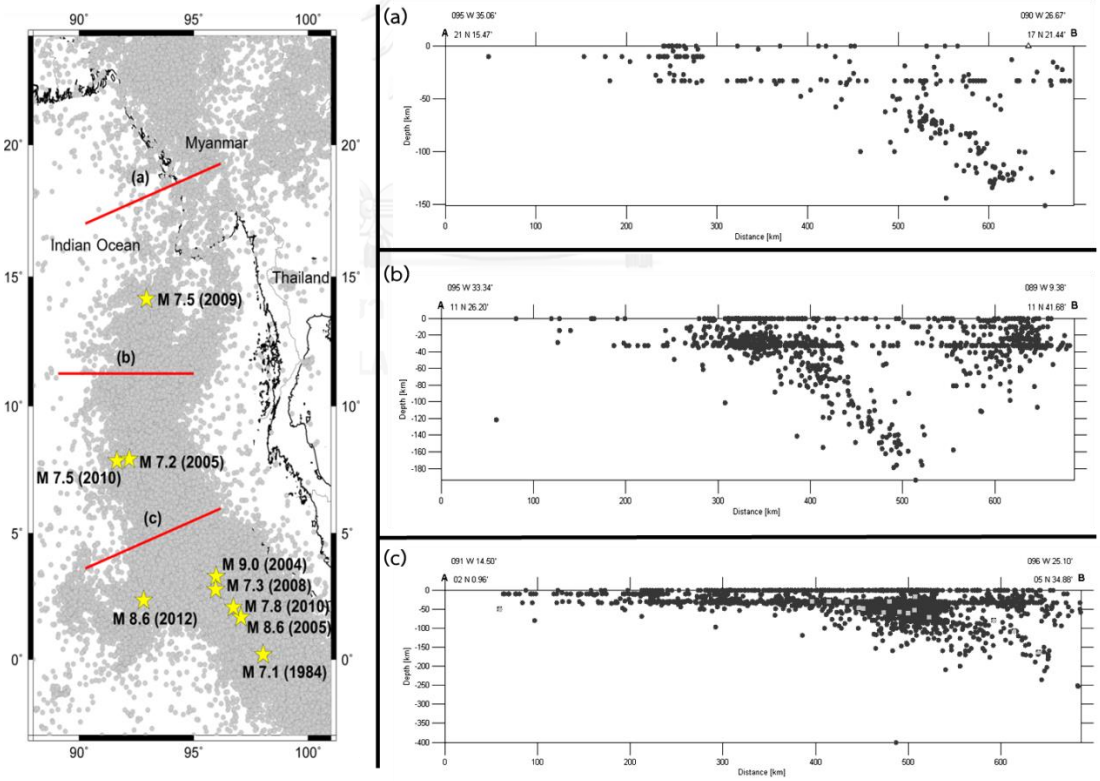

Figure3.8 Map of the SASZ showing cross section lines of earthquake distribution (Sukrungsri and Pailoplee, 2014).

CHAPTER IV
FOCAL MECHANISM

4.1. Focal Mechanism & Significant

The SASZ is often defined as high-risk potential hazard zones that can generate devastating earthquake and tsunami. Most of tsunamis are occurred by great shallow earthquakes with an epicenter near or on the seafloor. However, it should be noted that not all earthquakes can cause tsunamis. The principle generation mechanism depends on two important factors which are magnitude and tectonic activity. As stated by previous researches, it can be assumed that tsunamis are generated, the magnitude must exceed the threshold which is usually more than 7 Mw. Also, the tectonic activity must be normal or reverse fault. The sudden vertical displacements of a large volume of water produce tsunami waves. In this study, the mechanism of fault rupture was studied by focal mechanism. In spite of the fact that it was not real-time determination, the study resulted in the mechanism based on historical seismic events that potentially aiding prediction of the upcoming earthquakes and tsunami along the SASZ.

4.2. Total of Focal Mechanism along the Sumatra-Andaman subduction zone

The mechanism of fault rupture can be classified into four patterns which are normal, strike slip, reverse and oblique reverse faulting. The diagram of focal mechanism (beach ball) along SASZ, in Figure 4.1 is oblique reverse motion. However, the SASZ is 1,300 km long which can produce both of interplate and intraslab earthquakes. Therefore, we divided the study area into 11 segments that caused by different types of mechanism. The interplate and intraslab were determined by 0-50 km and 50-1,000 km, respectively. Division of interplate and intraslab studies by cossection in Figure 3.8, in chapter II.

First, we investigated the interplate zone. The focal mechanism solution suggests oblique reverse motion (Figure 4.2). While the sub segments result in various beach balls (Figure 4.4). There are five reverse faulting (no. 1-5), three strike slip motion (no. 6, 9 and 10), two oblique reverse (no. 7 and 8) and one normal motion (no. 11).

Next, the beach ball diagram of intraslab indicates oblique reverse motion (Figure 4.3). The results of each segment display different focal mechanisms with their actual distribution in Figure 4.5. There are four reverse faulting (no. 1, 3-5), four oblique reverse (no. 2, 6-8), two strike slip (no. 9 and 10) and one normal motion (no. 11). Furthermore, in each segment, we conducted a study to thoroughly analyze strike, dip and rake of fault rupture mechanism.

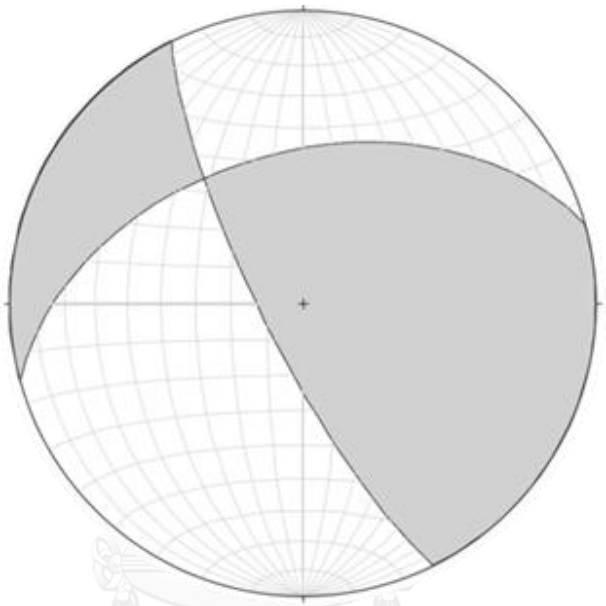

Figure4.1 Showing the total of focal mechanism (beach ball) along the SASZ is oblique reverse motion.

จุฬาลงกรณ์มหาวิทยาลัย
CHULALONGKORN UNIVERSITY

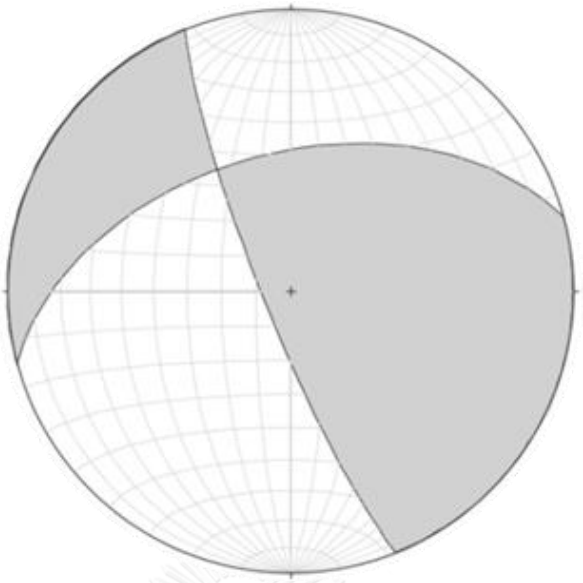

Figure4. 2 Showing the focal mechanism solution of interplate earthquake events is oblique reverse motion.

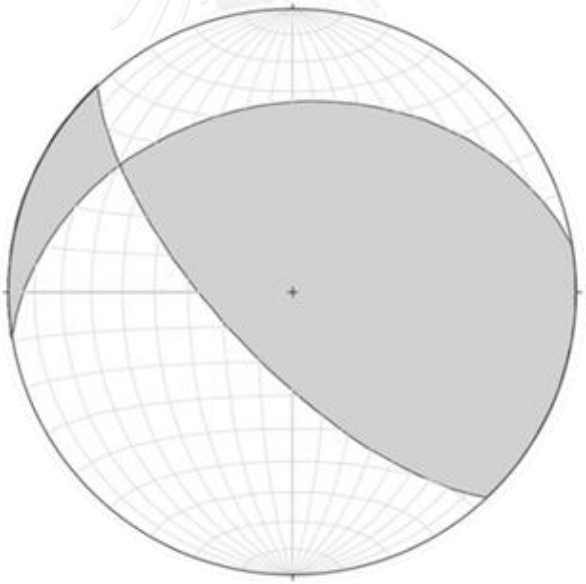

Figure4. 3 Showing the focal mechanism solution of intraslab earthquake event is oblique reverse motion.

4.3. Strike

The fault geometry data were distributed on a sphere around the focus. We can plot overall data and generate them into rose diagram of strike to summarize the

main direction of corresponding structure bearing. According to the earthquake catalogues, the types of strike can be divided into strike 1 and strike 2. In Figure 4.6, the rose petals indicated that the frequency of strike 1 showed two main direction which are S240E direction at 140° and N45W – N30W direction at 315°-330°. While the strike 2 indicated S45E direction at 135°. The overall strike of interplate provided the same result as the overall strike along the SASZ (Figure 4.7).

From the mention earlier, this research focused on study the fault mechanism in the details. Thus, we examined the strike, dip and rake of overall segments that should be taken into account to get the best possible reliable results.

4.3.1. Strike of interplate

First, the segment distribution of interplate presents the rose diagrams of strike 1 and strike 2 in Figure 4.8 and 4.9, respectively. The Table 4.1 shows the summary result of strike direction. The rose petals imply the main direction of each segment is in various distributions. It's all down to tectonic activity of the area.

The results give conclusion that the nearby segment strongly suggests the identical orientation. For example, the direction of segment no. 2-5 provided a range of N40W – N70W at 290°-330°. While some segments don't represent the obvious main direction in both of strike 1 and 2, such as, the segment no. 1 and 10.

จุฬาลงกรณ์มหาวิทยาลัย
Chulalongkorn University

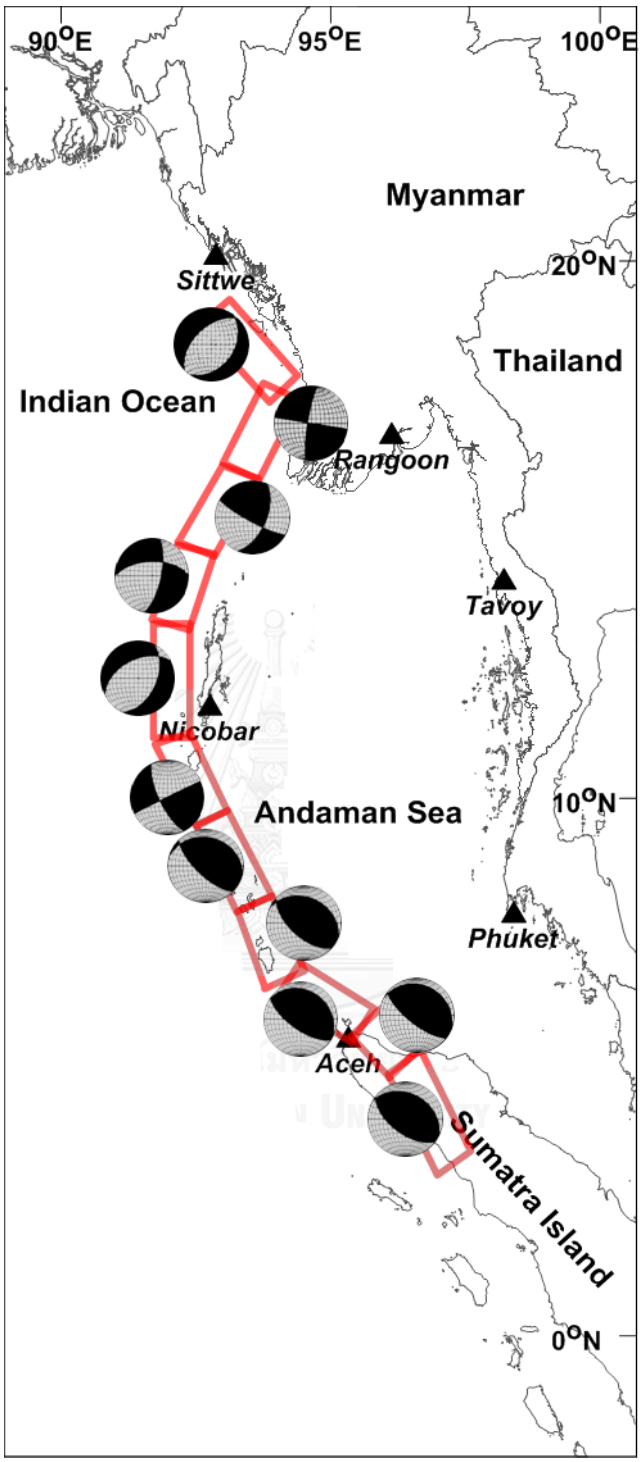

Figure4. 4 The segments of interplate (0- 50 kilometer) revealed different focal mechanism that occurred in each area. The focal mechanism of interplate is mix motions which are reverse, oblique reverse, normal and strike slip.

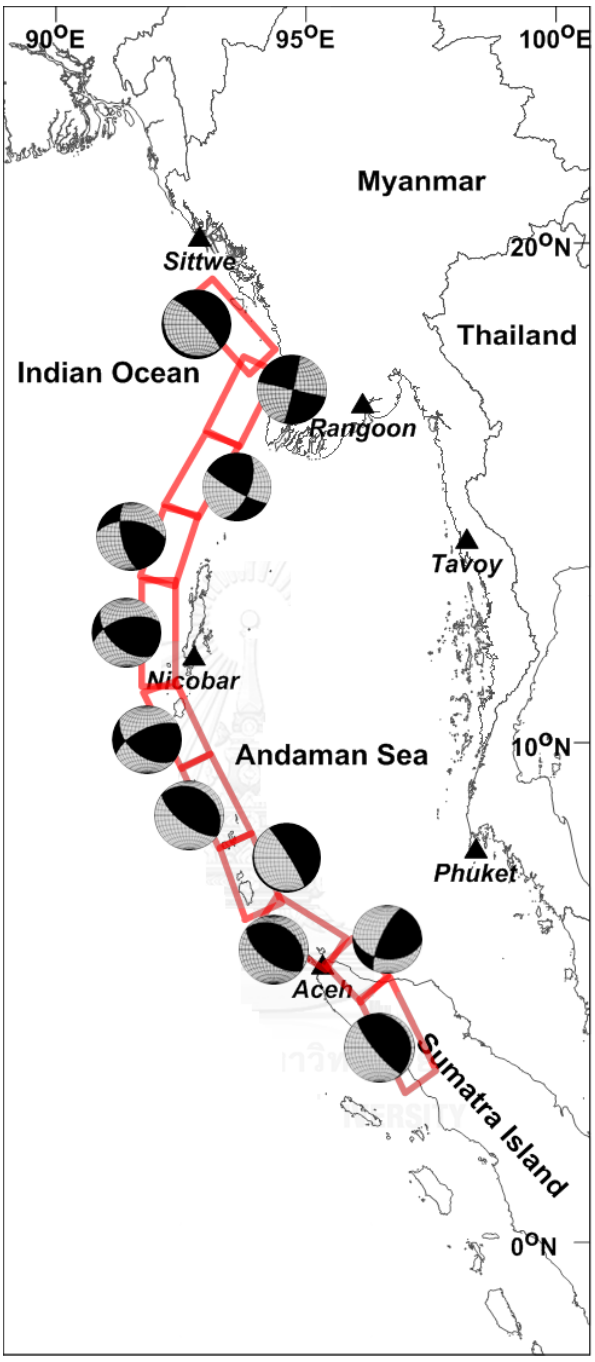

Figure4.5 The segments of intraslab (50-1,000 km) revealed different focal mechanism that occurred in each area. The focal mechanism of interplate is mix motions which are reverse, oblique reverse, normal and strike slip.

Table4.1 the results of strike 1 and 2 of interplate.

Segment no.	Location	Strike 1 of interplate	Strike 2 of interplate
1.	Sumatra Island	N70W at 70°, S70E – S30E at 110°-150°, N60W at 300°, N40W at 320°	S90E at 90°, S45E at 135°, S40E – S30E at 140°-150°, N45W at 315°
2.	Aceh city	N45W – N23W at 315°-337°	S55E – S45E at 125°-135°
3.	Northern section of Aceh city	N60W at 300°	S50E – S45E at 130°-135°
4.	The upper of no.3 in Andaman Sea	N70W – N45W at 290°-315°	S55E – S45E at 125°-135°
5.	Adjacent to no.4 in Andaman Sea	N45W – N40W at 315°-320°	S45E at 135°
6.	The bottom of Nicobar Island	S40E – S10E at 140°-170°	N45E – N65E at 45°-65°
7	Nicobar Island	N55E at 55°	S60W – S80W at 240°-260°
8.	The upper of Nicobar Island	N20E–N30E at 20°-30° S20W–S40W at 200°-220°	S10E and S80E at 170°
9.	Southern Ocean of Rangoon city	N22E at 22°	S50W at 230°
10.	Rangoon city	N18E at 18°, S90E at 90°, S70E at 110°, S60W at 240°	N45E at 45°, S30W at 210°, N80W at 280°, N60W at 300°
11.	Southern Ocean of Sittwe	N40W – N30W at 320°-330°	S45E at 135°

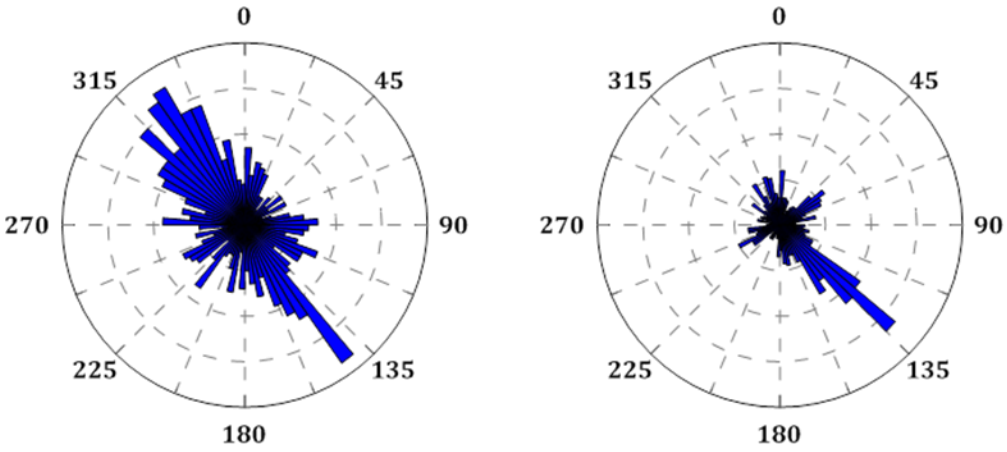

Figure4.6 Rose diagram is showing overall strike directions along the SASZ. It indicates two main direction which are S240E direction at 140° and N45W – N30W direction at 315°-330°.

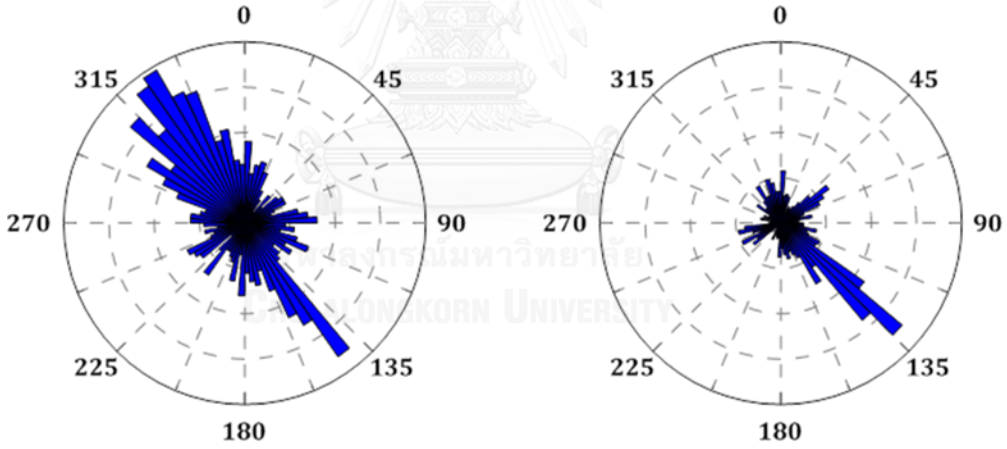

Figure4.7 Rose diagram is showing overall strike direction of interplate. The strike 2 indicated S45E direction at 135°.

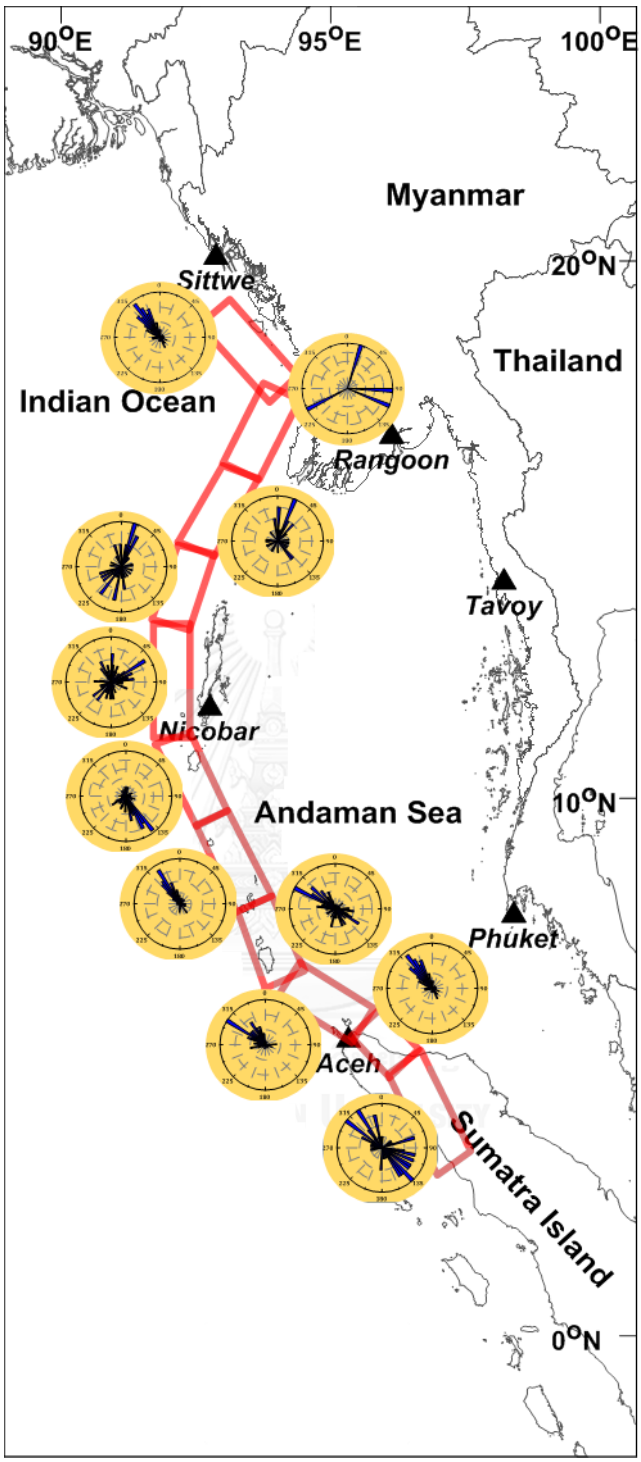

Figure4.8 Rose diagrams is showing strike 1 of the eleven segments from interplate events. The rose diagram indicates degree of strike.

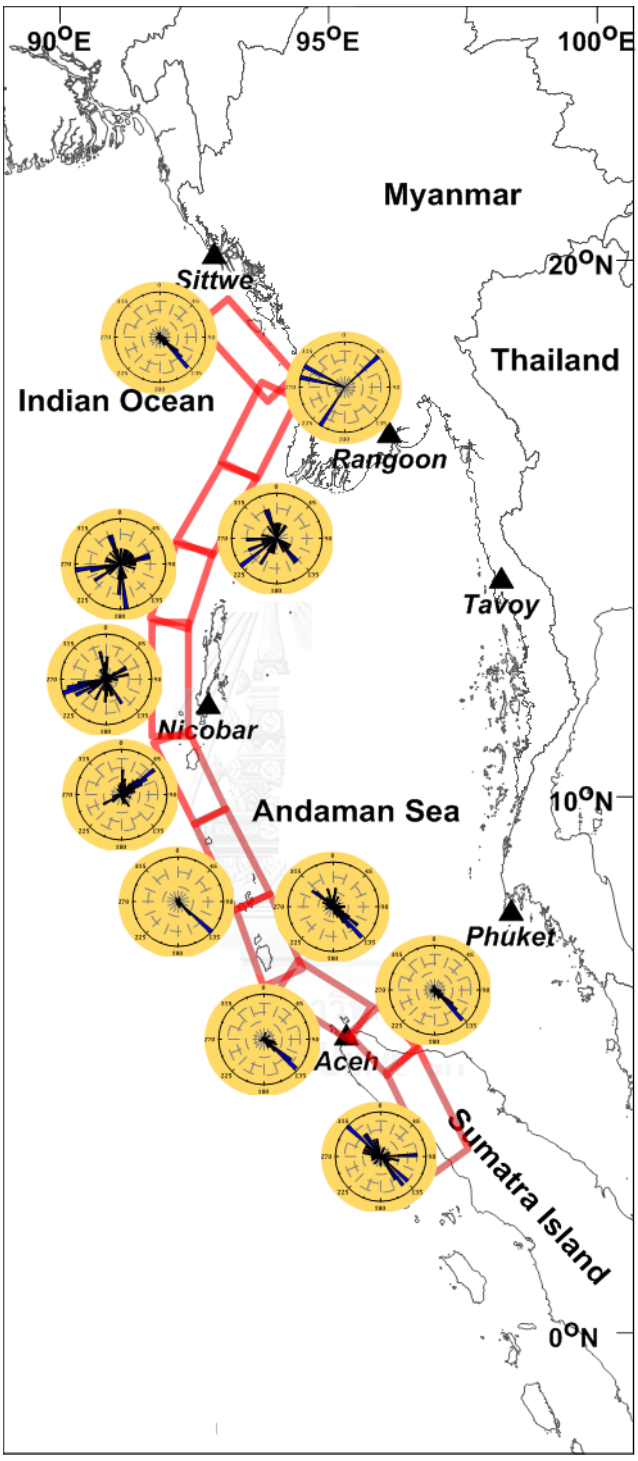

Figure4. 9 Rose diagrams is showing strike 2 of the eleven segments from interplate events.

4.3.2. Strike of intraslab

The following of interplate analysis, we also examined the strike of intraslab. The rose diagram represents the varied distribution of overall strike along the SASZ. The strike 1 is in a range of N90E – N23W direction at 90°-337°. While the strike 2 is S45E direction at 135° (Figure 4.10).

According to Figure 4.11 and 4.12, they consequently reveals strike 1 and strike 2 of sub segments**,** described in Table 4.2. The results are obviously different from interplate. Their rose petals show the varied main direction that they're definitely not related. Most of segments vary in the strike direction, whereas, some segments greatly suggest merely one orientation like segment no. 2, 9 and 10.

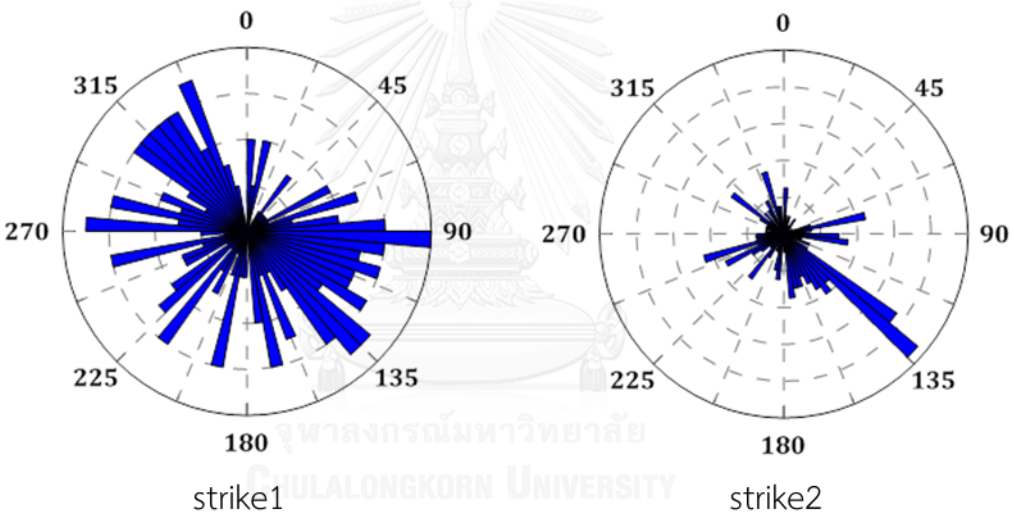

Figure4.10 The rose petals are showing the varied distribution of overall strike of intraslab. The strike 1 is in a range of N90E – N23W direction at 90°- 337°. The strike 2 is S45E direction at 135°.

Table4.2 the result of strike 1 and strike 2 of intraslab

Segment no.	Strike 1 of intraslab	Strike 2 of intraslab
1.	N65E at 65°, N80E at 80°, S30W at 210° and N35W at 315°	N80E at 80°
2.	S70E at 110°	S50E at 130° and S40W at 220°
3.	N55W at 305°	N55W – N45W at 305°-315°
4.	N70E – N90E at 70°-90°	N55W – N45W at 305°-315°
5.	N60W – N40W at 300°-320°	S45E at 135°
6.	N80W at 280°	S55E at 125° and S67W at 247°
7.	N at 0°	S60W at 240°
8.	S75W at 255° and W at 270°	S10E at 170°
9.	S80W at 100°	S50W at 230°
10.	N10E at 10°	N80W at 280°
11.	S68E, S15E and S at 112°, 165° and 180°	N70E at 70° and N35W at 325°

จุฬาลงกรณ์มหาวิทยาลัย
Chulalongkorn University

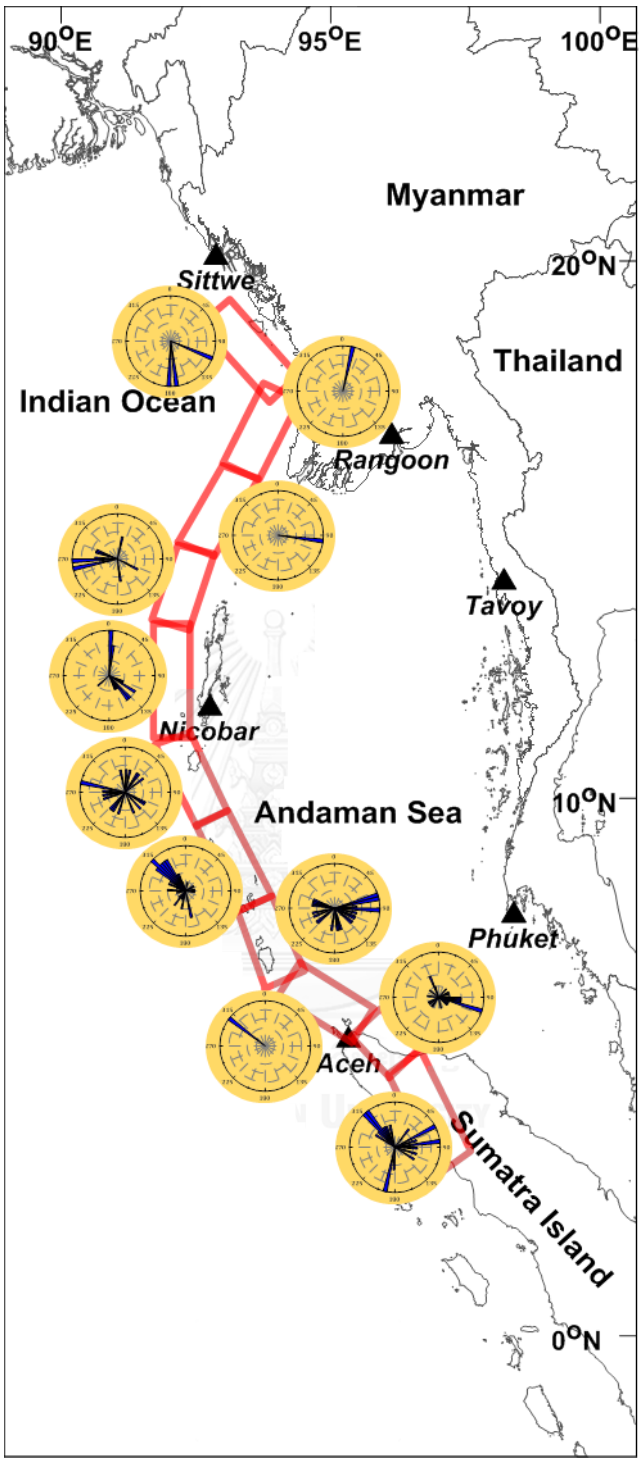

Figure4.11 The rose diagrams is showing strike 1 of intraslab of overall segments.

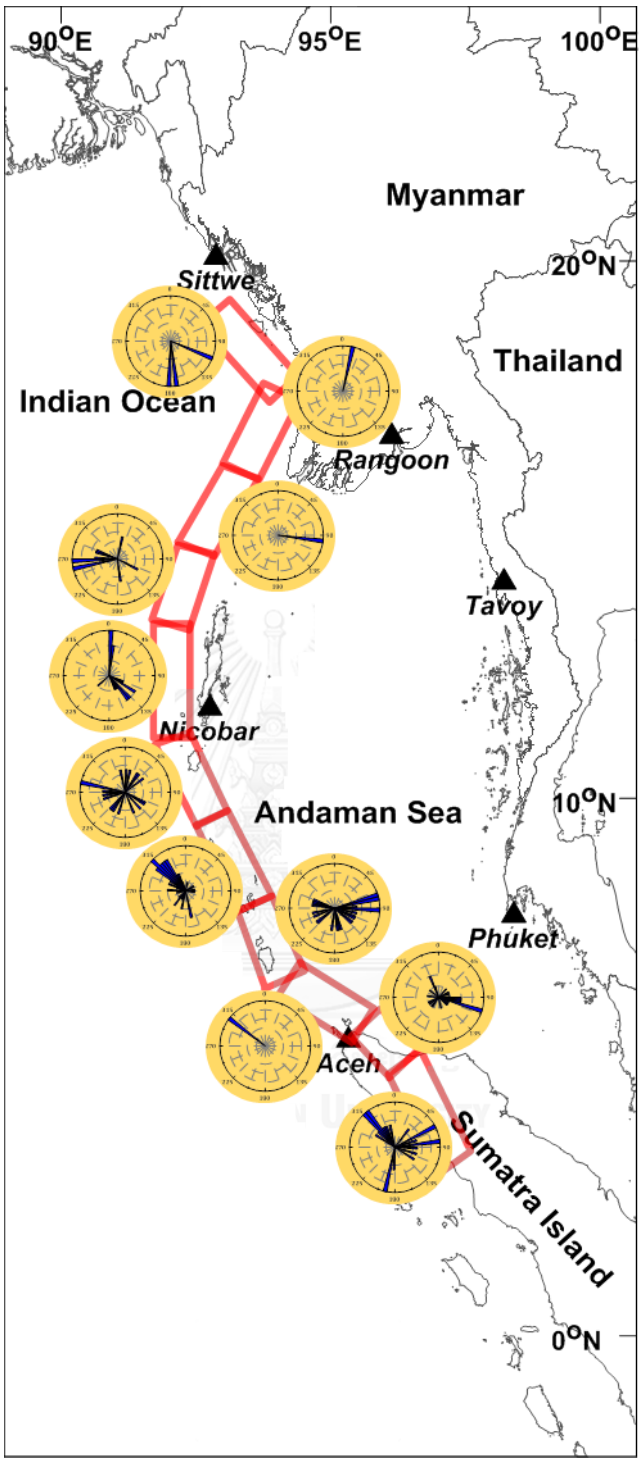

Figure4.12 Rose diagram is showing strike 2 of intraslab of overall segments.

4.4. Dip

The next step from strike, we examined dip angle long the SASZ. Likewise, it was divided into two genres which are dip 1 and dip 2 (Figure 4.13). The rose diagram of overall strike data along the SASZ shows that dip 1 and dip 2 are found the angle between 24°-45° and 55°-90°, respectively. Then, we analyzed the data of interplate only, the rose diagram provides the same result (Figure 4.14).

4.4.1. Dip of interplate

As reported by Table 4.3, it has been supported that every segment indicated in a similar way for both of dip 1 (Figure 4.15) and dip 2 (Figure 4.16). The rose petals present the frequency of dip 1 are mostly in a range of 25°-50°, whereas dip 2 are mostly dipped between 55°-70°. Comparing two sets of data, it strongly recommends that dip 2 provide the angle more than dip 1.

Table4.3 the result of dip 1 and dip 2 of interplate.

Segment no.	Dip 1 of interplate	Dip 2 of interplate
1.	45°-90°	30°-45°
2.	25°-45°	55°-70°
3.	11°-33°	55°-70°
4.	25°-45°	45°-65° and 80°
5.	22°-30°	60°
6.	33°-67°	78°-90°
7.	33°-40°	50°-67°
8.	45°	60° and 70°
9.	30°-55°	55°-90°
10.	20°, 30°-40° and 78°	45° and 70°
11.	15°-33°	55°-70°

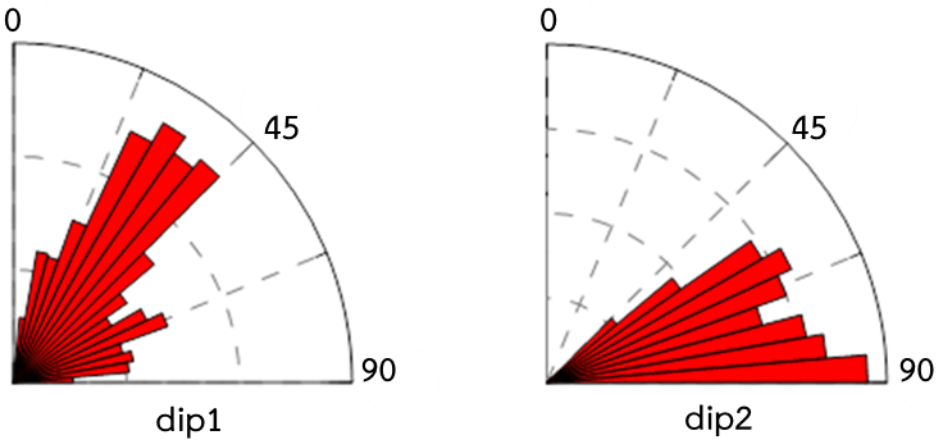

Figure4. 13 Rose diagram is showing the overall dip angle along the SASZ, 0° to 90°. The dip 1 is showing the angle between 24°-45°. The dip 2 is showing the angle between 24°-45° and 55°-90°.

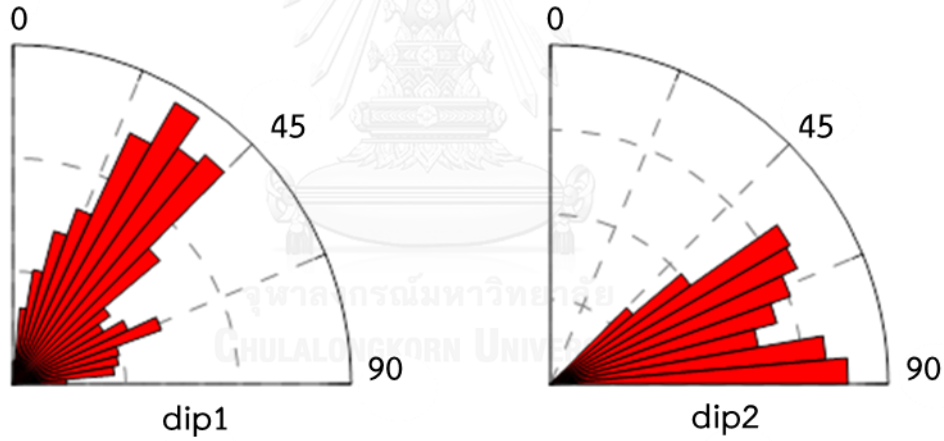

Figure4. 14 Rose diagram is showing the overall dip of interplate data. The dip 1 is showing the angle between 24°-45°. The dip 2 is showing the angle between 24°-45° and 55°-90°.

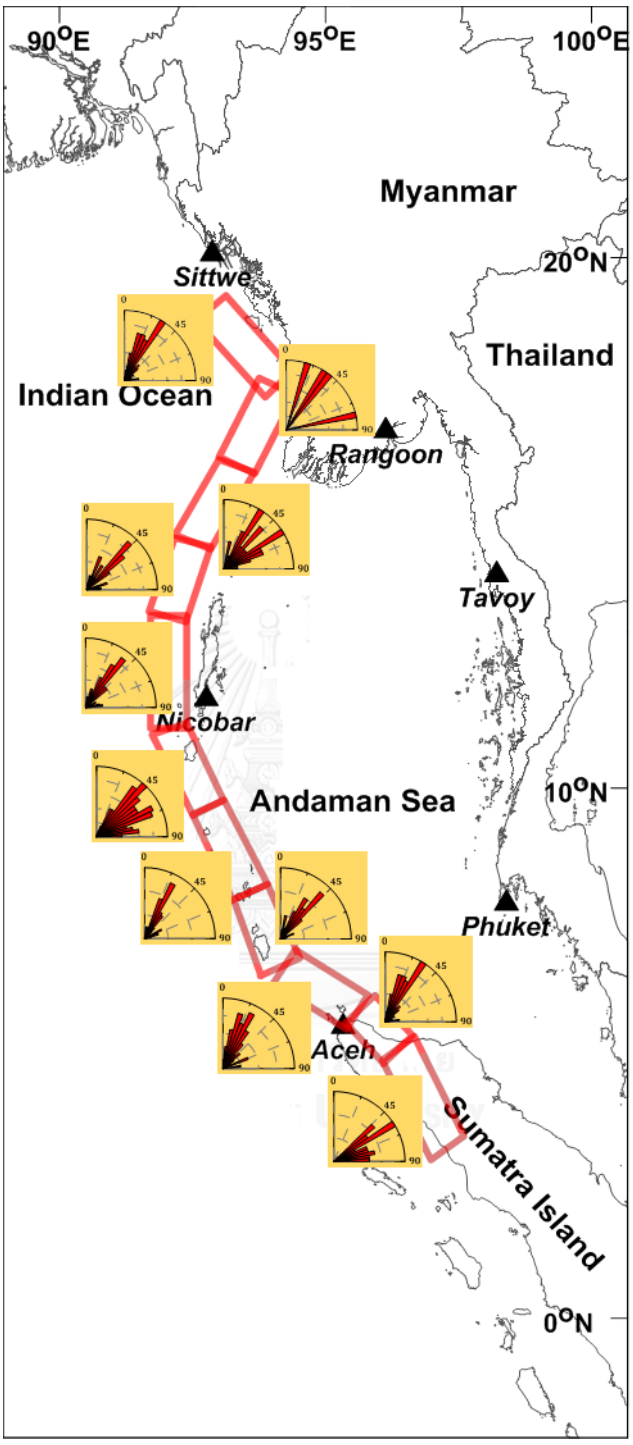

Figure4. 15 The rose diagram is indicating the frequency of dip 1 of interplate of 11 segments. The rose petals present the frequency of dip 1 are mostly in a range of 25°-50°.

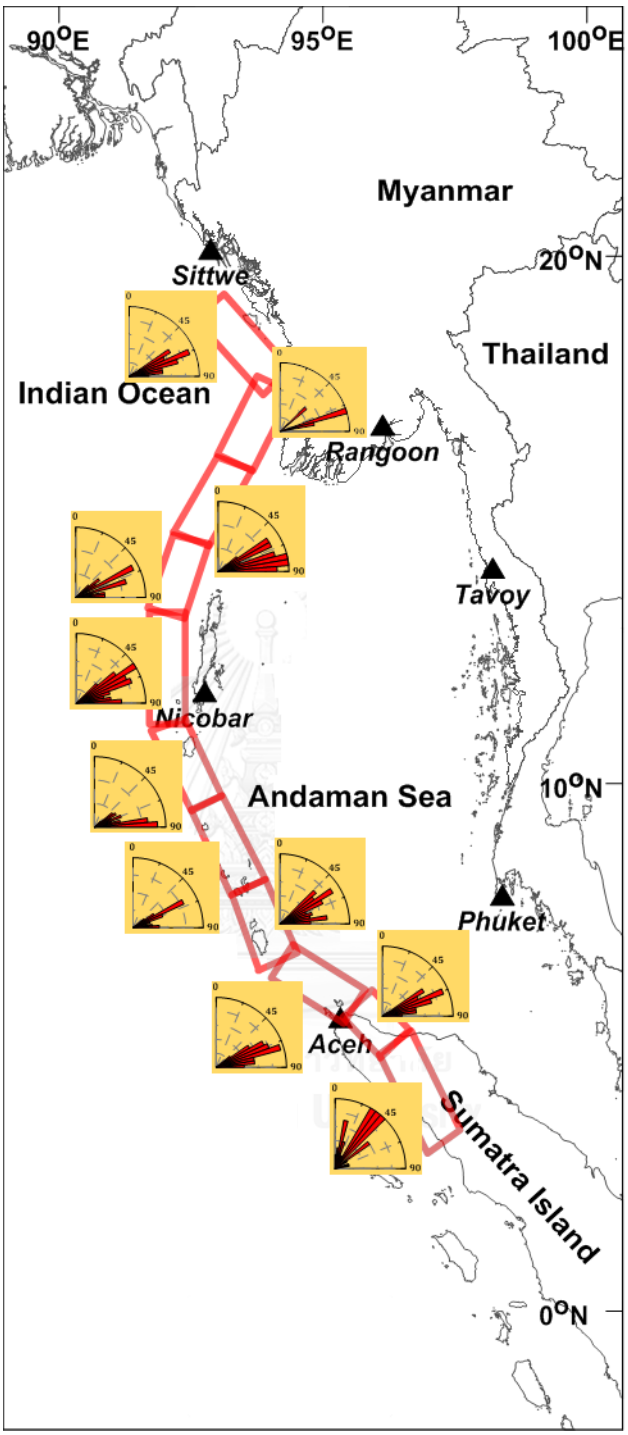

Figure4. 16 The rose diagram is indicating the frequency of dip 2 of interplate of 11 segments. The dip 2 is mostly dipped between 55°-70°.

4.4.2. Dip of intraslab

The following of interplate, we analyzed the intraslab data which consequently provided the results of dip 1 and dip 2 in Figure 4.15 and 4.16. It can be described that dip angle 1 are approximately 35° and dip 2 are found the angle between 55°-75°.

Table 4.4 provides the angles of dip 1 and dip 2 of intraslab. According to Figure 4.18 which represents dip 1, each segment has been rather a varied distribution of angles. While Figure 4.19 shows dip 2 that indicates the same manner as intraplate described above. However, their angles are slightly more than intraplate, in a range of 65°-90°. Although, dip 1 varied in the dip angles, it can be assumed in the similar way as intraplate that most of dip 1 were found the angles less than the dip 2.

Table4.4 the results of dip 1 and dip 2 of intraslab

Segment no.	Dip 1 of intraslab	Dip 2 of intraslab
1.	35°-50°	55°-60°
2.	25°-45°	67°-90°
3.	30°	57°
4.	10°-20° and 35°-45°	67°-90°
5.	30°-35°	55°-60°
6.	45°-55° and 80°	67°and 90°
7.	35°and 55°	56°-75°
8.	50° and 80°	67°, 80° and 90°
9.	22°	75°
10.	90°	90°
11.	10°-20° and 45°	85°

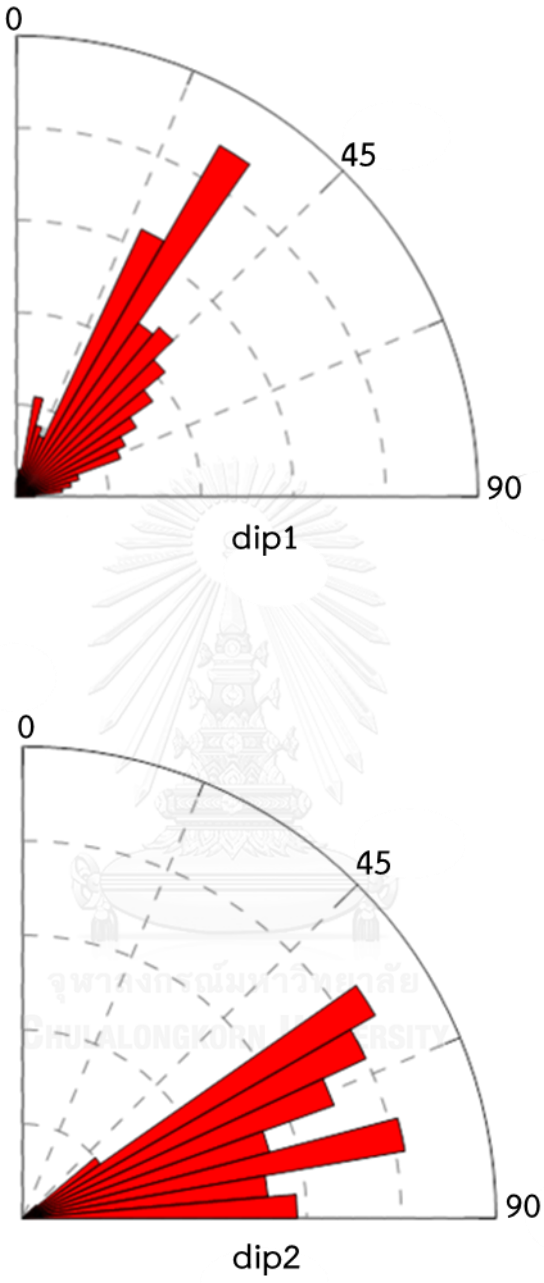

Figure4.17 Showing the overall dip rose diagram of intraslab. The dip angle 1 is approximately 35°. The dip 2 is the angle between 55°-75°.

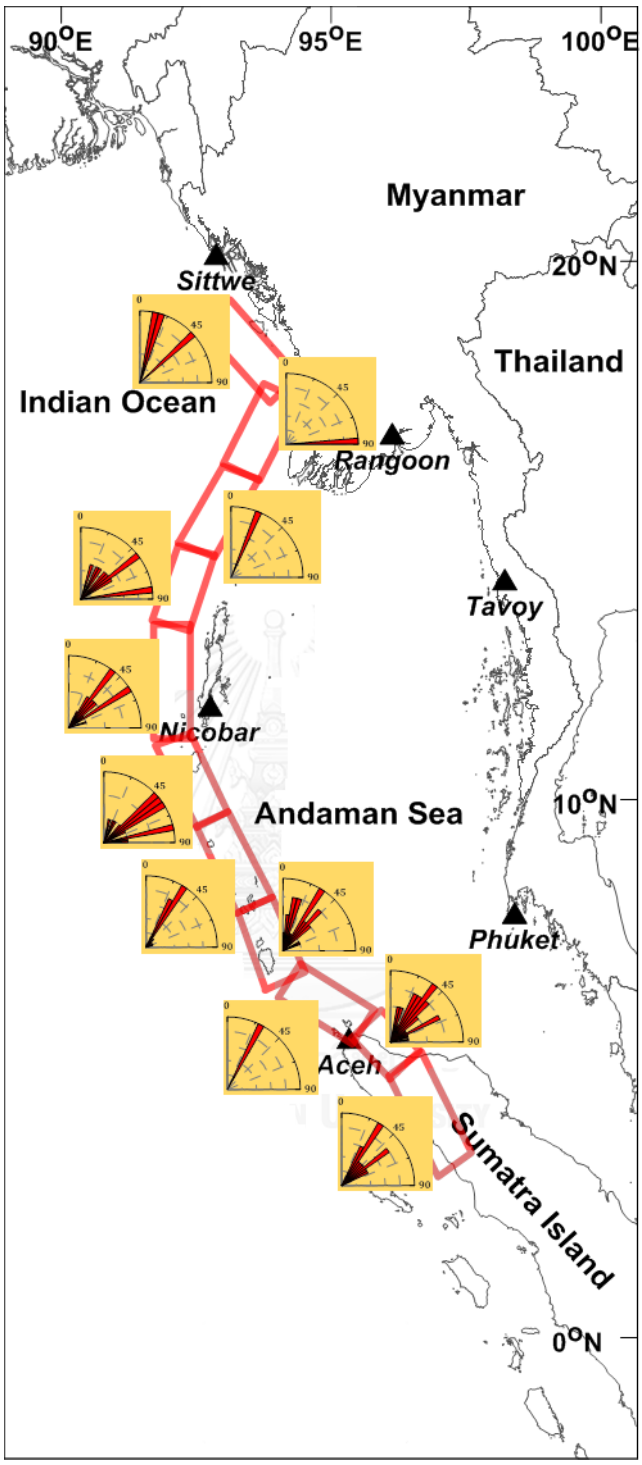

Figure4. 18 Showing dip 1 rose diagrams of intraslab in 11 segments. The average of dip 1 is 45°.

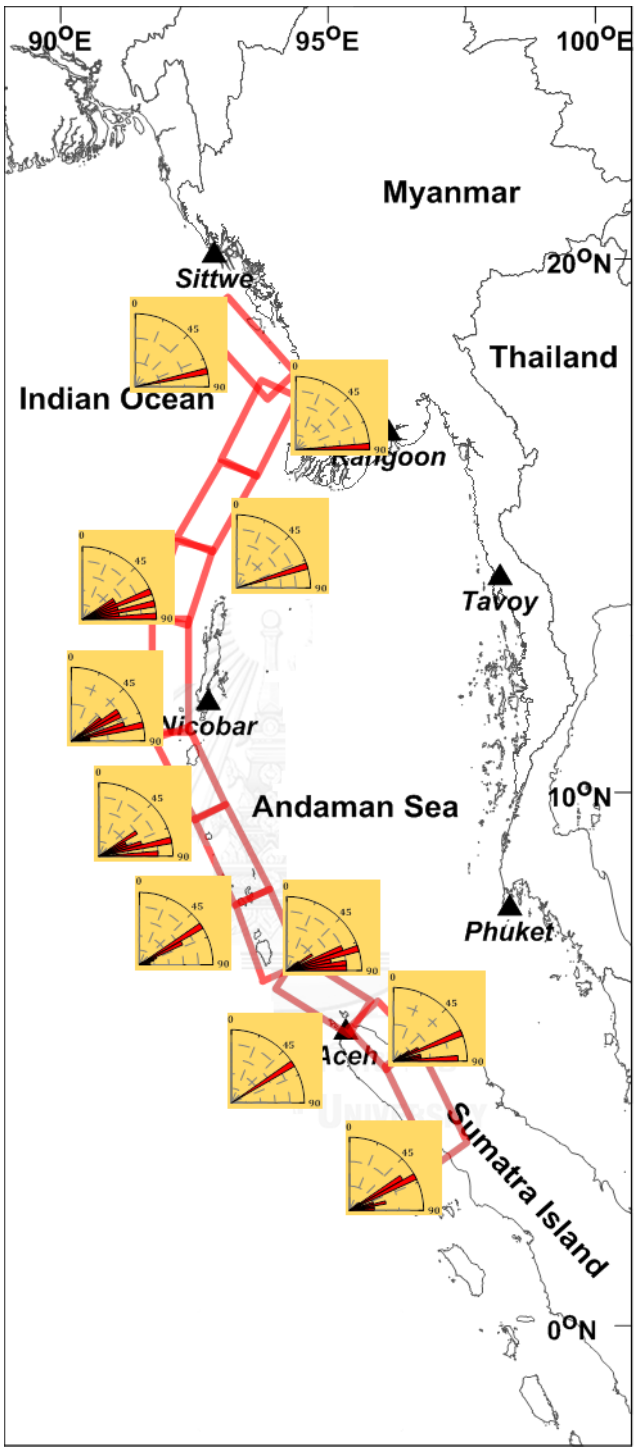

Figure4.19 Showing dip 2 rose diagram of intraslab in 11 segments. The average of dip 2 is 70°.

4.5. Rake

The final parameter analysis of focal mechanism is rake angle which can be separated into rake 1 and rake 2 as well (Figure 4.20). The rake angle can be interpreted as the direction a hanging wall block moves during rupture. In the other hand, the results gave a movement on the fault plane. In this study area, the overall rake along the SASZ signified that rake 1 is thrust-right motion. While the rake 2 of 90° indicated thrust motion. Likewise, the rake of interplate is in the same way as mentioned earlier (Figure 4.21).

4.5.1. Rake of interplate

The results of each segment indicate of rake of interplate described in Table 4.5., In each segment divides into rake1 (As reported in Figure 4.22, rake 1 quite varies in faulting motion. However, most of the lower parts of study area (segment no. 1-4) imply thrust motion. While the central to upper parts (segment no. 5-10) show normal motion. It can inferred from and rake 2 (Figure 4.23 that).the lower segment (no. 1-5) present thrust motion. While the rest segments vary in degree that suggest both of thrust and normal motion.

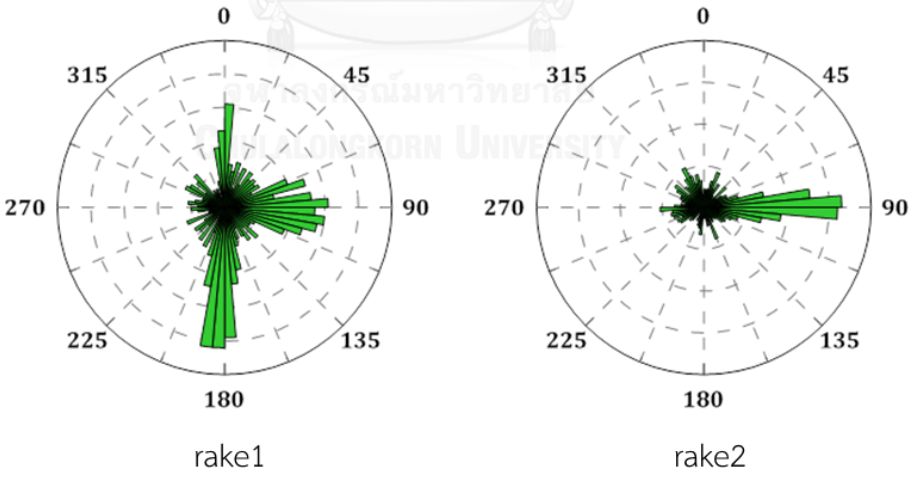

Figure4.20 Rose diagram is showing overall rake along the SASZ. The rake 1 is thrust-right motion. The rake 2 is thrust motion.

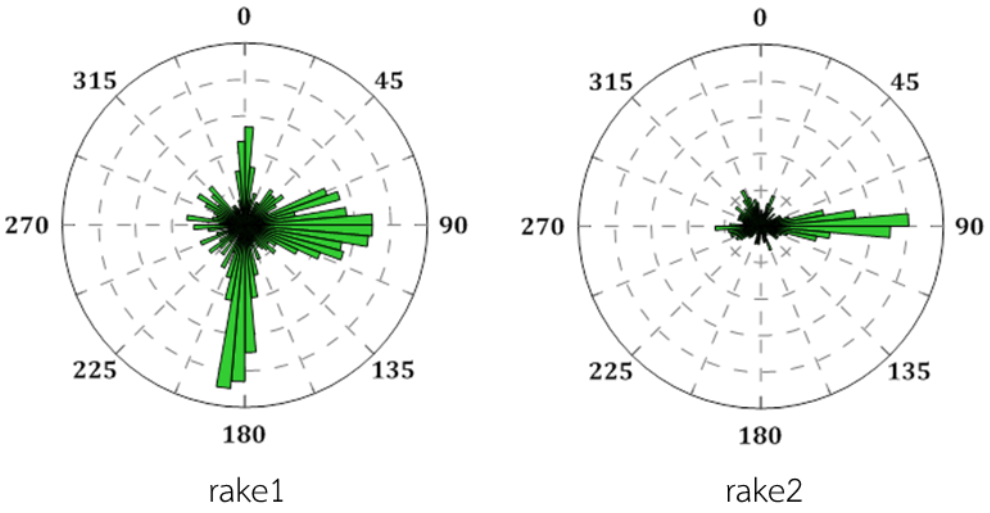

Figure4.21 The rake rose diagram of overall interplate events. The rake 1 is thrust-right motion. The rake 2 is thrust motion.

Table4.5 the results of rake 1 and rake 2 of interplate.

Segment no.	Rake 1 of interplate	Rake 2 of interplate
1.	thrust-right, thrust and normal-right motion	thrust motion
2.	thrust motion	thrust motion
3.	thrust and normal-right motion	thrust motion
4.	thrust-right motion	thrust motion
5.	normal-right motion	thrust motion
6.	normal motion	normal-left motion
7.	normal-right and normal-left motion	normal motion
8.	normal-right motion	normal-left motion
9.	normal-left motion	thrust-left and normal-right motion
10.	thrust, normal-right and normal-left motion	thrust, normal-right, normal and normal-left motion
11.	thrust motion	thrust motion

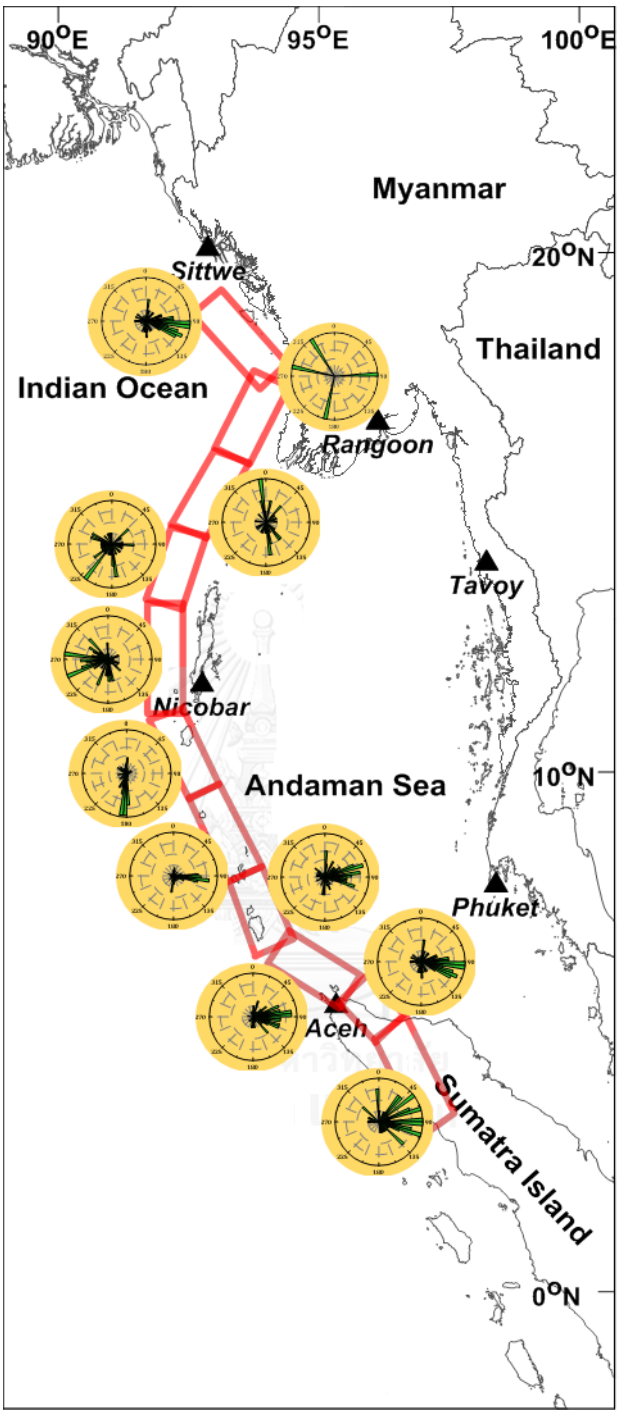

Figure4.22 Showing rose diagram of rake 1 from interplate events in 11 segments. The almost of rake 1 are thrust and normal motion.

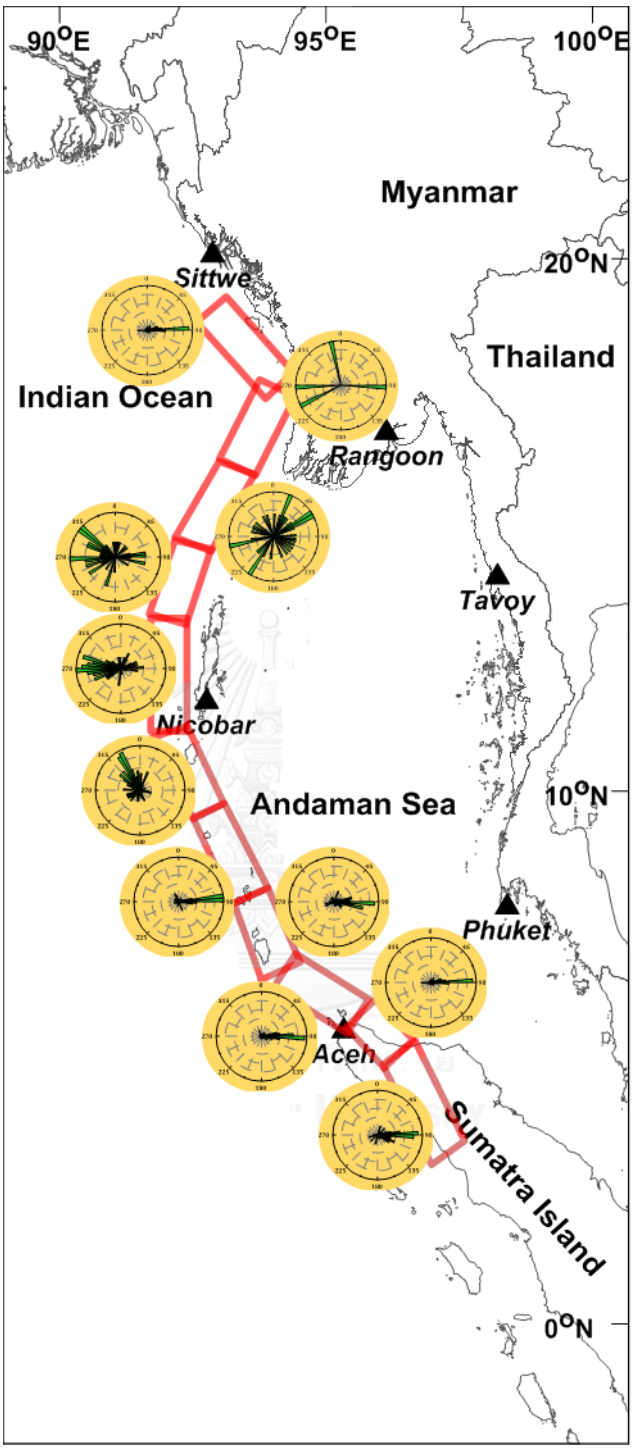

Figure4.23 Rose diagram is showing the rake 2 of from interpolate events (0–50 km) in 11 segments. The almost of rake 2 are thrust and normal motion.

4.5.2. Rake of intraslab

The last parameter we examined is the rake of intraslab which were divided into rake 1 and rake 2 as well. According to Figure 4.24, which shown rake rose diagram of overall intraslab data, it has been suggested that rake 1 and rake 2 are thrust-right motion thrust-left, respectively.

The results of rake from intraslab earthquake data are given in Table 4.6. As shown in Figure 4.25 and 4.26, which referred to rake1 and rake2 rose diagrams, both of them vary in fault motion and differ from interplate. For rake 1, both of thrust and normal motion are equally likely. While most of segments indicate thrust motion in rake2.

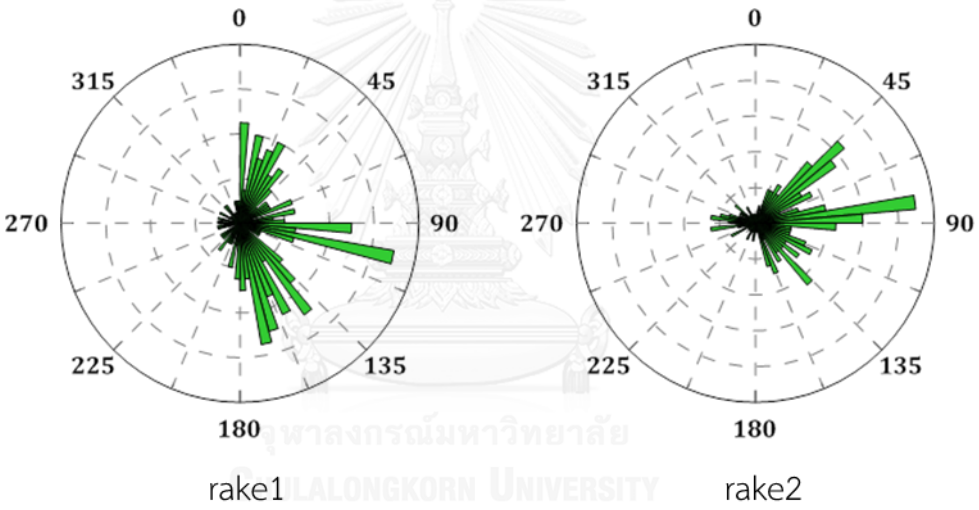

Figure4.24 Rake rose diagram of overall intraslab. The rake 1 and rake 2 are thrust-right motion thrust-left, respectively.

Table4.6 the results of rake1 and rake2 of intraslab.

Segment no.	Rake 1 of intraslab	Rake 2 of intraslab
1.	thrust-right motion	thrust-left motion
2.	thrust, thrust-right and normal-right motion	thrust-right motion
3.	thrust motion	thrust motion
4.	normal-right motion	normal-right motion
5.	thrust, thrust-right motion	thrust-left motion
6.	thrust-left, thrust-right and normal motion	normal-right motion
7.	thrust-left, normal-right and normal-left motion	thrust-left motion
8.	thrust-left motion	thrust-right motion
9.	thrust-right motion	thrust-left motion
10.	thrust-right motion	normal-left motion
11.	thrust-left, normal-right and normal-left motion	thrust-right, normal-right and normal-left motion

จุฬาลงกรณ์มหาวิทยาลัย
Chulalongkorn University

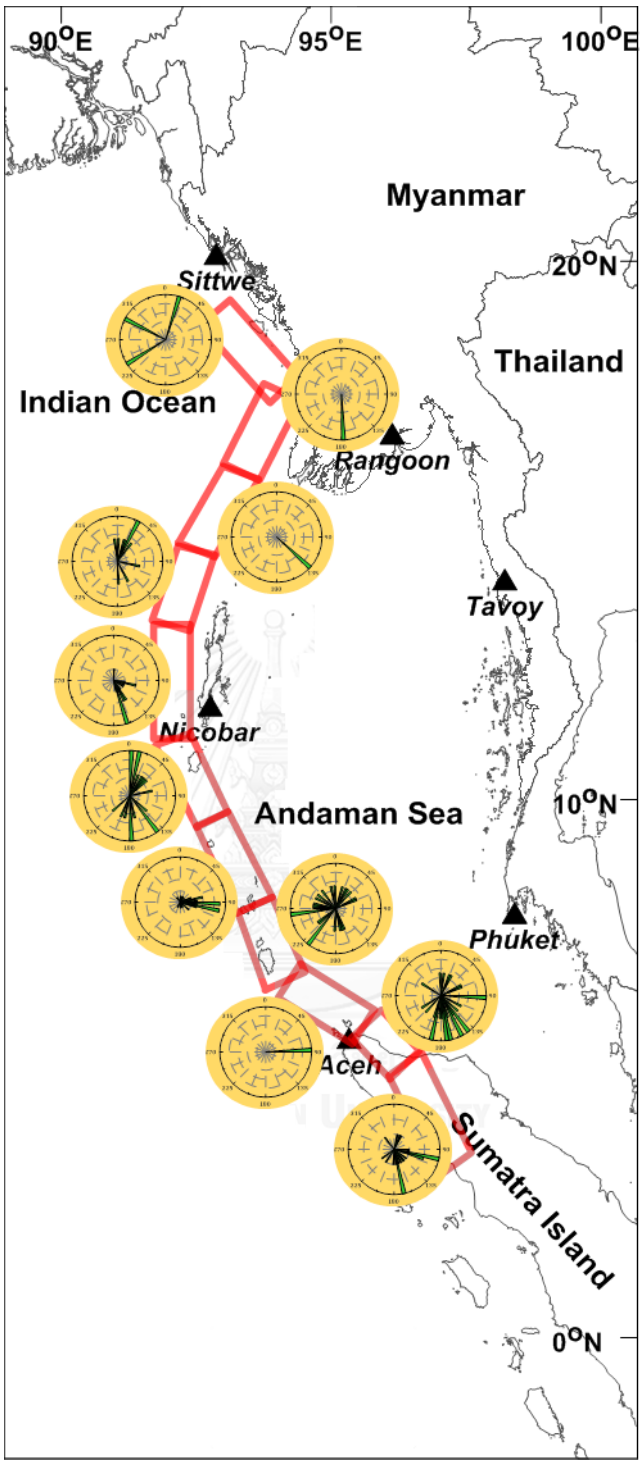

Figure4. 25 Showing rose diagram of rake 1 from intraslab earthquake event of 11 segments. The almost of rake 1 is thrust motion.

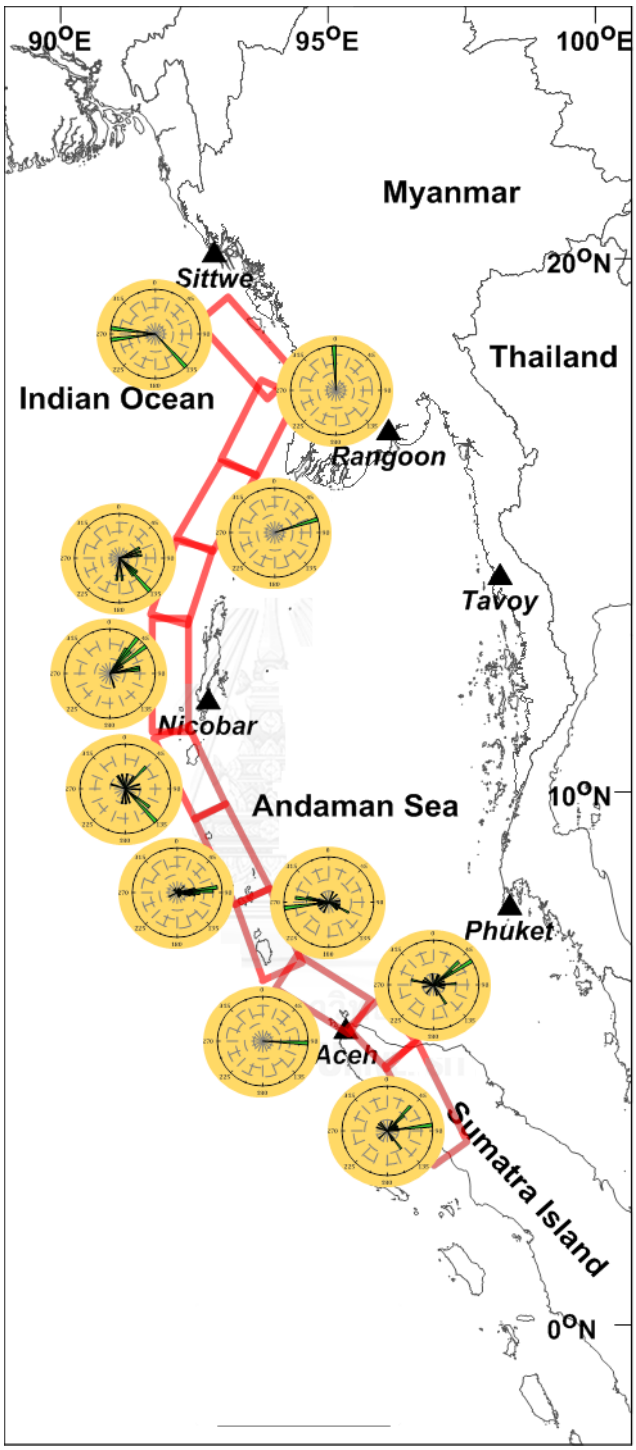

Figure4. 26 Showing rose diagram of rake 2 from intraslab earthquake event of 11 segments. The almost of rake 2 is thrust motion.

CHAPTER V
FRACTAL DIMENSION AND B VALUE

5.1. Fractal Dimension and b value & Significant

The SASZ is potential hazardous area and can generate the great earthquake. The researches have been investigated to predict the future earthquake. There are many methods for earthquake prediction, such as, Pattern Informatics, Z value, RTL, as we mentioned previously. This research analyzed by studying fractal dimension (Dc value) and b value method. Fractal Dimension (Dc value) can indicate seismic pattern of earthquake area. Likewise, b value directly relates to tectonic stress ((Mogi, 1967); (Scholz, 1968)). The low b value means that the anomalous area has been accumulated high stress which can lead to earthquake in the future. Therefore, this study examined two processes which are (i) spatial (ii) temporal of fractal dimension and b value.

5.2. Spatial Distribution of Fractal Dimension and FMD Parameters (b value)

From the completeness seismicity data (detail in Chapter III), we analysed the fractal dimension in the SASZ, Dc value is 2.37 ± 0.02. The distance of epicentre between range 1 and range 2, is 10.1-91.0 kilometres (Figure 5.1a). The graph indicates that slope is non- distribution. As stated by the equation of FMD power law for estimation the total of earthquake, the results yield 5.63 of a value and 0.84 ± 0.03 of b value. The graph shows a typical frequency magnitude of this study (Figure 5.1b).

5.2.1. Resolution map

In this method, we focused on merely interplate earthquake because the SASZ can generate severe earthquakes within 40 km- depth which already shows the cross section in Figure 3.11. To obtain the highest potential results, we need to examine 2 groups of seismicity data which are (i) before declustering and (ii) after declustering. The FMD equation can analyze by completeness seismicity data but not for fractal dimension investigation. Before declustering, the seismic data consist of mainshock, foreshock and aftershock. However, after declustering, we removed foreshock and

aftershock, the remaining seismic data which is main shock would show directly the released tectonic activity.

A high-resolution map would be presented by a high density of earthquake and small grid spacing. Thus, we divided the study area into 25x25 km subarea and found out the most appropriate earthquake number for fractal dimension analysis. It has been observed that sampling with 70 numbers of events showed significant result. Therefore, we fixed 70 events in any radius in kilometer.

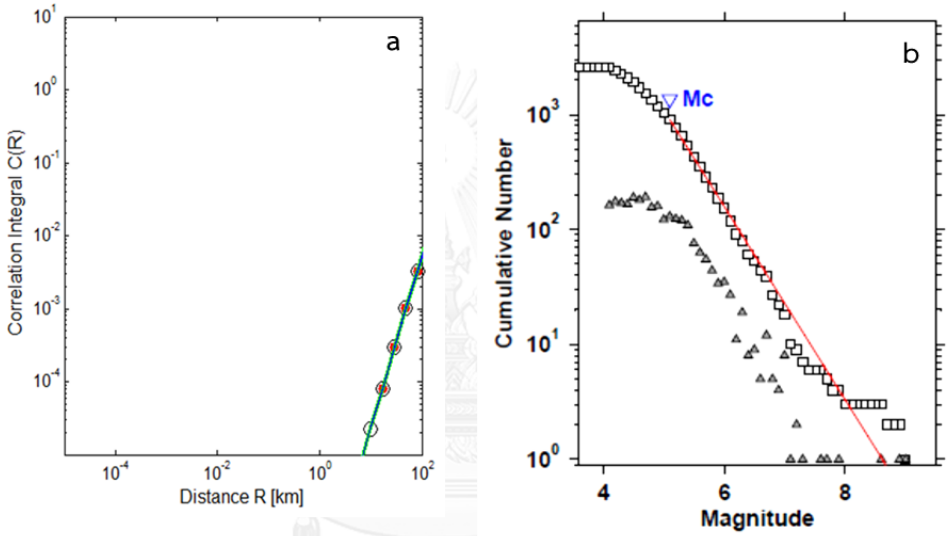

Figure5. 1 (a) Showing the relation of fractal dimension. The red points indicate distribution of slope. The green line indicates slope of fractal dimension. (b) Showing a typical frequency magnitude of the study. The red line indicates the magnitude of completeness and the rectangles indicate the cumulative number of events.

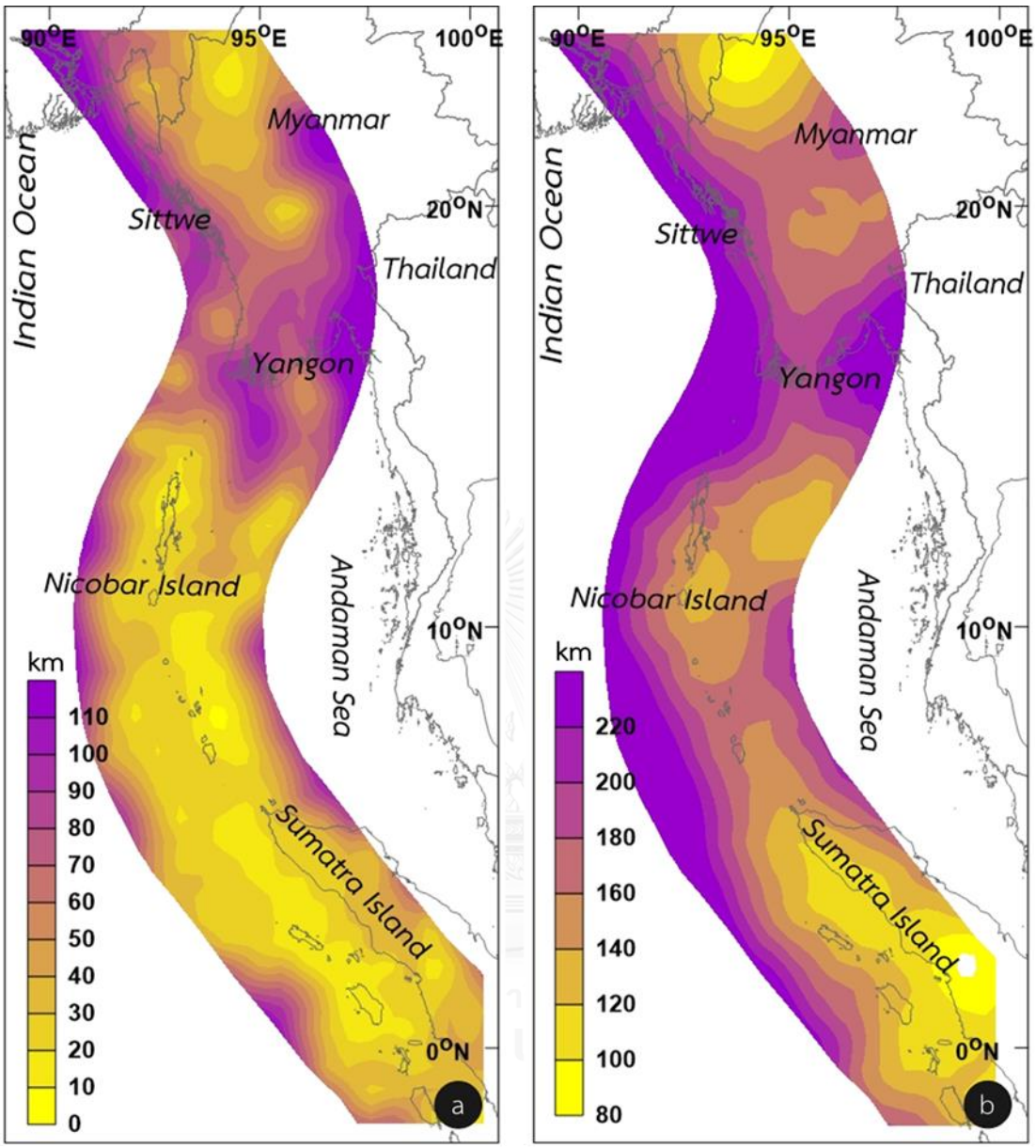

Figure5.2 Showing the distribution of radius map, covered 70 events from intraplate earthquakes, comparing between (a) before declustering and (b) after declustering.

It can be described from Figure 5.2a of before declustering data that the radius of grid spacing ranged from 0 to 90 km for 70 events. In some cases, such as, Yangon in Myanmar and northeastern of Sittwe city, they presented the low seismicity data. Hence, their radiuses of grid spacing are set the wide spread, around 110 km. In summary of before declustering data, the area was separated into a grid of 1° spacing

or around 110 km. The next is after declustering data (Figure 5.2b), the radius of grid spacing is wider than non-declustering data. The data quantity is less than before declustering due to mainshock only. According to Figure 5.2b, the radius of grid spacing is around 80-220 km**.** For some areas like Sumatra Island, Nicobar Island and northern of Sittwe city take to radius between 80-120 km. While the radius of outer boundary of the SASZ ranged from 180 to 220 km. As a result of after declustering data, the area was divided into a grid of 2° spacing or around 220 km for fractal dimension and b value analysis in the next step.

5.2.2. Spatial distribution of fractal dimension

- The result of before declustering data

This study presents Dc values in four case study areas along the SASZ (Figure 5.3), i.e., (a) Sittwe city and (b) Yangon city in Myanmar, (c) Nicobar city in India and (d) Aceh city in northern of Sumatra Island, Indonesia. The results of fractal dimension suggest that the slope is clearly non-distribution.

It can be seen in Figure 5.4a that the Dc value of study area ranged from 1.0 to 2.5. However, the Dc value of main area varied between 1.5 and 2.2. The western Myanmar indicates high Dc value of 2.5. While the western of Yangon city, where is located at western offshore of Myanmar, implies Dc values of approximately 1.0 to 1.4. The offshore of Sumatra Island to the southern of Nicobar Island is 1.9-2.2 Dc value. And the rest zones varied between 1.4 and 1.9 Dc value.

As illustrated by Figure 5.4b, the error of Dc value indicated <0.04. It has been supported that the error of Dc value is low fluctuation. The range of distance indicated by Figure 5.4c, the shortest of distance (range 1) is <10 km, whereas, the longest of distance (range 2) is approximately 60-110 km (Figure 5.4d). These results combined confirm the range of distance between 10-110 km.

(a) Sittwe city

Dc = 1.89±0.02, Range = 4.1-78.2

(b) Yangon city

Dc = 1.76±0.02, Range = 5.5-118.6

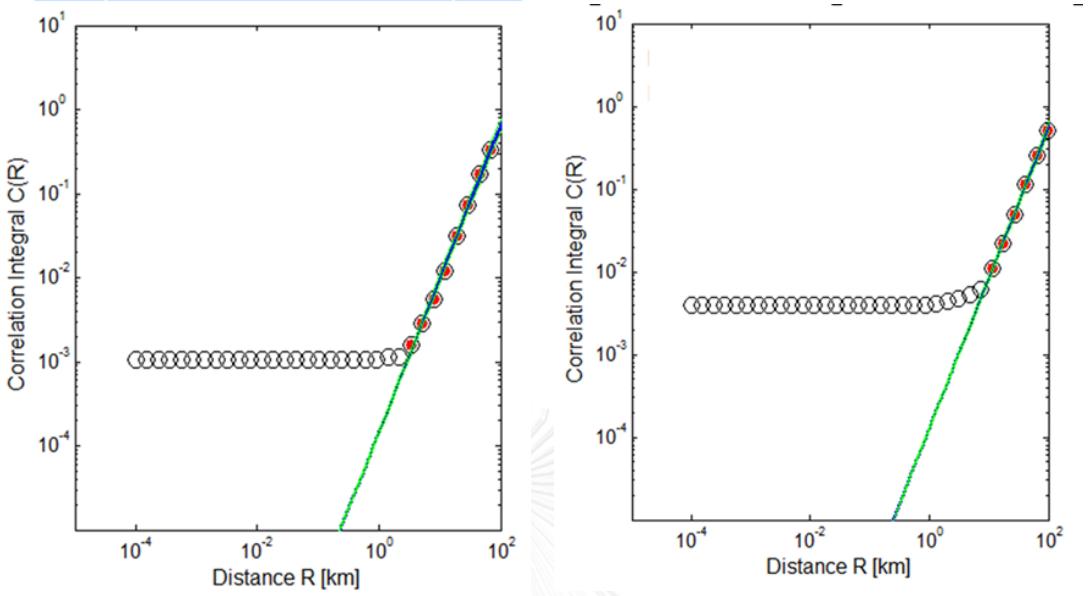

(c) Nicobar city

Dc = 1.79±0.01, Range = 3.1-101.9

(d) Aceh city

Dc = 1.98±0.02, Range = 1.4-87.6

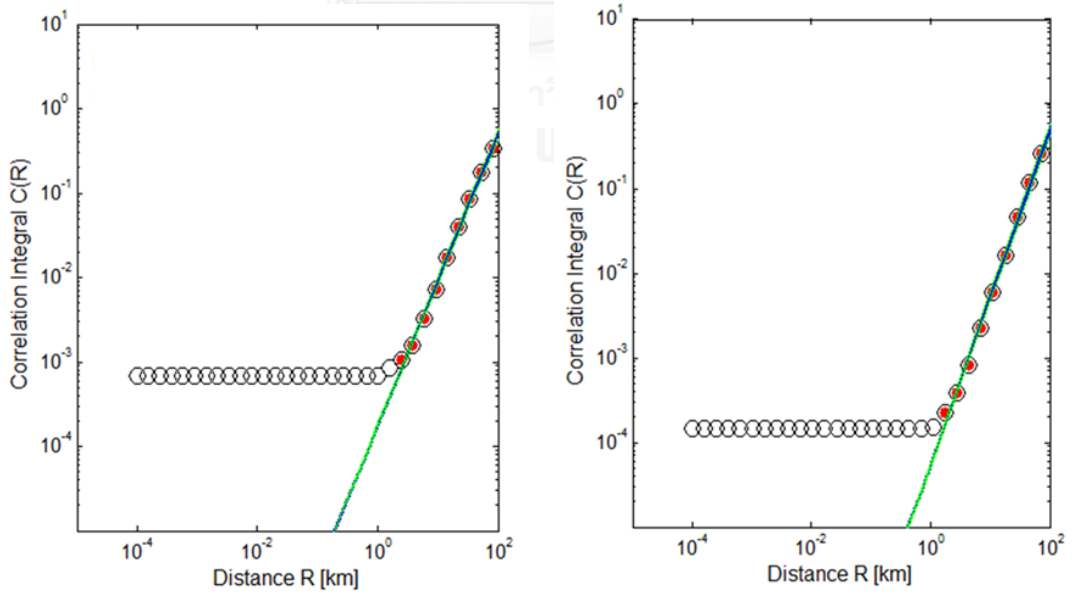

Figure5. 3 The graph showing Dc values in four case study areas along the SASZ of before declustering data.

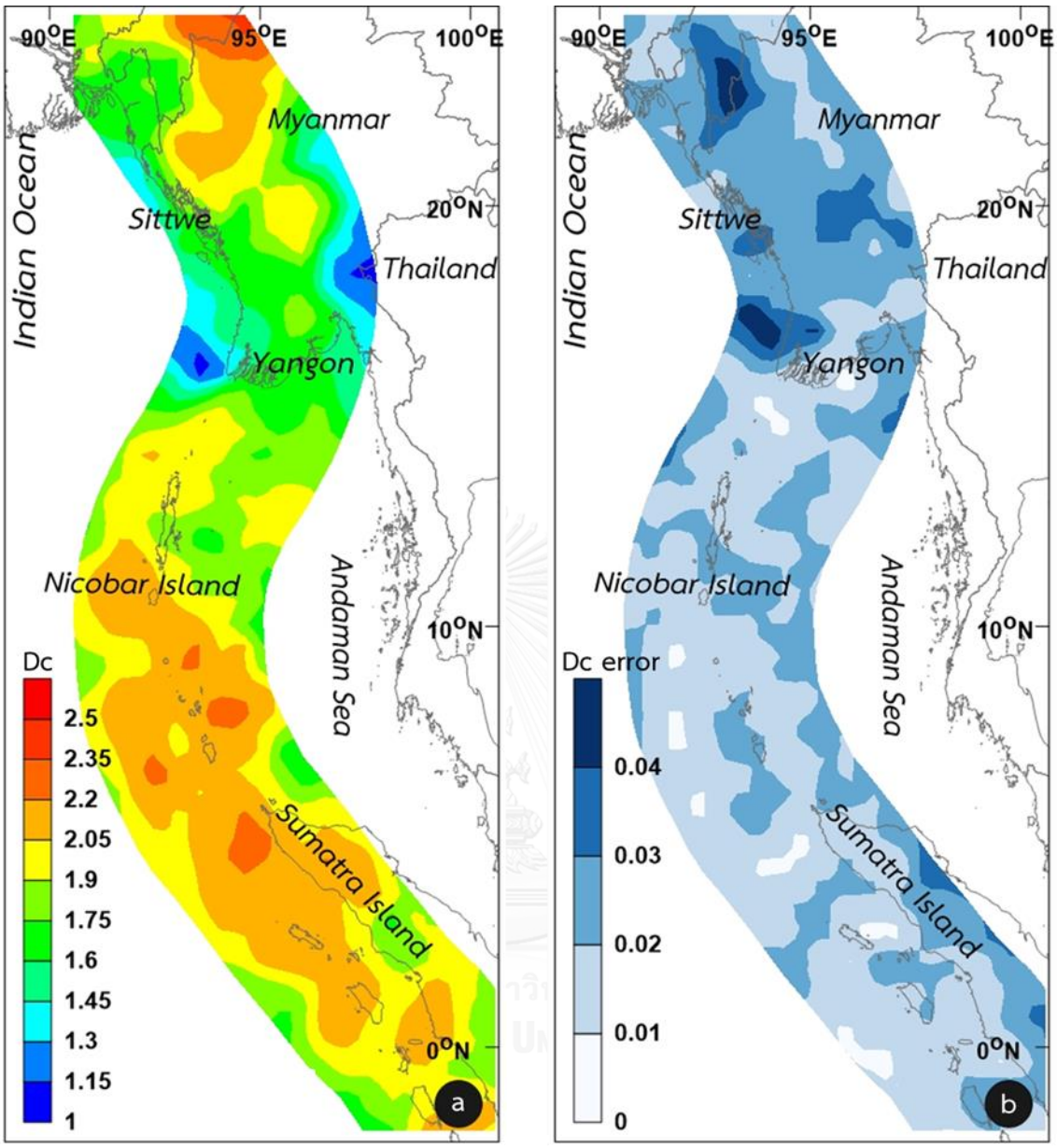
90°E
95°E
100°E
Myanmar
Indian Ocean
Sittwe
20°N
Thailand
Yangon
Nicobar Island
Andaman Sea
10°N
Dc
2.5
2.35
2.2
2.05
1.9
1.75
1.6
1.45
1.3
1.15
1
Sumatra Island
0°N
a
Dc error
0.04
0.03
0.02
0.01
0
b

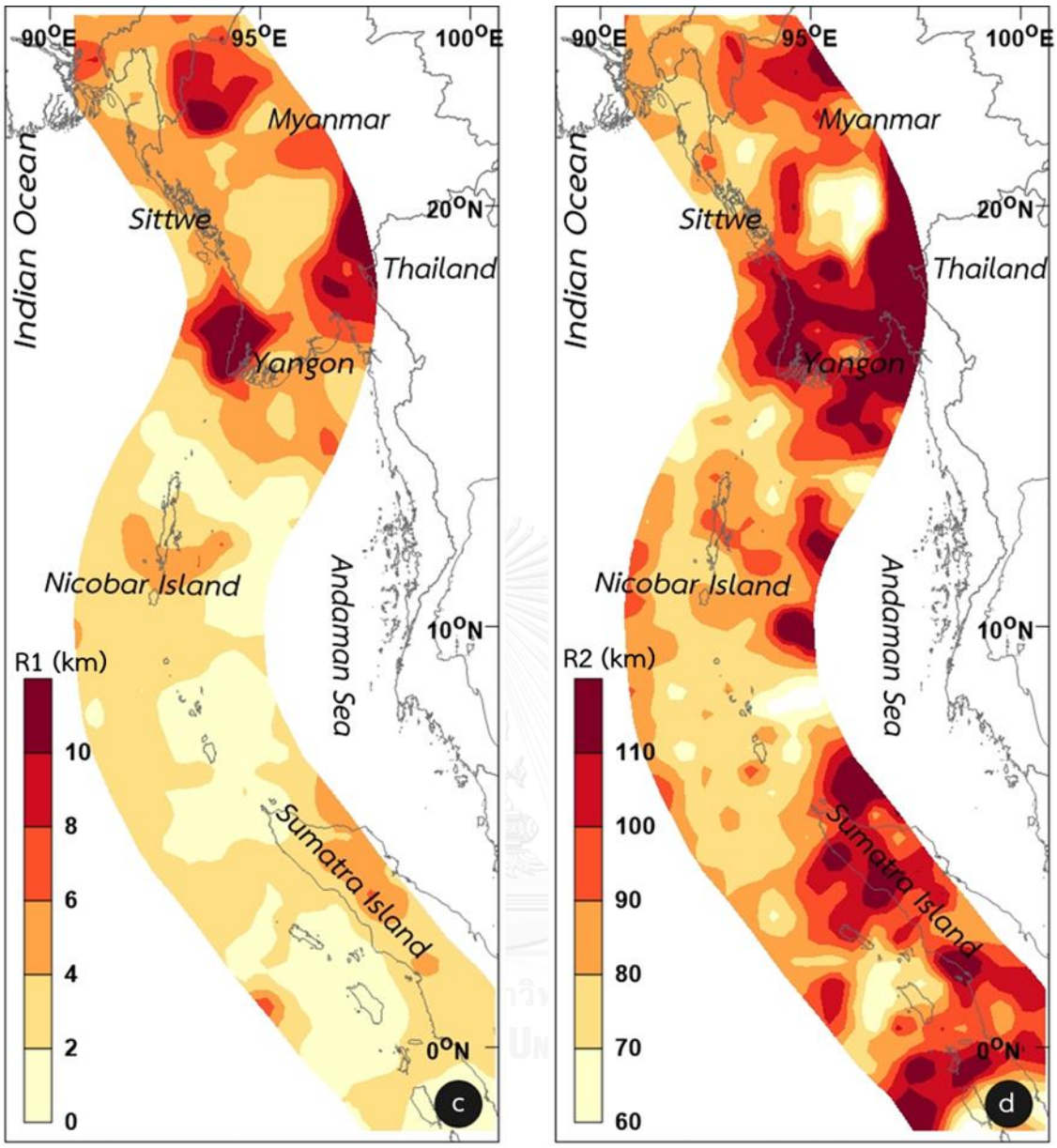

Figure5.4 The SASZ map of before declustering data can indicate the distribution of (a) Dc value, (b) error of Dc value, (c) range 1 of Dc value and (d) range 2 of Dc value.

- The result of after declustering data

The study also demonstrates the relation of Dc values in four case study areas in Figure 5.5. According to Figure 5.6a, the entire study area yields Dc value of 1.5-2.5. There are four areas of high Dc values, which are (1) around the Sittwe city, western of Myanmar (2) southeastern offshore of Nicobar Island (3) around the Aceh city and (4)

offshore of Sumatra Island, Indonesia (southeastern of study area). From Figure 5.6b it is clear that the error of Dc value is <0.04, which means Figure 5.6a strongly suggests high reliable data of Dc value.

It can be seen from Figure 5.6c that the shortest distance (range 1) ranged from 8 to 16 km of the main area which came from the relation of fractal dimension. The longest range is located on Southwestern offshore of Nicobar Island, about 40 km range 1. The shortest range is situated on Sumatra Island of Indonesia, <8 km. While the longest distance (range 2) ranged from 110 to 130 km in most of study areas (Figure 5.6d).

(a) Stiiwe city

Dc = 2.25±0.03, Range = 29.2-123.1

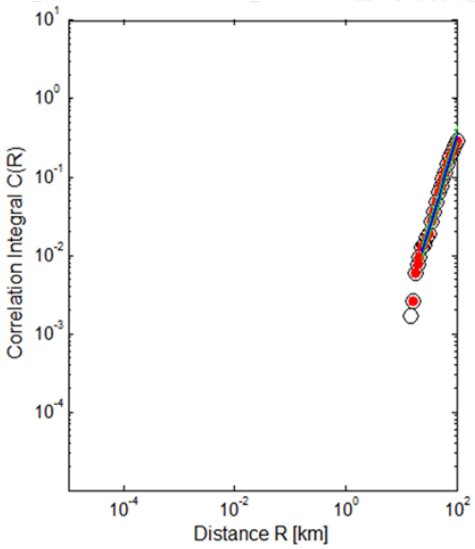

(b) Yangon city

Dc = 1.9±0.01, Range = 13.7-118.6

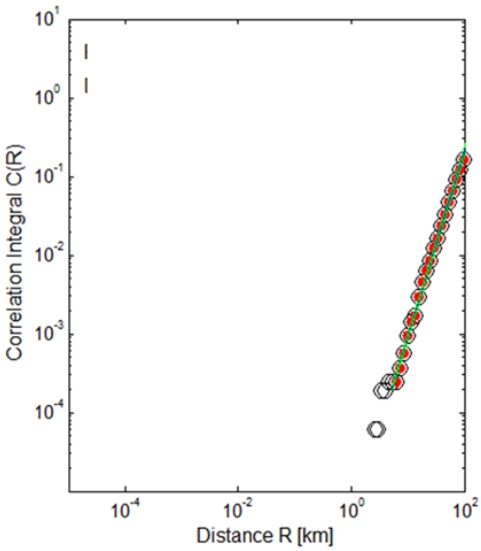

(c) Nicobar city

Dc = 2.11±0.01, Range = 6.7-105.8

(d) Aceh city

Dc = 2.09±0.02, Range = 6.9-173.1

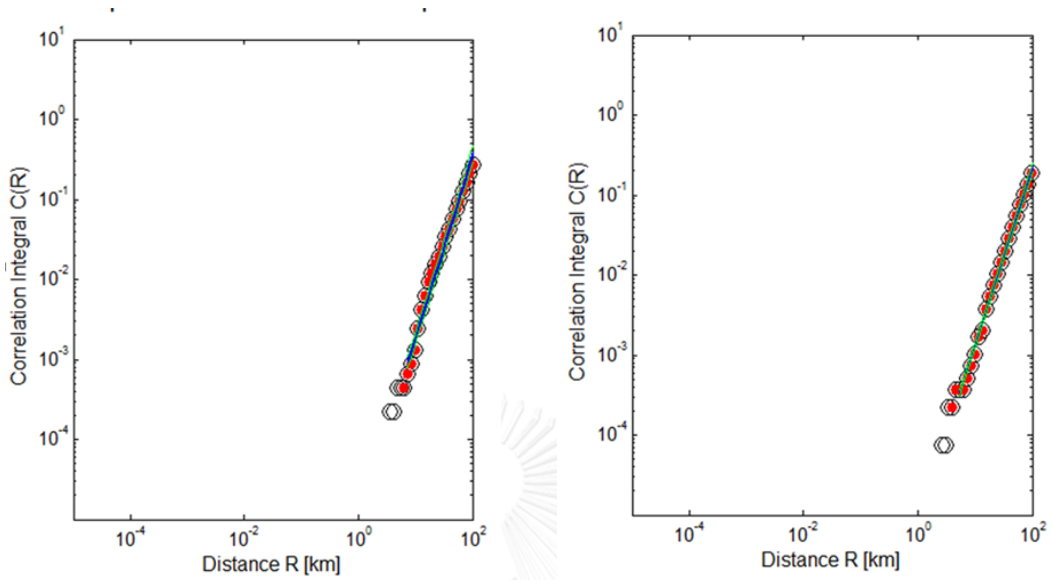

Figure5. 5 The graph showing Dc values in specific areas along the SASZ of after declustering data.

5.2.3. Spatial distribution of b value

- The result of before declustering data

Following, we analysed FMD relation of four specific areas as we mentioned above, shown in Figure 5.7. They vary in b value. For example, the western Sittwe city of Myanmar, gridded with 1° spacing or around 110 km, represents b value of 0.97 ± 0.07 and Mc value of 4.5.

As can be seen in Figure 5.8a, we found the anomalous of low b value around Yangon and Sittwe city of Myanmar, which means this is a risk area for earthquake because of increasing in stress accumulation than surrounding area in the SASZ.

The standard deviation (SD) of study area shows in Figure 5.8b, which is <0.2. It indicates that the error of analysis is low fluctuation. Then, magnitude of completeness or Mc is defined the least magnitude the networks can receive correctly value. As shown in Figure 5.8c, Mc values of the study area are between 3.5 and 5.5,

which are higher than Mc values of Southeast Asia that indicates Mc values of 3.5-5.0. The reason may come from distances between the study area and seismic stations.

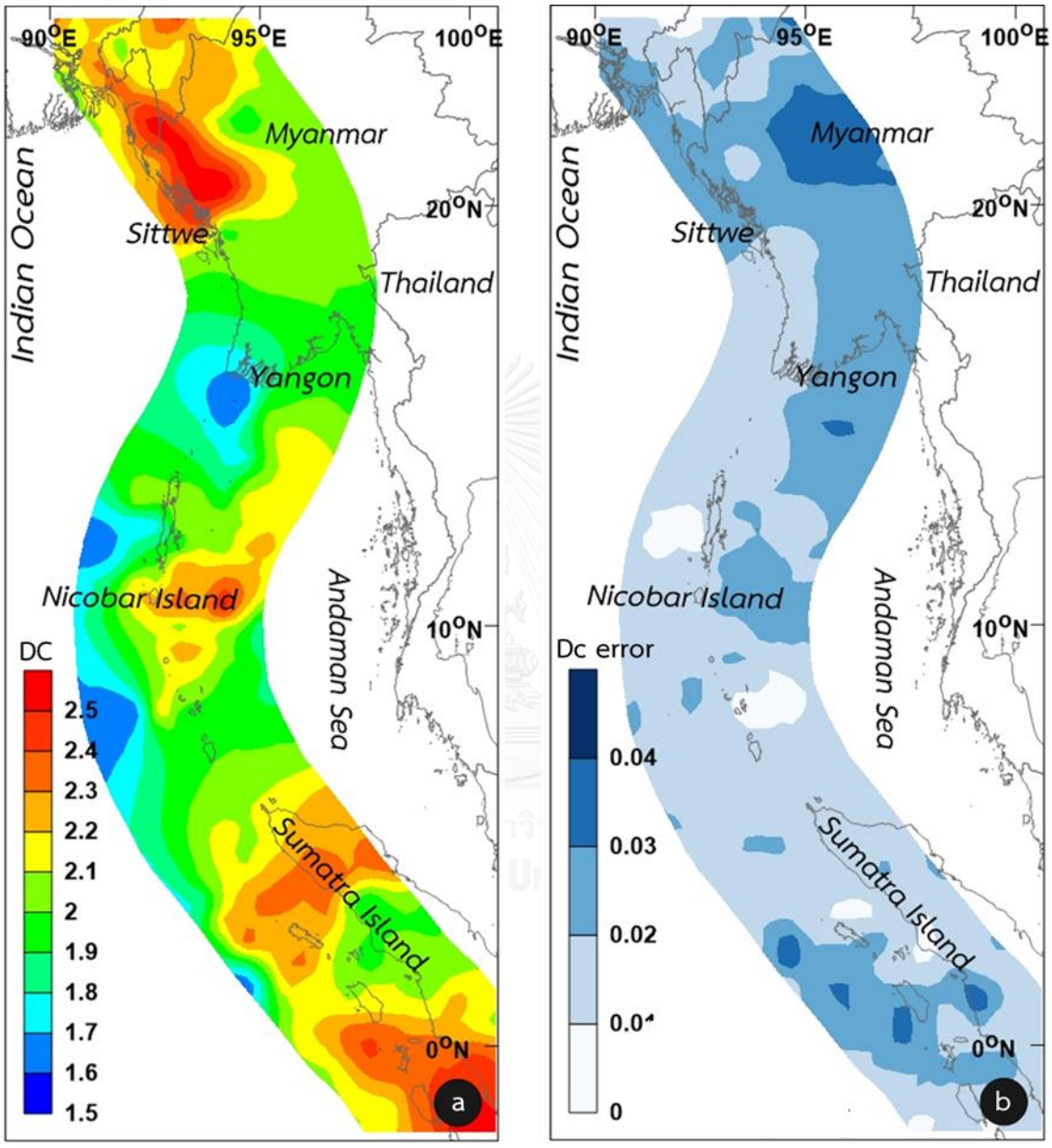

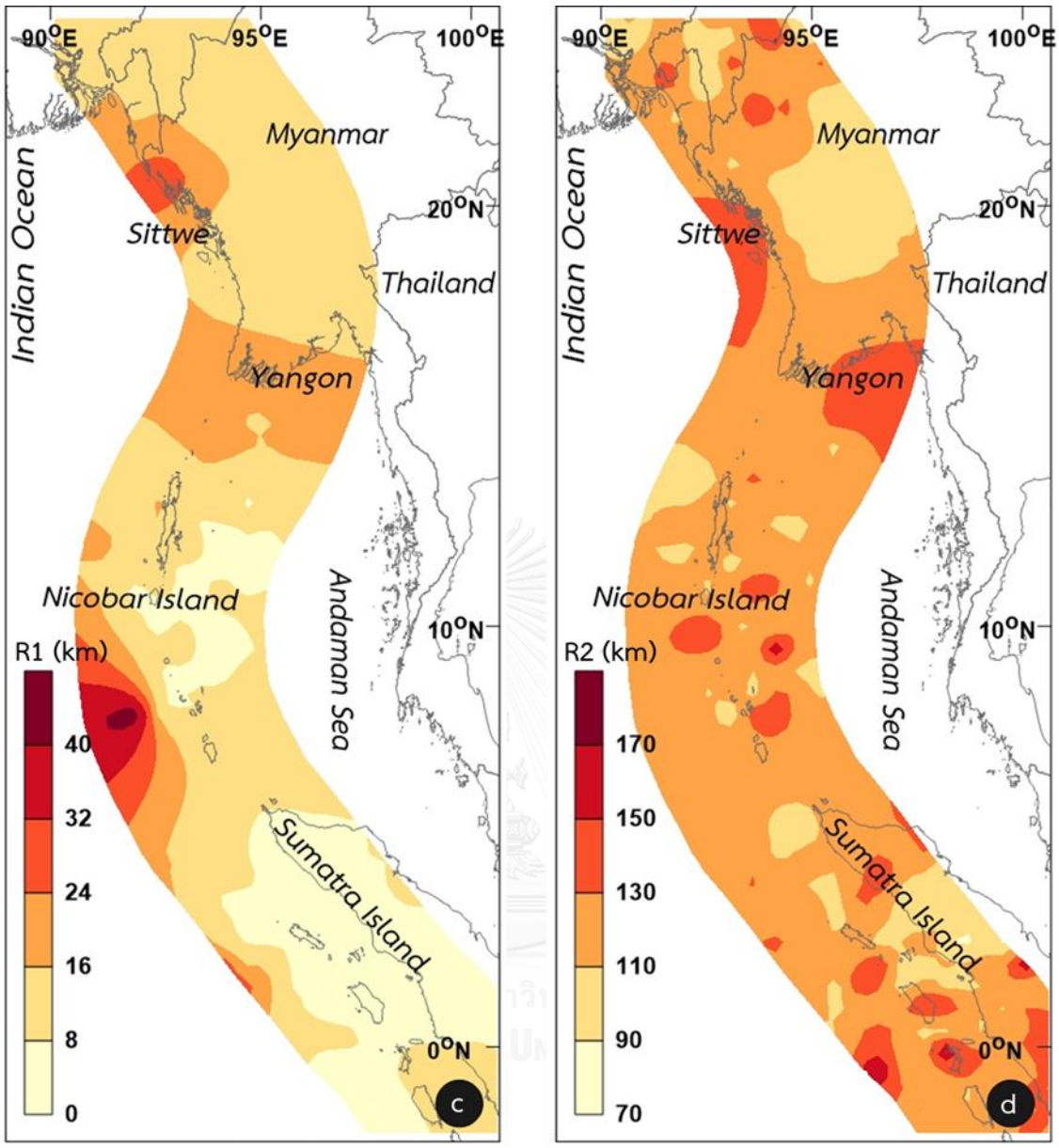

Figure5.6 The SASZ map after declustering data indicates the distribution of (a) Dc value, (b) error of Dc value, (c) range1 of Dc value and (d) range2 of Dc value.

(a) Sittwe city

a = 6.27, b =0.97±0.07, Mc = 4.5

(b) Yangon city

a = 5.00, b =0.76±0.10, Mc = 4.2

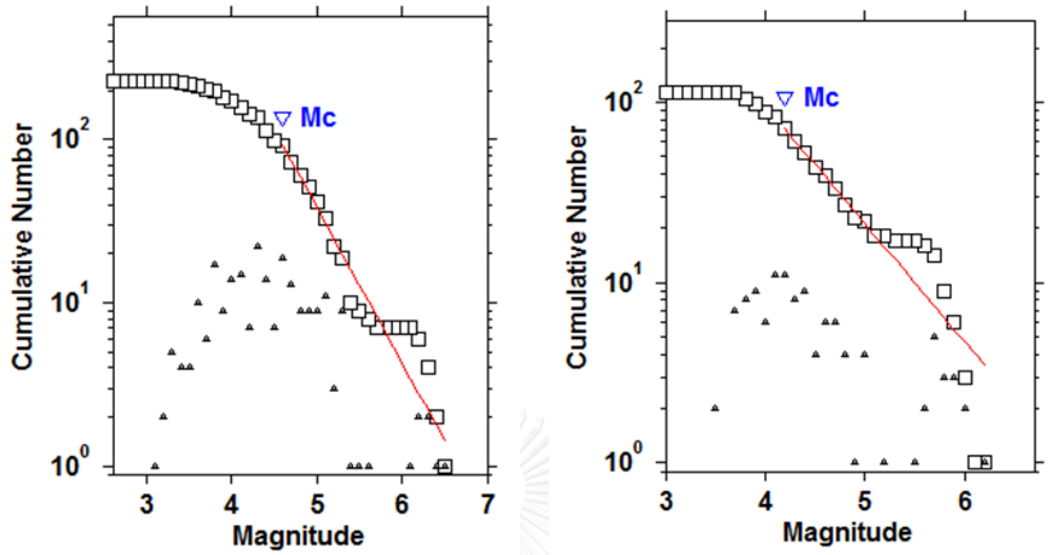

(c) Nicobar city

a = 12.21, b =1.83±0.27, Mc =5.8

(d) Aceh city

a = 11.66, b =1.68±0.21, Mc =5.8

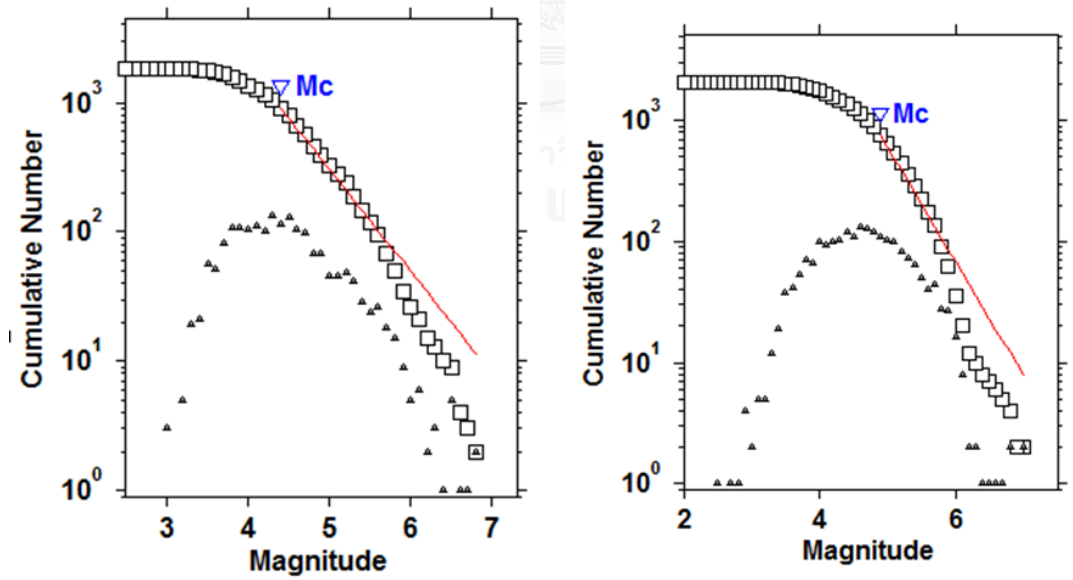

Figure5. 7 The graph showing FMD relation of specific areas along the SASZ before declustering data.

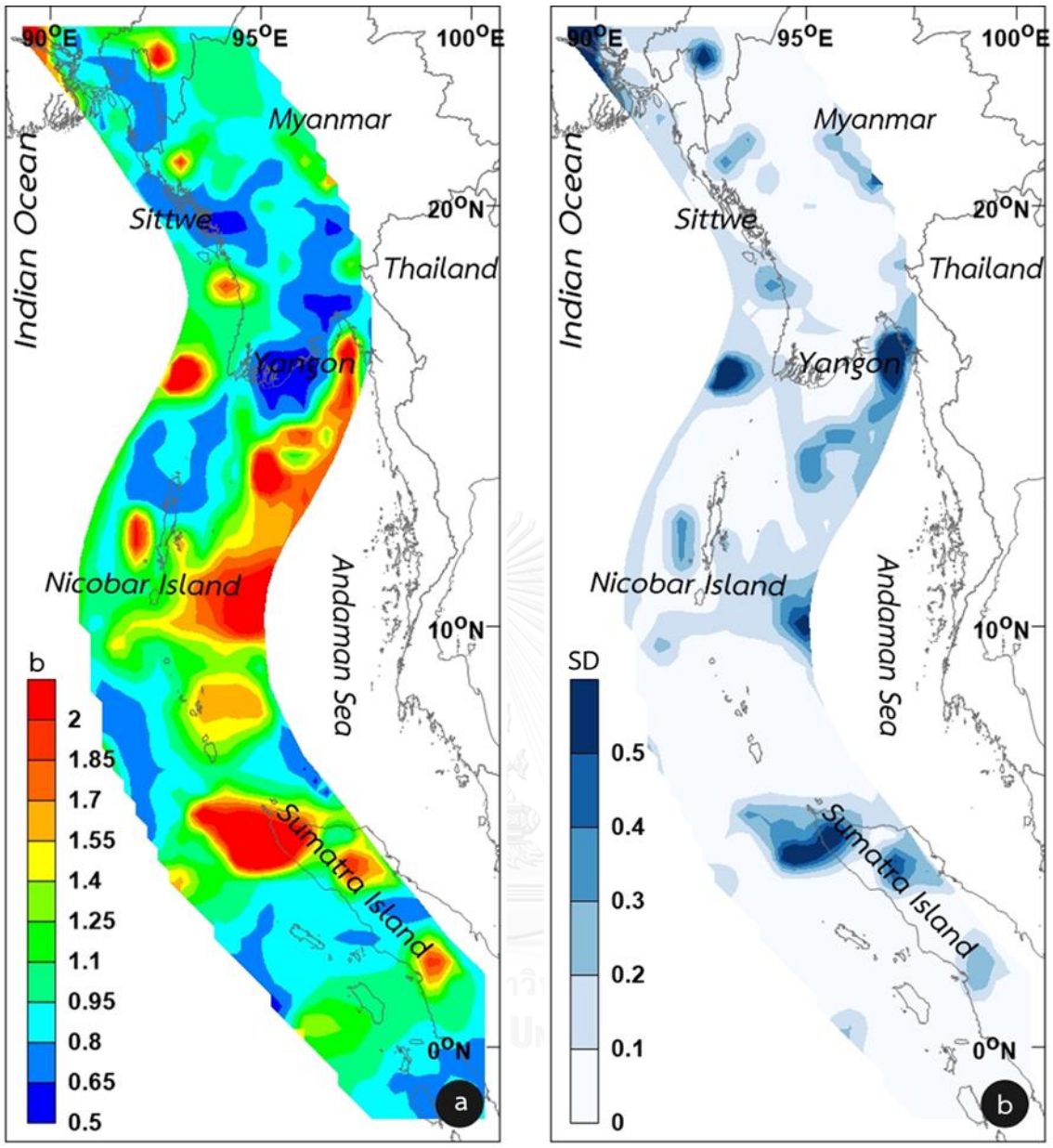
90°E
95°E
100°E
Myanmar
Indian Ocean
Sittwe
20°N
Thailand
Yangon
Nicobar Island
Andaman Sea
10°N
b
2
1.85
1.7
1.55
1.4
1.25
1.1
0.95
0.8
0.65
0.5
Sumatra Island
0°N
a
SD
0.5
0.4
0.3
0.2
0.1
0
b

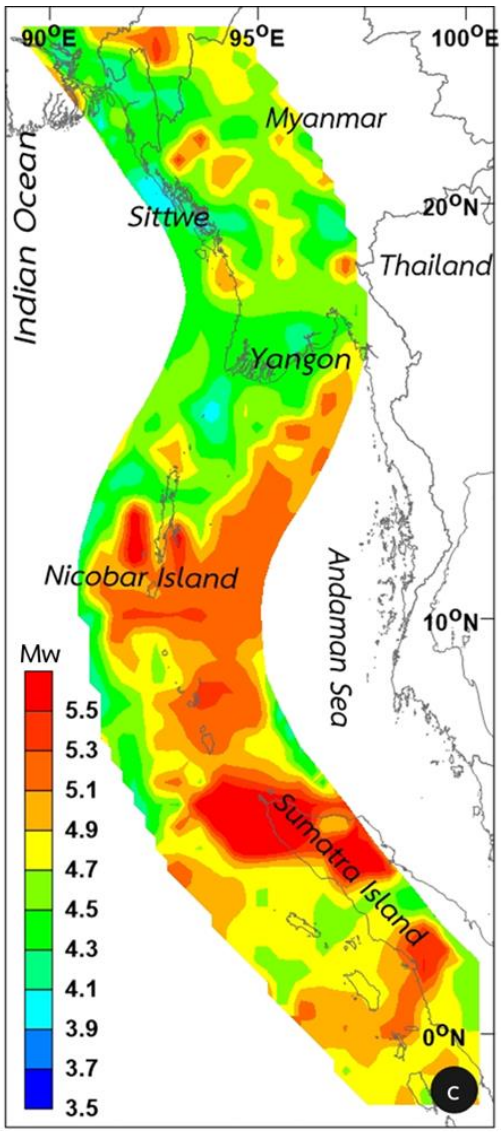

Figure5.8 The SASZ map of before declustering data indicates the distribution of (a) b value, (b) SD value, and (c) Mc.

- The result of after declustering data

After that, we analyzed FMD equation from after declustering data of four case study areas, as mentioned previously (Figure 5.9). It has been slightly provided different results from non-declustering data. Such as, b value of SASZ ranged from 0.2 to 2.0. The most anomalous low b value is located on offshore of Sumatra Island, which means it is the high-risk hazardous area (Figure 5.10a). The SD of the study area is presented in Figure 5.10b, which is <0.2. The low SD indicates high accurate and precise

result. Lastly, according to Figure 5.10c, Mc value is between 3.5 and 5.5, which equals to the value before declustering.

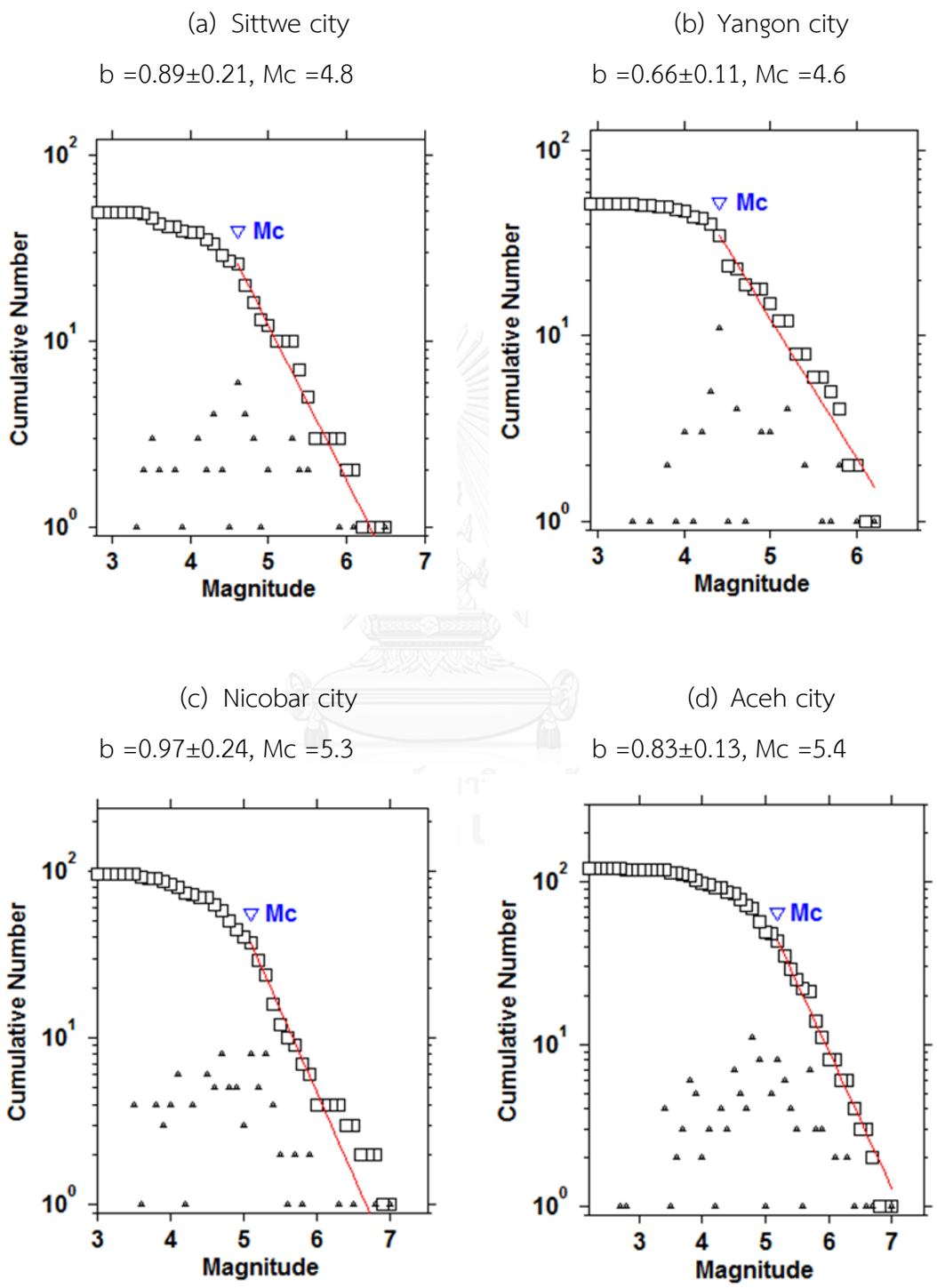

Figure5. 9 The graph showing FMD relation of specific areas along the SASZ after declustering data.

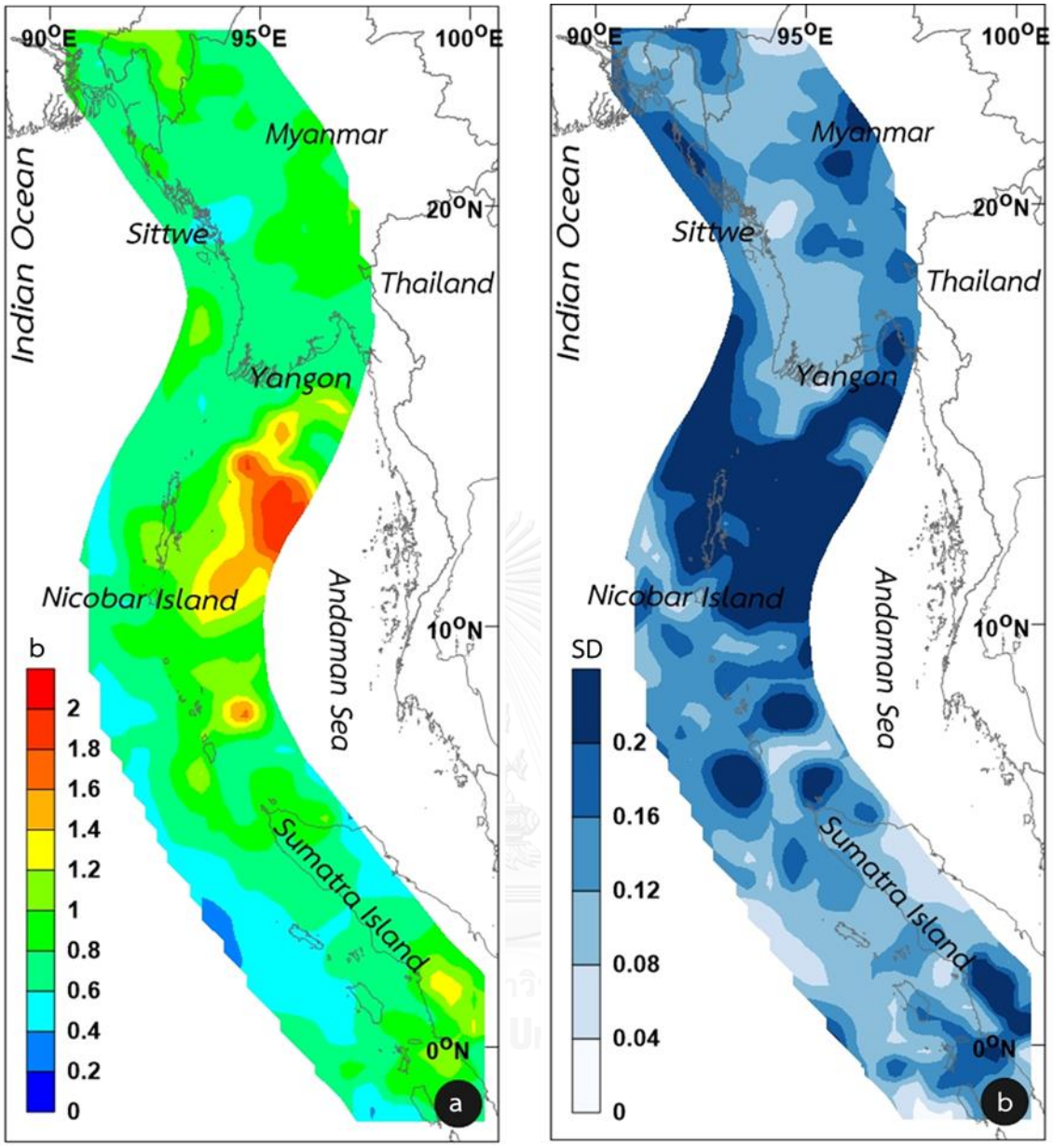
90°E
95°E
100°E
Myanmar
20°N
Sittwe
Thailand
Indian Ocean
Yangon
Nicobar Island
Andaman Sea
10°N
b
2
1.8
1.6
1.4
1.2
1
0.8
0.6
0.4
0.2
0
Sumatra Island
0°N
a
SD
0.2
0.16
0.12
0.08
0.04
0
b

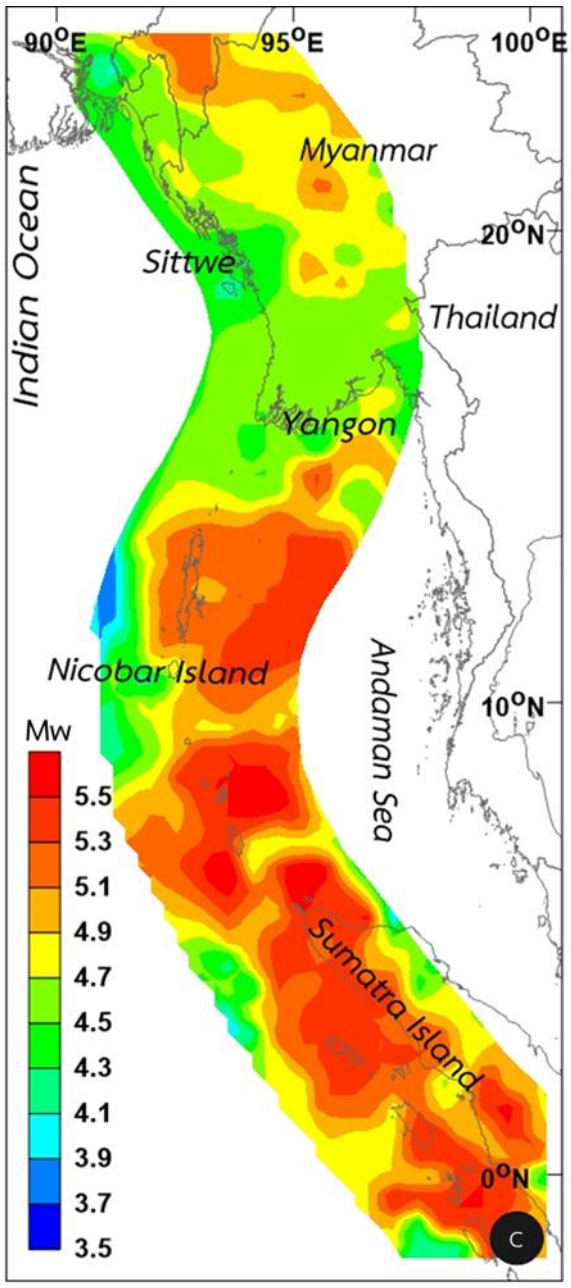

Figure5.10 The SASZ map of after declustering data indicates the distribution of (a) b value, (b) SD value, and (c) Mc.

5.3. Temporal Variation of Fractal Dimension and FMD Parameters (b value)

As we gave a consideration to the large earthquakes, we selected six specific events (Table 5.1). On condition that each event must have more than Mw 8.0. We still divided data set into two groups, which are (i) after declustering and (ii) before

declustering. The area was separated into a grid of 3° spacing or around 300 km. This research is analysed by using fractal dimension (Dc value) and b value.

Table5.1 The 6 case studies which has the magnitude up to Mw 8.0.

event	long	lat	d/m/y	Depth (km)	Mw	EQ number	b	Dc
1	94.26	3.09	26/12/2004	29	9.0	204	0.54	2.24
2	95.98	3.29	26/12/2004	30	8.9	318	0.55	2.24
3	97.07	1.67	28/03/2005	26	8.6	414	0.59	2.24
4	100.99	-3.78	12/09/2007	24	8.5	369	0.88	2.35
5	92.82	2.35	11/04/2012	46	8.6	71	0.45	2.10
6	92.31	0.90	11/04/2012	55	8.2	44	0.37	1.91

5.3.1. The result of before declustering

Firstly, the b value of event 1 continuously decreased range of 0.94 to 0.83, from 1978 to 1993. During 1993 to 2004, the b value remained steadily at approximately 0.83-0.76. Then, the fractal dimension or Dc value was a gradually increase from 1.99-2.16 between 1978 and 1983. Then in 1983-2003, there was a slightly growth in range of 1.99 to 2.24 before it went down to 2.17 in 2004 (Figure 5.11a).

In case of event 2, the b value fluctuated widely in range of 1.20 to 0.84, from 1968 to 1988. Then, it remained fairy at 0.87-0.75 between 1988 and 2004. While in 1968 to 1983, the Dc value fluctuated as well, at range of 1.76 to 2.16. After that, there was a continuously increase from 0.75-0.87, until 2004 (Figure 5.11b).

As regards event 3, the period between 1968 and 1993 indicated a downward fluctuation of b value at 1.35-0.77. Then in 1993-2005, it remained constantly at 0.86-0.77. The Dc value also fluctuated at 1.63-2.18 from 1968-1983 and it continuously increased in range of 2.08 to 1.73 until 2005 (Figure 5.11c).

In the case study 4, In 1973-1998, the b value fell gradually in range of 1.34 to 0.95 from 1973 to 1998. For the following two years, it dramatically dropped to 0.74

and constantly remained until 2007. While the Dc value remained steadily at 1.91-2.16 from 1973 to 2007 (Figure 5.11d).

Next in 1995-2005 of event 5, the b value was fluctuated from 1995 to 2005 at range of 0.89-0.62. From 2005 to 2012, the b value was continuously decreased to 0.79. The fractal dimension, Dc value, was remained steady at 1.99 from 1995 to 2005. The Dc value was continuously decrease on range of 1.58-1.99 from 2005 to 2012 (Figure 5.11e).

Eventually, in 2005-2012 of the case study 6, the b and Dc values were remained steadily in range of 0.67-0.56 and 1.59-1.69, respectively (Figure 5.11f).

(a) Mw 9.0 26/12/2004

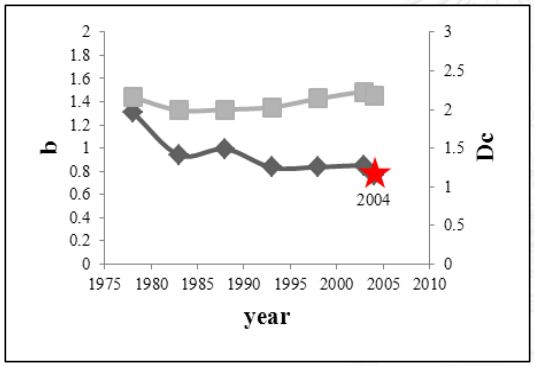

(b) Mw 8.9 26/12/2004

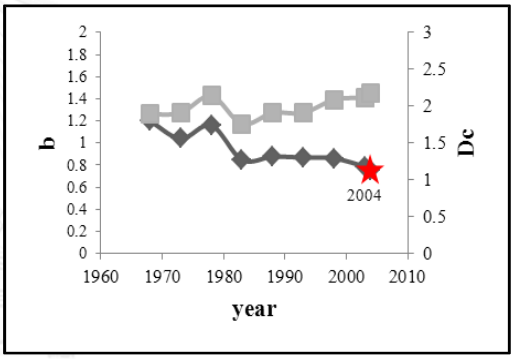

(c) Mw 8.6 28/03/2005

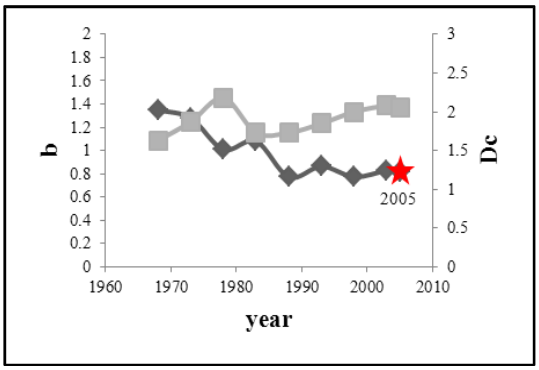

(d) Mw 8.5 12/09/2007

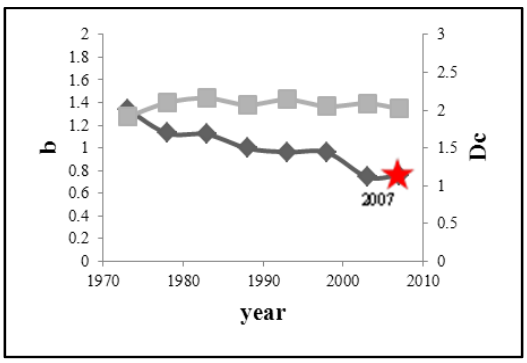

(e) Mw 8.6 11/04/2012 (f) Mw 8.2 11/04/2012

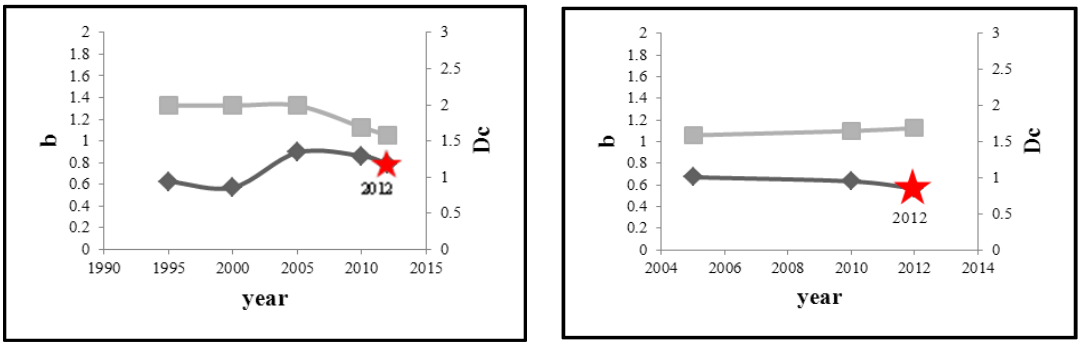

Figure5.11 Showing the before declustering data of 6 case studies which were (a) event 1, (b) event 2, (c) event 3, (d) event 4, (e) event 5 and (f) event 6. Graph showing relationship between b values, Dc values and year in temporal term. The dark grey lines indicate b values and the light grey lines indicate Dc values.

5.3.2. The result of after declustering

First, as illustrated by the graph in Figure 5.12a, the b value of event 1 remained steadily at approximately 0.67 from 1977-2003. Then over the next year, it dropped to 0.59 before the Mw 9.0 earthquake happened in the northern Sumatra-Andaman Island in 2004. The Dc value fluctuated in range of 1.85 to 2.21. Until 1998, it remained at around 2.21.

In the matter of event 2 generated Mw 8.9 aftershock of event 1. In 1988, the b value was 0.93 and continuously decreased to 0.61 in 2004. The Dc value increased from 1.2 to 1.4, in 1988-1993. Then, it remained stable in range of 1.38-2.16 until 2004 (Figure 5.12b).

In case of event 3 which generated Mw 8.6 in the same area of event 1, in 2005. In 1988, the b value was 0.70 and it slightly fell to 0.65 in 2005. There was gradually growth of Dc value from 1988 to 2005 at 1.75-2.26 (Figure 5.12c).

Next, the event 4 generated Mw 8.5 in the southern Sumatra-Andaman in 2007. The b value was downward fluctuation in range of 1.28-1.16. It continuously dropped

to 0.91 in 2007. While the Dc value from 1973 to 2007 gradually increase at 1.75-2.95 (Figure 5.12d).

Regarding the event 5, generated Mw 8.6 in the Indian Ocean in 2012. Between 2000 and 2010, the b value was continuously decreased to 0.79-0.54 and dramatically fell to 0.45 in 2012. The Dc value slightly rose in range of 1.98-2.24 between 2000 and 2012 (Figure 5.12e).

Ultimately, the event 6 generated Mw 8.2 earthquake at the same area of event 5 in 2012. In 2000-2010, the b and Dc value were remained steady in range of 0.49-0.47 and 1.69-1.96, respectively. After that, before 2012 earthquake, the b value was dramatically decreased to 0.36, whereas, the Dc value increased to 1.92 (Figure 5.12f).

(a) Mw 9.0 26/12/2004

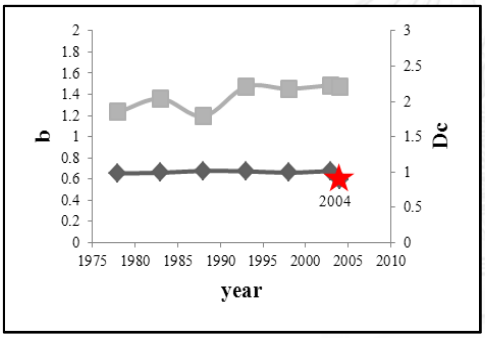

(b) Mw 8.9 26/12/2004

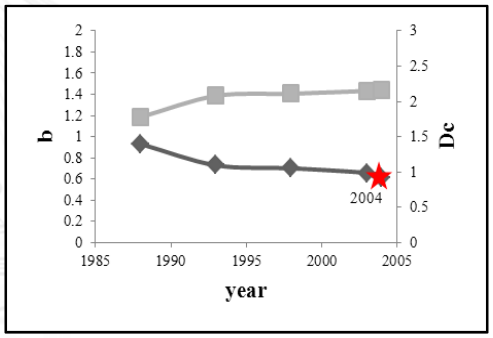

(c) Mw 8.6 28/03/2005

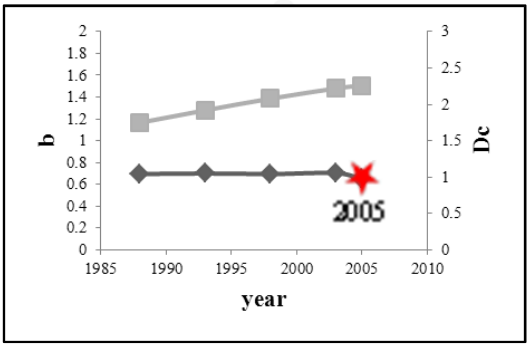

(d) Mw 8.5 12/09/2007

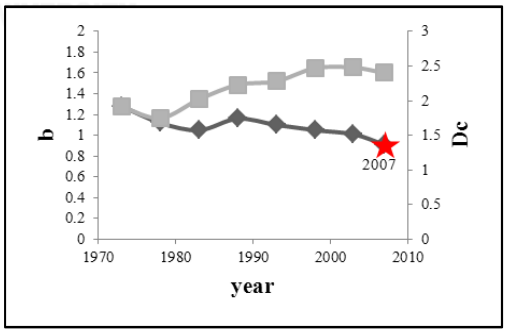

(e) Mw 8.6 11/04/2012

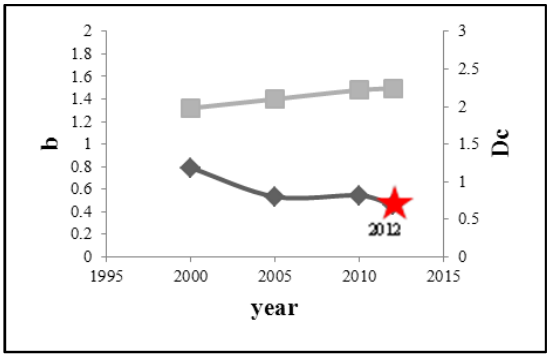

(f) Mw 8.2 11/04/2012

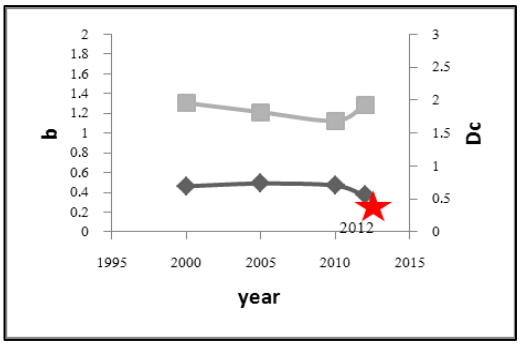

Figure5.12 The graphs of 6 case studies showing the relationship between b value, Dc value and year in the temporal term after declustering data, which were (a) event 1, (b) event 2, (c) event 3, (d) event 4, (e) event 5 and (f) event 6. The dark grey lines indicate b value and the light grey lines indicate Dc value.

จุฬาลงกรณ์มหาวิทยาลัย
Chulalongkorn University

CHARPTER VI
DISCUSSION

In order to confirm that the focal mechanism indicates mechanism of fault rupture and the fractal dimension indicates seismic pattern along the SASZ. In this chapter, the results in previous chapters were considered with each other and comparing with the previous researches which corresponded to this study.

6.1. Earthquake Magnitude Conversion

From the convert earthquake data, The process began with the development of relationships between these different magnitude scales and converted them to the standard Mw . This research was converted Mb scale to the standard Mw. It shows the equation, $Mw = 0.18mb^2 - 1.00mb + 5.60$, $R^2 = 0.78$. It was converted Ml scale to Mw scale which is showing the equation, $Mw = 0.07Ms^2 - 0.17Ms + 4.41$, $R^2 = 0.90$ (Figure 6.1). However, we studied the other previous research. They are convert magnitude same as this research. For example, Sukrungsri and Pailoplee, 2015 was converted Mb and Ms to the standard Mw. The equation is $Mw = 0.19mb^2 - 0.95mb + 5.19$, $R^2 = 0.76$ and $Mw = 0.08mb^2 - 0.17mb + 4.31$, $R^2 = 0.93$, respectively (Figure 6.2). And the research of Pailoplee, 2017, He was converted Mb and Ms to Mw scale. It indicate by equation, $Mw = 0.31mb^2 - 2.28mb + 8.78$, $R^2 = 0.77$ and $Mw = 0.11mb^2 - 0.58mb + 5.4$, $R^2 = 0.92$, respectively (Figure 6.3). As the seen that we compare R^2 between this research and previous research, it is close to 1 which is indicates that the equation is conform to data earthquake.

6.2. Cumulative Number of Earthquake

The main purpose of this stage was to remove foreshocks and aftershocks, to get the best possible estimate for the rate of mainshocks that directly indicate the released energy from tectonic stress. Therefore, the data obtained from the previous procedures needed to be decluttered by filtering only main shocks from an enormous number of foreshocks and aftershocks.

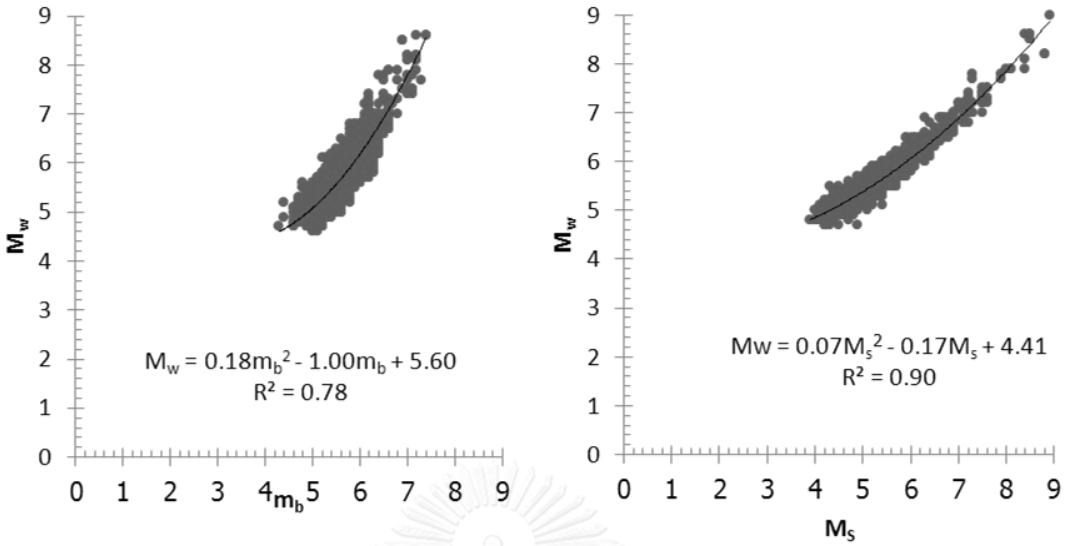

Figure6. 1 Graph is showing to convert Mb and Ms to the standard Mw of this research.

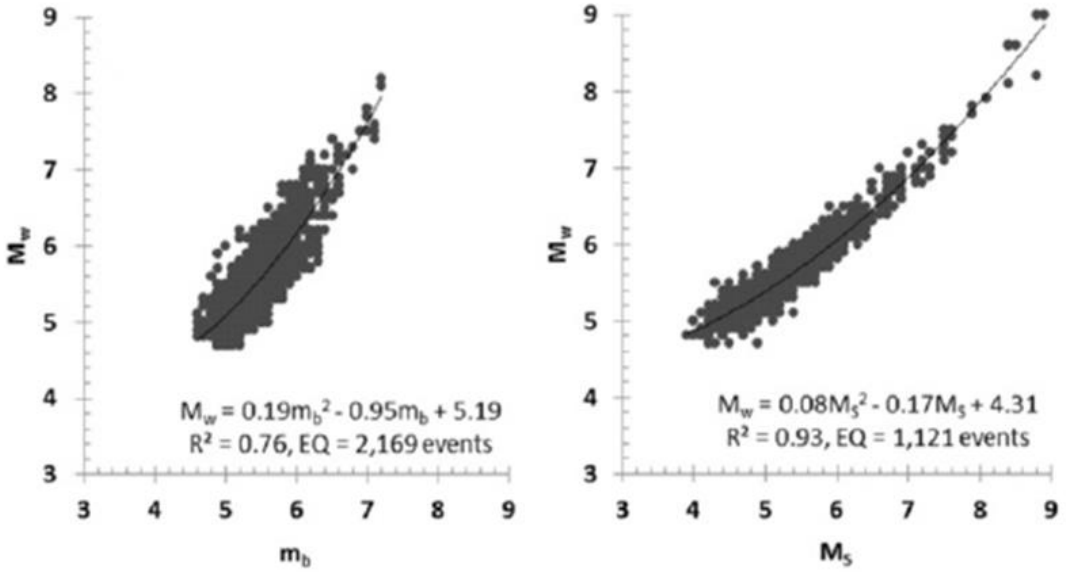

Figure6. 2 Graph is showing to convert Mb and Ms to the standard Mw of Sukrungsri and Pailoplee (2015) (Sukrungsri and Pailoplee, 2015).

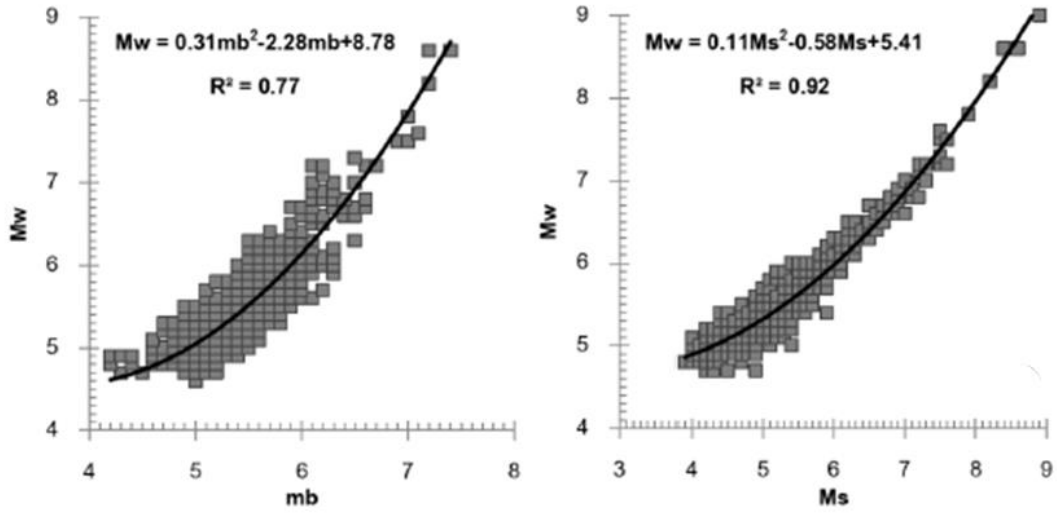

Figure6. 3 Graph is showing to convert Mb and Ms to the standard Mw of Pailoplee (2017) (Pailoplee, 2017).

When we compare between before declustering data and after declustering data, it shows that the cumulative number graph of after declustering data is rather straighter than before declustering. However, we were plotted the both earthquake data. It shows that although before declustering data is not straight because It is not decluster data and manmade. After declustering data is more linear because It is remove foreshock and aftershock. Even though In 2005, It is a few curve but It is straighter than before declustering (Figure 6.4). In addition, we compare with other previous research, i.e., Pailoplee (2017) and Pailoplee el at. (2013) (Figure 6.5). Almost It is linear but we compare between previous research and this research. It shows that the previous research is straighter because It removed foreshock, aftershock and manmade. However, this research, fractal dimension does not need to remove manmade. From Pailoplee (2017) and Pailoplee el at. (2013), It removes foreshock, aftershock and manmade. There are 1,960 and 1,920 events, respectively. This research, It removes foreshock and aftershock but not remove manmade. There are 3,632 events. In summary, this research is more data than other previous research. However, fractal dimension analyses by range1 and range 2. It is not use magnitude data.

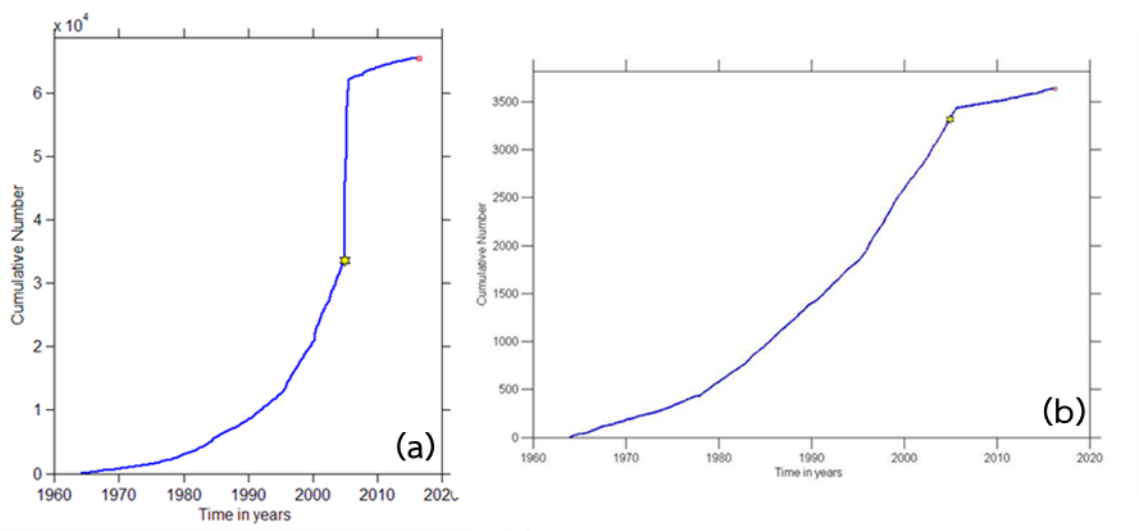

Figure6. 4 The graph is showing the cumulative number of this research. (a) Non-declustering (b) declustering.

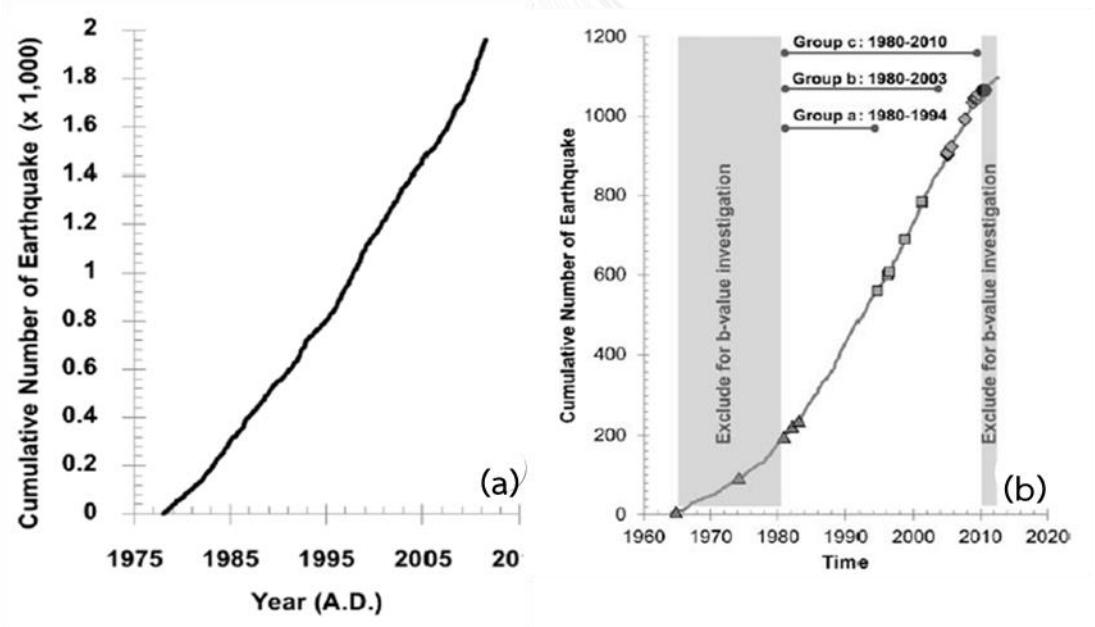

Figure6.5 The graph is showing the cumulative number of this research. (a) Pailoplee (2017) (b) Pailoplee el at. (2013) (Pailoplee, 2017; Pailoplee el at., 2013).

6.3. Focal Mechanism

6.3.1. Strike

Because the focal mechanism is loaded from Harvard moment centroid which are 2 data groups, the choosing a data group, we will observe from the direction of the orientation of the segment that each segment will use the data of any set. In the interplate, we divided into 11 segments along the Sumatran Andaman. According to the direction of the subduction of each segment, we can choose the data group is the first set of 11 segments. It shows in the map is green. The Table 6.1 shows the summary result of strike direction of interplate. (Figure 6.6)

Table6.1 The results of strike of interplate.

Segment no.	Location	Strike of interplate
1.	Sumatra Island	N70W at 70°, S70E – S30E at 110°-150°, N60W at 300°, N40W at 320°
2.	Aceh city	N45W – N23W at 315°-337°
3.	Northern section of Aceh city	N60W at 300°
4.	The upper of no.3 in Andaman Sea	N70W – N45W at 290°-315°
5.	Adjacent to no.4 in Andaman Sea	N45W – N40W at 315°-320°
6.	The bottom of Nicobar Island	S40E – S10E at 140°-170°
7.	Nicobar Island	N55E at 55°
8.	The upper of Nicobar Island	N20E–N30E at 20°-30° S20W–S40W at 200°-220°
9.	Southern Ocean of Rangoon city	N22E at 22°
10.	Rangoon city	N18E at 18°, S90E at 90°, S70E at 110°, S60W at 240°
11.	Southern Ocean of Sittwe	N40W – N30W at 320°-330°

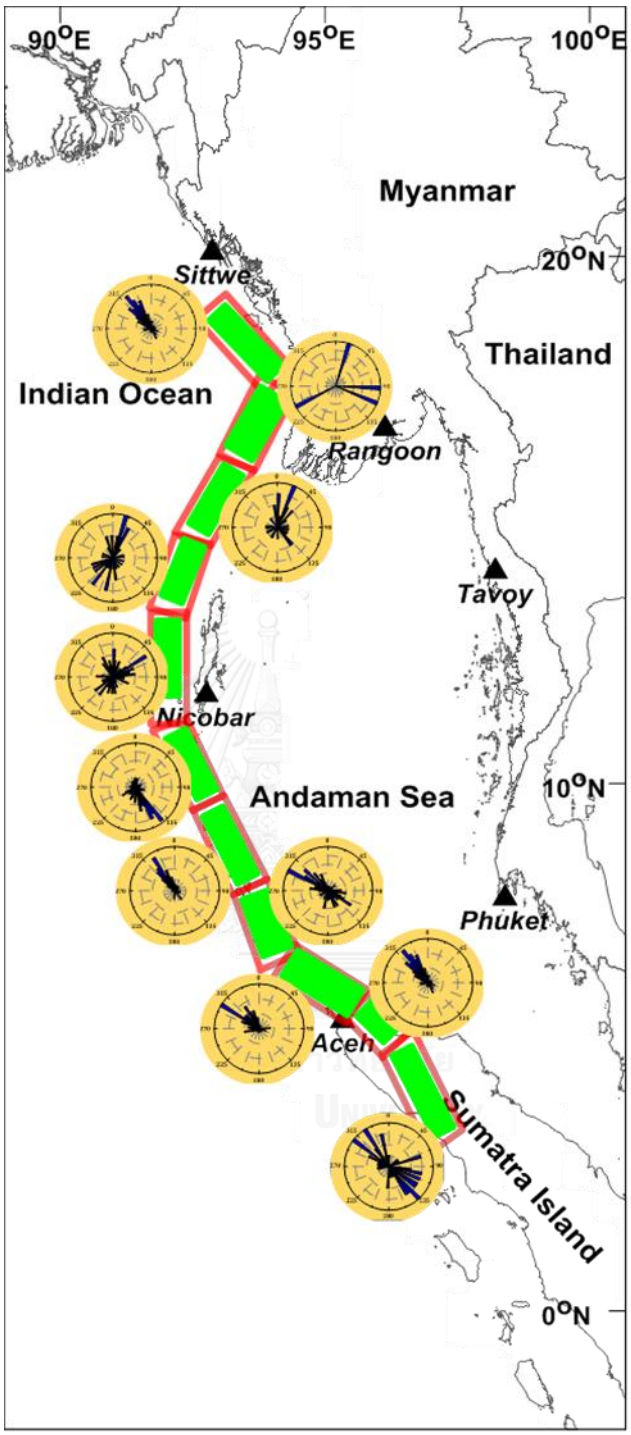

Figure6.6 Showing the results of strike of interplate. The green segment is showing the first data group of strike.

In the intraslab of the direction of subduction, it shows that there are 3 segments that choose the 2nd data group which is segments 4, 9 and 11. It shows in the map is pink. For other segments, we choose the first data group. It shows in the map is green. The Table 6.2 shows the summary result of strike direction of interplate. (Figure 6.7)

Table6.2 The results of strike of intraslab.

Segment no.	Strike of intraslab
1.	N65E at 65°, N80E at 80°, S30W at 210° and N35W at 315°
2.	S70E at 110°
3.	N55W at 305°
4.	N55W – N45W at 305°-315°
5.	N60W – N40W at 300°-320°
6.	N80W at 280°
7.	N at 0°
8.	S75W at 255° and W at 270°
9.	S50W at 230°
10.	N10E at 10°
11.	N70E at 70° and N35W at 325°

จุฬาลงกรณ์มหาวิทยาลัย
Chulalongkorn University

6.3.2. Dip

From choosing strike in the interplate, Strike1 matched with the SASZ. As a result, we choose to study dip1. In the interplate, Dip angle is diverse. From the 11 segments can be grouped into 3 groups. The first group, the dip angle is in the same direction, is 20°-45°. There is 2, 3, 4, 5, 7, 8 and 11 segment. It shows in the map are green. Next, the dip angle is 45°-50° directions. That is segment 1 which shows in the map is blue. However, there are 3 groups which the dip angle is distributed. There is 6, 9 and 10 segment. It shows in the map are yellow (Figure 6.8a). From the different dip angle of each segment, It may be because the accretionary complex of each fault segment is same or different direction. The accretionary complex is sediments which

is the top layer of material on a tectonic plate. It is accumulate and deform where oceanic and continental plates collide. These sediments are scraped off the top of the down going oceanic crustal plate and are appended to the edge of the continental plate (Figure 6.9).

In the intraslab, the dip angle of intraslab can be divided into 3 groups. The first group, the dip angle is 30° directions. There is 1, 3 and 5 segment. It shows in the map are blue. Next, the dip angle is 70°-90° direction. That is segment 9, 10 and 11 which shows in the map are green. The last group, the dip angle is distributed which are 2, 4, 6, 7 and 8 segment. It shows in the map is yellow (Figure 6.8b).

จุฬาลงกรณ์มหาวิทยาลัย
Chulalongkorn University

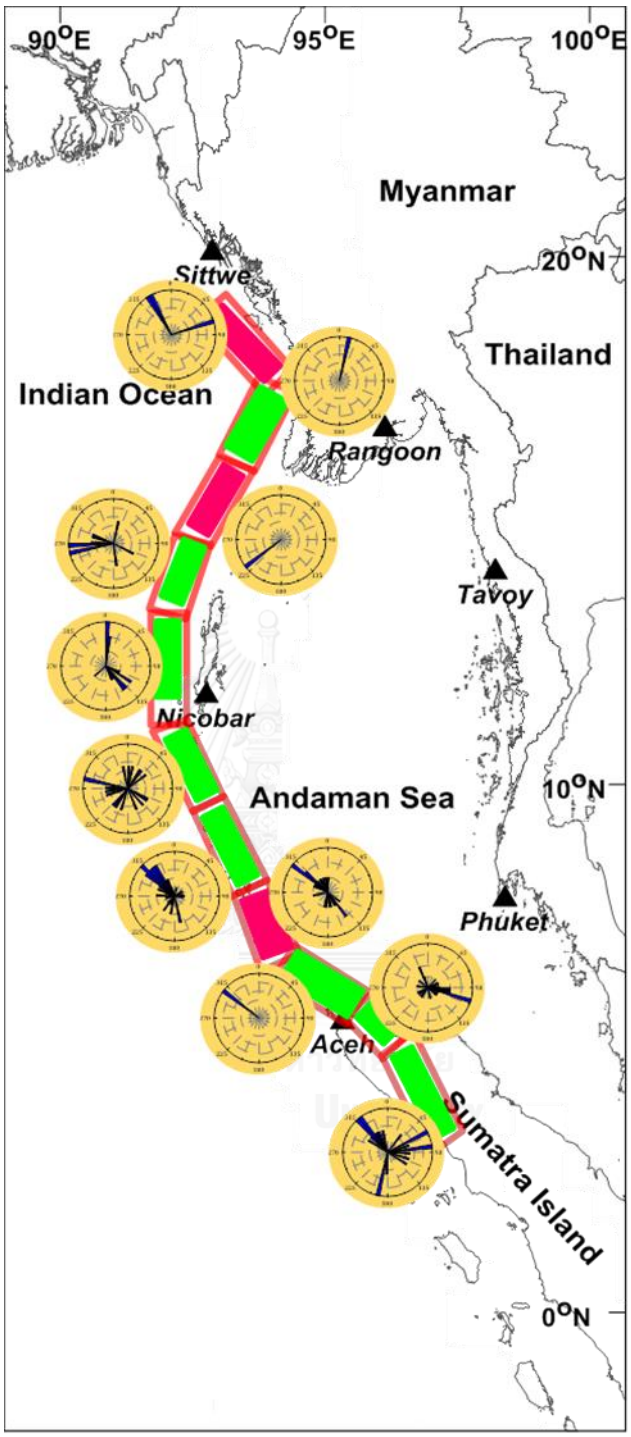

Figure6.7 Showing the results of strike of intraslab. The green segment is showing the first data group of strike. The pink segment is showing the 2nd data group.

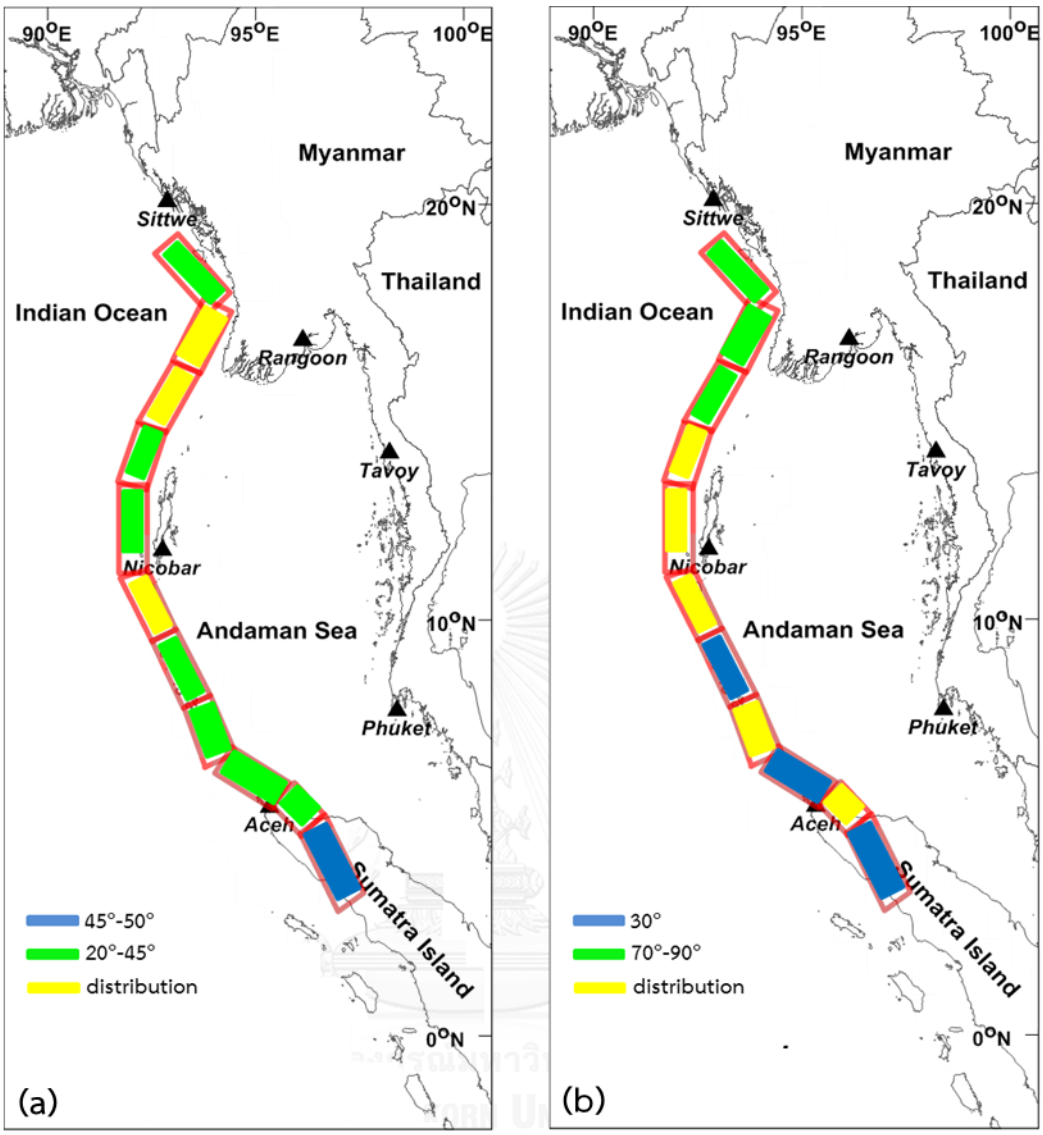

Figure6.8 The map is showing group of dip angle in (a) interplate (b) intraqslab.

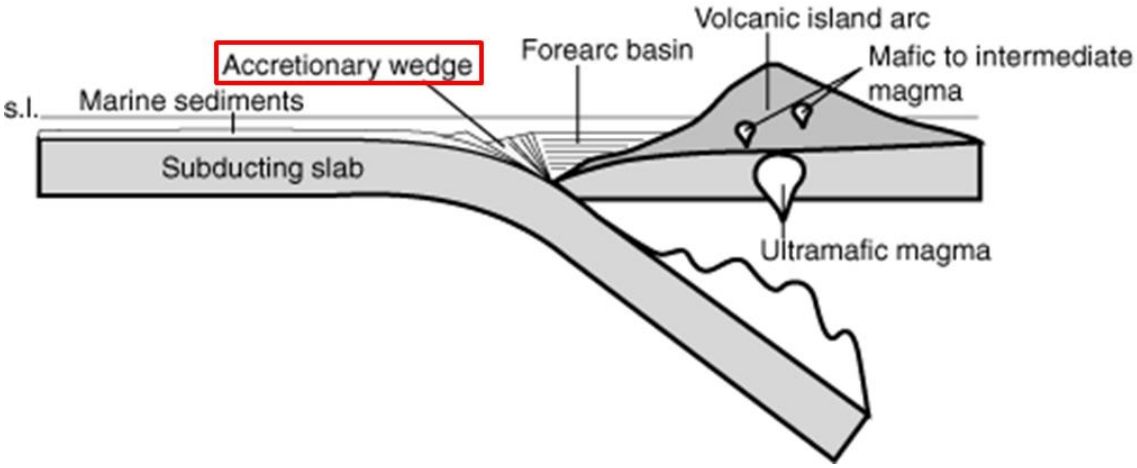

Figure6. 9 Showing the accretionary wedge. It indicates dip angle. The accretionary complex is sediments which is accumulate and deform where oceanic and continental plates collide (www.geol.umd.edu).

6.3.3. Rake

In this research divided the drift faulting into two types which are vertical and horizontal motion. The vertical motion caused a tsunami but the horizontal did not a tsunami. From choosing strike and dip in the interplate, Strike1 and dip1 matched with the SASZ. As a result, we choose to study rake1. It shows that almost the SASZ is vertical motion. It is divided into 8 segments, ie, 1 2 3 4 5 7 8 11 segment. It shows in the map is green. Next, there are 2 segments which is horizontal motion, 6 and 9 segments. It shows in the map is blue. The last, there are 1 segment appearing every motion. It shows in the map is pink (Figure 6.10). This may be due to insufficient data to study. Therefore, the segment is vertical motion which is a hazard zone. The segment is horizontal motion which is a save zone.

In the intraslab, It was generated deep earthquake and large earthquake. It means that when the crust is collapsed, it does not lock whit anything like an interplate and no accumulate energy but It occurs an earthquake. This causes, we want to know about the mechanism of intraslab. This research, we found that almost of drift faulting can be vertical motion. It may be because when the plate is collapsed, it interacts with the convection current. By convection current, the elbows are pulled out until the final slab is absent which is extension (Figure 6.12). The pull of convection current

causes vertical motion. It shows in the map is green. But there are two segments which are horizontal motion. That is 6, 10 segment. It shows in the map is blue (Figure 6.11). The relate with previous research of Myhill, 2013, he studied focal mechanism of deep earthquake in the Marianas slab, In chapter II. Almost of the focal plane solution was vertical motion but there are some drift faulting of horizontal motion.

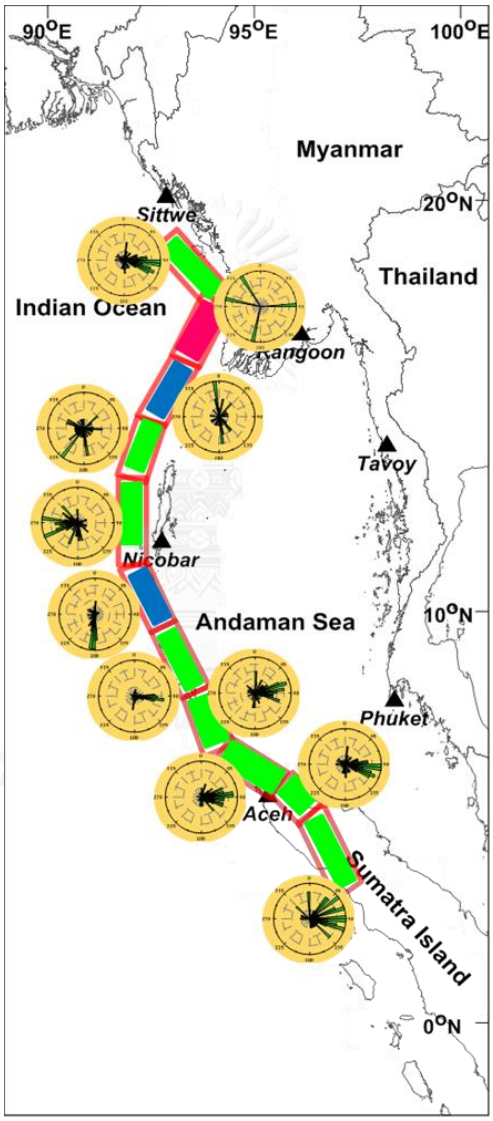

Figure6.10 Showing the results of rake of interplate. The green segment indicates vertical motion. The blue segment indicates horizontal motion. The pink segment indicates distribution motion.

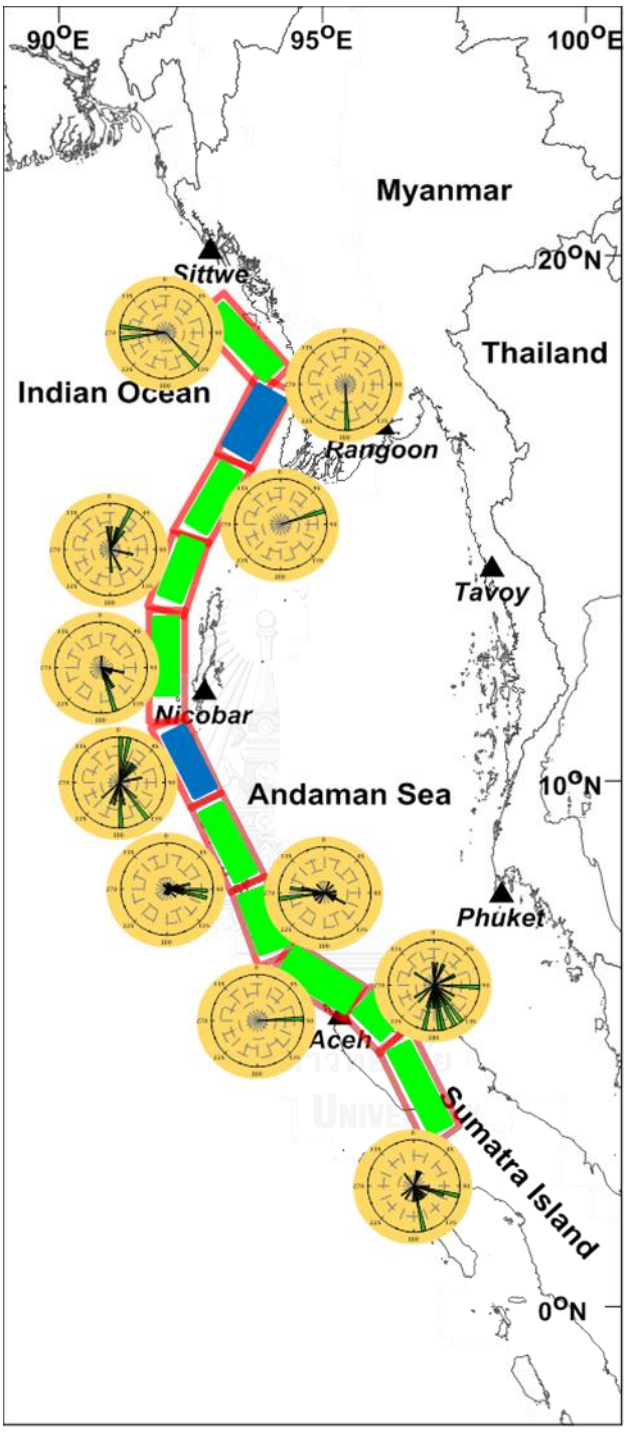

Figure6.11 Showing the results of rake of intraslab. The green segment indicates vertical motion. The blue segment indicates horizontal motion.

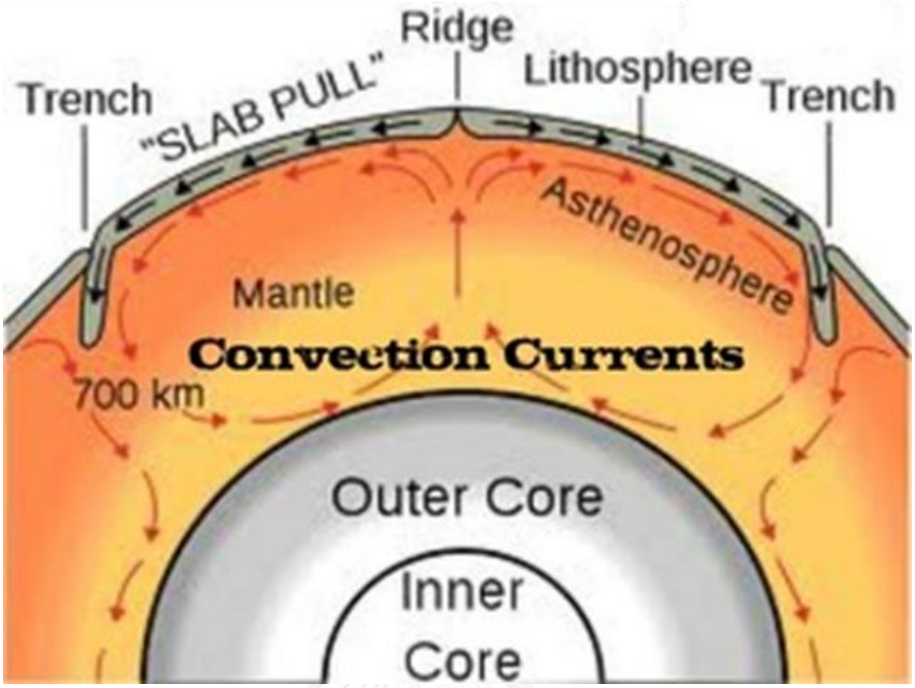

Figure6.12 Showing the convection current. By convection current, the elbows are pulled out until the final slab is absent which is extension. The pull of convection current causes vertical motion (Planet Earth).

6.3.4. Relate with the risk area

Due to the tsunami, there are two factors which are (i) magnitude earthquake, 7 up (ii) drift faulting which is vertical motion. The great earthquake occurred in the past. Such as, In 2004, the SASZ was generated the great earthquake, Mw 9.2. It caused a tsunami disaster which was damaged Thailand. The drift faulting of the plate is a vertical motion. From Figure 6.13, It shows mechanism of fault rupture which is pink beach ball (Lay et al., 2005). In 2012, It was generated the great earthquake, Mw 8.6 and 8.2. It did not a tsunami because the drift faulting of the plate is a horizontal motion. From Figure 6.14, It shows mechanism of fault rupture which is green beach ball (Duputel et al., 2012). Therefore, we can summery that the vertical motion caused a tsunami but the horizontal did not a tsunami.

However, in a research article by Pailoplee et al. (2013) who applied b value analysis, he studied the risk area of earthquake in the SASZ. It showed the three obvious anomalous low b value areas which are (i) the southward offshore region of

the Nicobar Islands (ii) the offshore area north of the Nicobar Islands and (iii) the West coast of Myanmar. However, this research studies mechanism of fault rupture (focal mechanism) in the SASZ. So, we relate between risk area of earthquake map (Figure 6.15a) and focal mechanism map (Figure 6.15b). It shows that there are three risk areas are vertical motions which are (i) the southward offshore region of the Nicobar Islands, It indicates reverse motion (ii) the offshore area north of the Nicobar Islands, It indicates oblique motion and (iii) the West coast of Myanmar, It indicates normal motion.

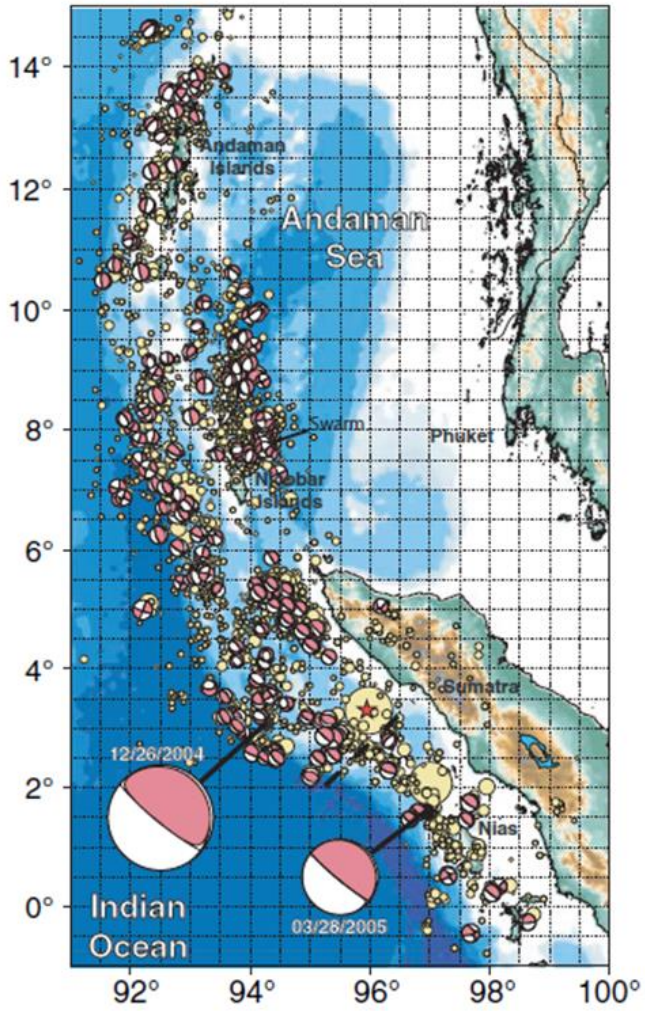

Figure6.13 Map showing mainshock and aftershock in the SASZ of December 26th 2004 earthquake event. The focal mechanism (pink beachball) indicates thrust motion (Lay et al., 2005).

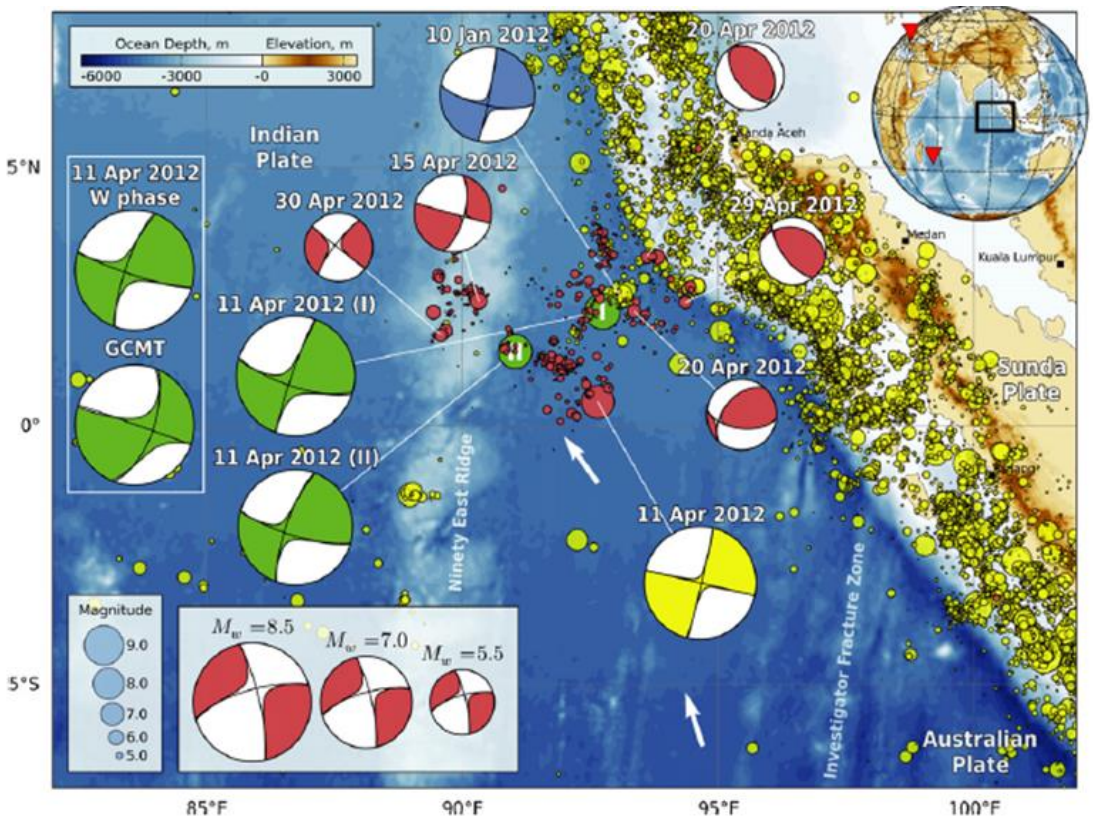

Figure6.14 Map of the 2012 Sumatra great earthquake region of April 11st 2012. The mainshock shows green mechanisms. The foreshock shows blue mechanism. The aftershock shows yellow and red mechanism (Duputel et al., 2012).

จุฬาลงกรณ์มหาวิทยาลัย
Chulalongkorn University

6.4. Fractal Dimension (Dc value) and B value

6.4.1. Temporal variation

This research, we divide into 2 groups data which are (i) before declustering and (ii) after declustering. From the result in Figure 5.11 and 5.12 in chapter V, It indicates that before declustering data is better than after declustering data because before declustering data is more variable than after drclustering data. It means that after decclustering data is meaningless. From Nuannin el at. (2012) and Cao and Gao (2002), the b value is decrease continuously (Figure 6.16). It indicates that the stress in area is the stress is high which can be the risk area of earthquake in the future. From the Figure 6.16 and 5.11, the b value is decrease continuously before occurring the

great earthquake. Therefore, the b value can be precursor. In part of Dc value, It is fluctuation. So, It cannot be precursor.

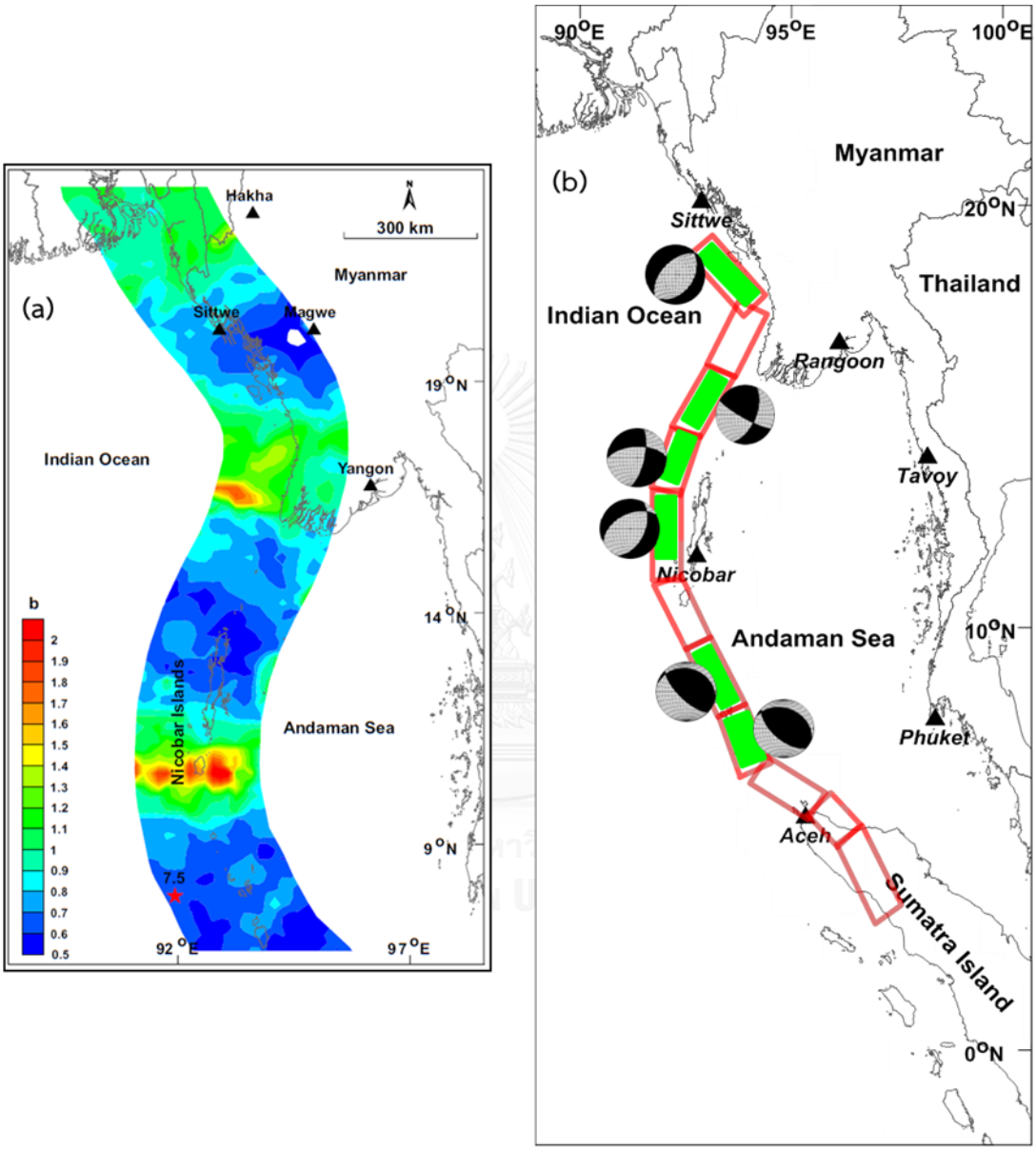

Figure6. 15 Map showing relate between (a) risk area of earthquake map and (b) focal mechanism map. It shows that there are three risk areas are vertical motion (Pailoplee et al., 2013).

6.4.2. Dc value and b value relationship of temporal term

From temporal variation of Dc value and B value, we focus the result of before declustering data because before declustering data is more variable than after drclustering data and the result of before declustering can be precuesor.

The Dc/b ratio has been suggested as an effective indicator of seismic hazards (Bayrak and Bayrak 2011; 2012). The Dc/b can either be a positive or negative correlation. For example, Bayrak and Bayrak (2012) examined this study at Western Anatolia and the relationship of b and Dc was negative correlation (Figure 6.18). Ozture (2012) studied the Turkish earthquake and the correlation of b and Dc was negative (Figure 6.19). This research, we analyzed relationship between Dc value and b value of before declustering data (Figure 6.17) of six specific events, as already stated above. The results give a conclusion that the b value and Dc value relationships of all case studies are negative (Table 6.3).

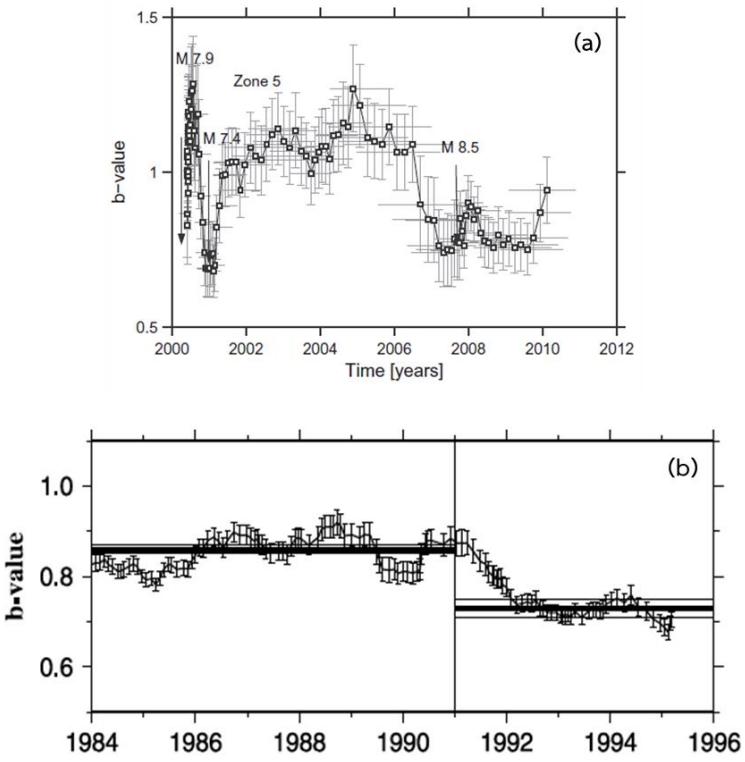

Figure6. 16 Graph showing relationship between b values, Dc values and year in temporal term. (a) (Nuannin et al., 2012) (b) (Cao and Gao, 2002) and Gao,

2002. The b value is decrease continuously before occurring the great earthquake. The b value can be precursor (Nuannin el at., 2012; Cao and Gao, 2002).

Table6.3 Showing b value and Dc value relationship of 6 events

event	Before		
	Dc/b	r^2	relation
1	Dc = -0.76b + 2.73	0.69	negative
2	Dc = -0.15b + 2.13	0.02	negative
3	Dc = -0.38b + 2.27	0.20	negative
4	Dc = -0.12b + 2.19	0.10	negative
5	Dc = -0.62b + 2.31	0.20	negative
6	Dc = -2.15b + 3.03	0.89	negative

(a) Mw 9.0 26/12/2004

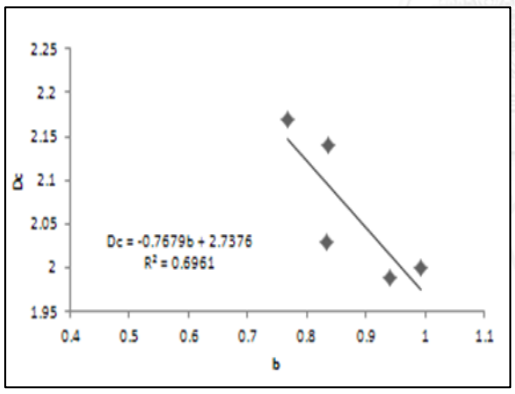

(b) Mw 8.9 26/12/2004

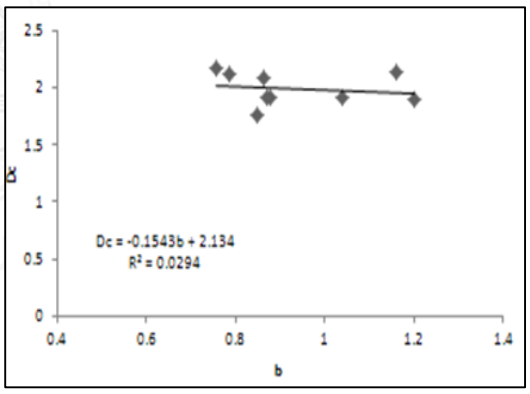

(c) Mw 8.6 28/03/2005

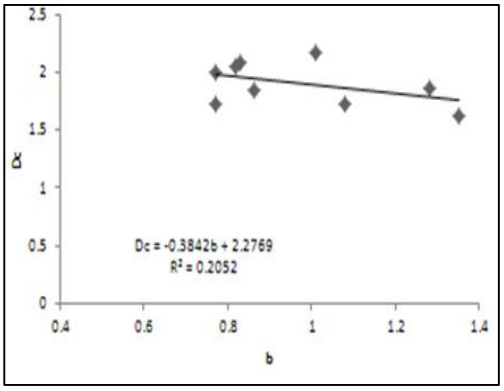

(d) Mw 8.5 12/09/2007

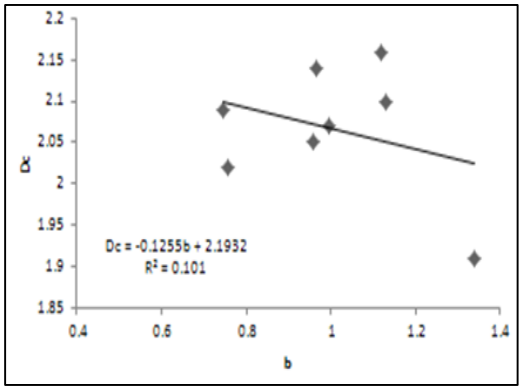

(e) Mw 8.6 11/04/2012

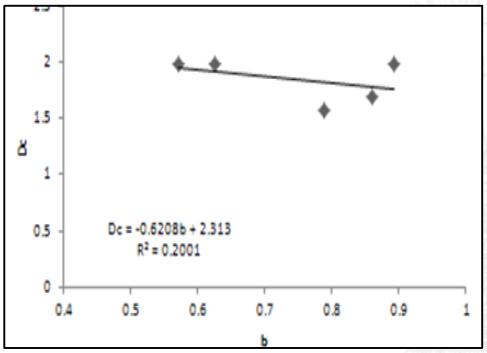

(e) Mw 8.2 11/04/2012

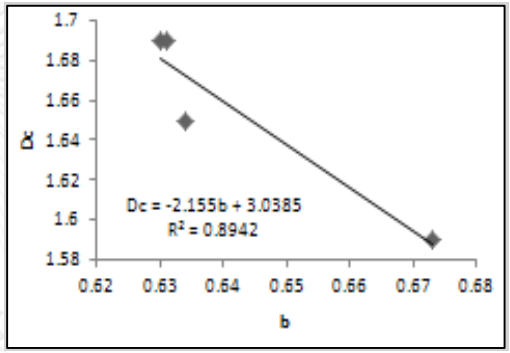

Figure6.17 The graphs showing relationship between Dc value and b value of 6 specific events (before declustering data). The Dc/b relationship of overall area is negative.

จุฬาลงกรณ์มหาวิทยาลัย
Chulalongkorn University

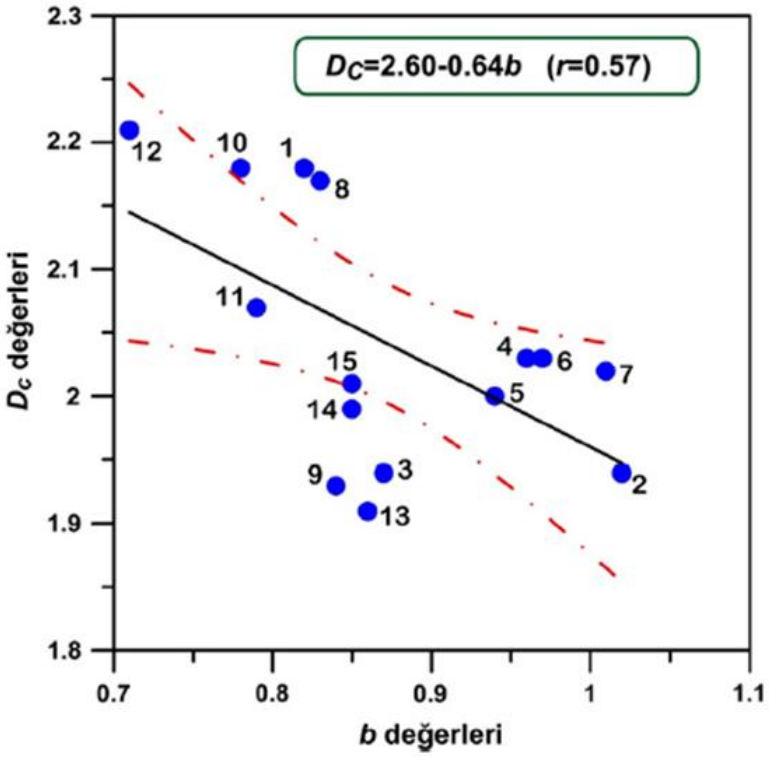

Figure6. 18 The graphs showing relationship between Dc value and b value of Bayrak and Bayrak (2012). The Dc/b relationship is negative (Bayrak and Bayrak, 2012).

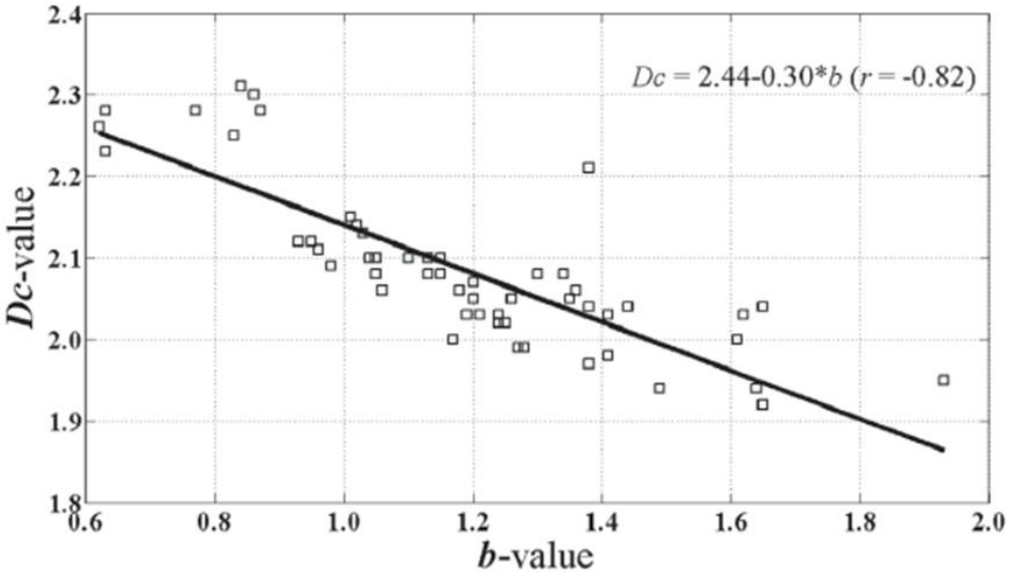

Figure6.19 The graphs showing relationship between Dc value and b value of Ozture (2012) in temporal term. The Dc/b relationship is negative (Ozturk, 2012).

6.4.3. Spatial variation

Because of discussion of temporal term, before declustering data is better than after declustering data, we focus before declustering data. However, from a research article by Aki (1981), he observed to characterize a pattern of seismic system. As we mentioned before in Chapter II, if a Dc value closes to 3, it can signify that fractures are filling up a volume of the crust. A value closes to 2, implies that a plane is filling up and a value closes to 1 means its predominant feature is line sources. Refer to this information; most of characteristic of fault system in this study area is a plane. However, some areas, such as, offshore of Sumatra Island to southern of Nicobar Island, is a volume of the crust. Thus, the seismic patterns of earthquake are plane and volume, which shows the similar of distribution earthquake in spatial and depth terms (Figure 6.20b).

From the comparison between b value map and seismic pattern map, It shows that the anomalous of low b value are Yangon and Sittwe city of Myanmar. The low b value is around 0.5-0.65 (Figure 6.20a). The seismic pattern of area is the low b value which is plane.

จุฬาลงกรณ์มหาวิทยาลัย
Chulalongkorn University

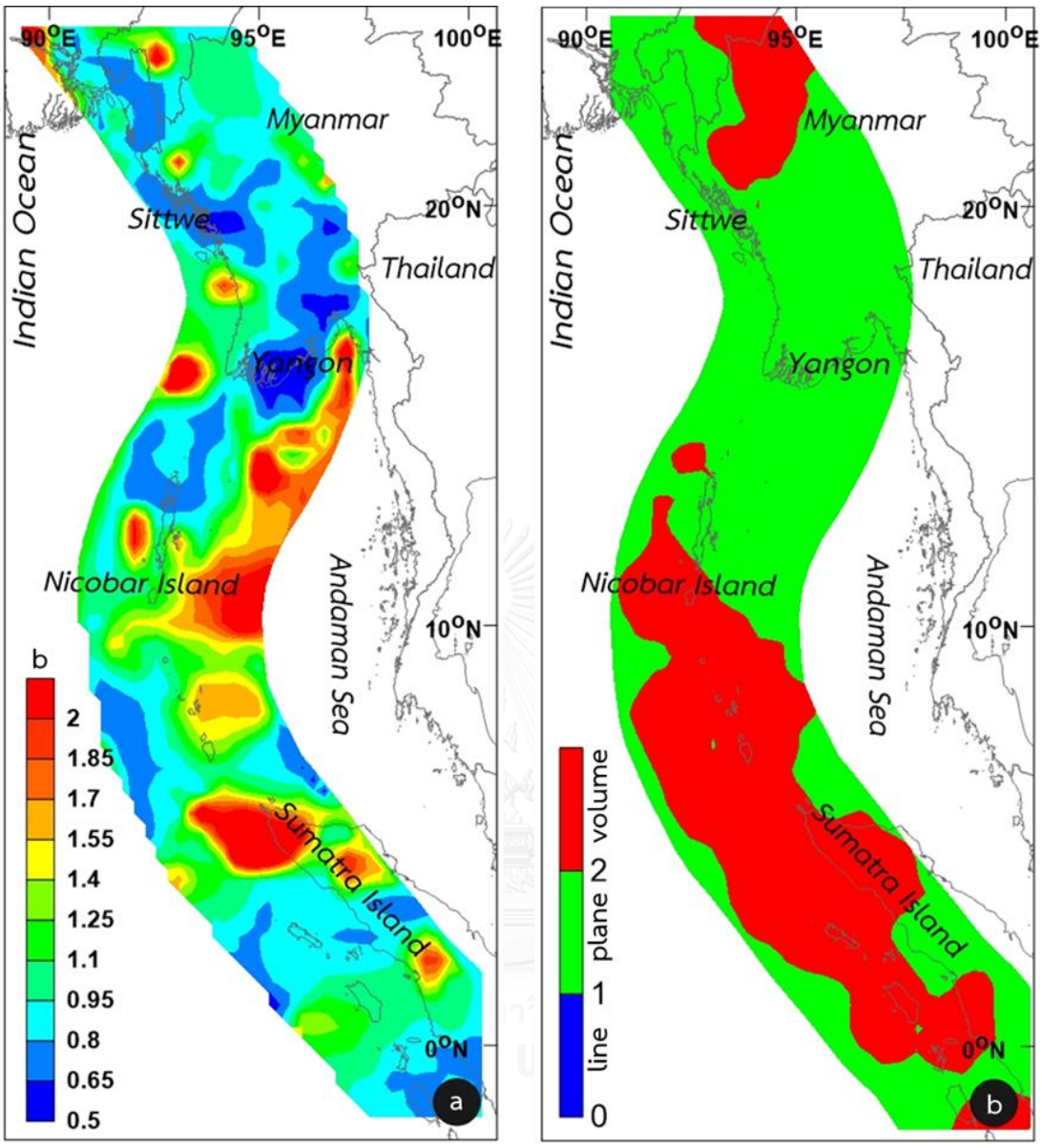

Figure6.20 The SASZ map of before declustering data indicates (a) b value (b) the seismic pattern.

6.4.4. Dc value and b value relationship of spatial term

From the Figure 6.21, we found the Dc value and b value relationship of spatial term. It indicates relation by $Dc = -0.07b^2 + 0.23b + 1.76$. The along SASZ, the b value and Dc value relationships is negative. It means that the cumulative of stress is increase and Dc value is decrease. The same as other previous research is Barton el at. (1999).

He found the Dc value and b value relationship of earthquakes at Long Valley caldera, California. The b value and Dc value relationships is negative (Figure 6.22).

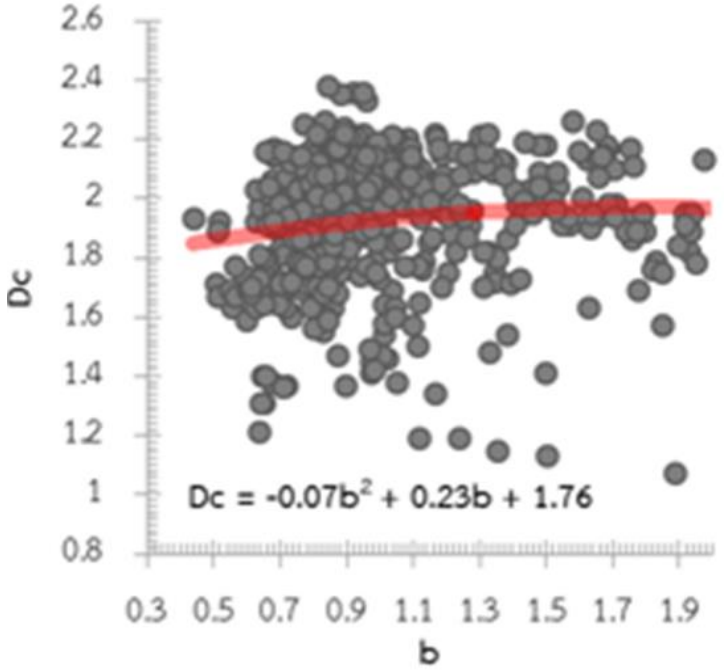

Figure6. 21 The graphs showing relationship between Dc value and b value of spatial term (before declustering data). The Dc/b relationship is negative.

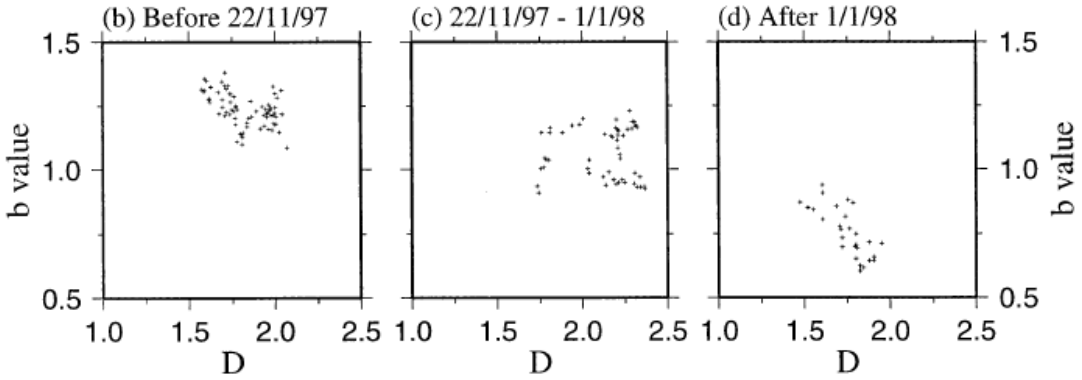

Figure6. 22 The graphs showing relationship between Dc value and b value of Barton el at. (1999) in spatial term. The Dc/b relationship is negative (Barton el at., 1999).

CHARPTER VII
CONCLUSION AND RECOMMENDATION

7.1. Conclusion

This study attempt to investigate the mechanism of fault rupture and seismic pattern along the SASZ by using both focal mechanism and fractal dimension method, respectively. The obtained results lead to the conclusion as follows;

7.1.1. Earthquake Magnitude Conversion

From the convert earthquake data to the standard Mw, we compare R^2 between this research and previous research. It is close to 1 which is indicates that the equation is conform to data earthquake.

7.1.2. Cumulative Number of Earthquake

The cumulative number graph of after declustering data is rather straighter than before declustering because It is remove foreshock and aftershock but not remove manmade. There are 3,632 events. In summary, this research is more data than other previous research. However, fractal dimension analyses by range1 and range 2. It is not use magnitude data.

7.1.3. Focal Mechanism

- Strike

In the interplate, we can choose the data group is the first set of 11 segments. In the intraslab, there are 3 segments that choose the 2nd data group. For other segments, we choose the first data group.

- Dip

From choosing strike in the interplate, Strike1 matched with the SASZ. As a result, we choose to study dip1. In the interplate, the dip angle average of the 8 segments is around 45° and 3 segments which the dip angle is distributed. In the intraslab, dip angle of intraslab are steep and oblique but 5 segments which the dip angle is distributed.

จุฬาลงกรณ์มหาวิทยาลัย
Chulalongkorn University

- Rake

From choosing strike and dip in the interplate, Strike1 and dip1 matched with the SASZ. As a result, we choose to study rake1. The interplate of along the SASZ, there are 8 segments is vertical motion. There are 2 segments which is horizontal motion. In the intraslab, almost of drift faulting can be vertical motion. But there are two segments which are horizontal motion.

- Relate with the risk area

In this research, we relate between risk area of earthquake map by Pailoplee et al., 2013 and focal mechanism map**.** It shows that three risk areas are vertical motions which are (i) the southward offshore region of the Nicobar Islands, It indicates reverse motion (ii) the offshore area north of the Nicobar Islands, It indicates oblique motion and (iii) the West coast of Myanmar, It indicates normal motion.

7.1.4. Fractal Dimension (Dc value) and B value

- Temporal variation

The b value is decrease continuously before occurring the great earthquake. Therefore, the b value can be precursor. In part of Dc value, It is fluctuation. So, It cannot be precursor.

- Dc value and b value relationship of temporal term

This research, we analyzed relationship between Dc value and b value of before declustering data. The b value and Dc value relationships of the SASZ is negative.

- Spatial variation

Because of discussion of temporal term, before declustering data is better than after declustering data. So, we focus before declustering data. It shows that the seismic patterns of the SASZ are plane and volume, which shows the similar of distribution earthquake in spatial and depth terms. From the comparison between b value map and seismic pattern map, the seismic pattern of area is the low b value which is plane.

- Dc value and b value relationship of spatial term

The b value and Dc value relationships is negative. It means that the cumulative of stress is increase and Dc value is decrease.

7.2. Recommendation

7.2.1. Focal mechanism

In the interplate, we know that the moment of another segment is dip slip or strike slip. In the future, It could be to study focal mechanism of small earthquake in the risk area for observing the focal mechanism which are many motion or alike motion. In the part of intraslab, this research studies basic of the convection current. More people are interested to study in the part of solid earth geophysics. Such as rheology of the earth.

7.2.2. Fractal dimension

In the temporal term, the Dc value is cannot be precursor. It may be not enough data. In the future, If there is enough information. You can study for confirmation that the Dc value is can precursor. In the spatial term, almost of the seismic pattern in the SASZ is plane. However, we cannot found the relation between plane pattern and tectonic activity. So, in the future, It could be to found the relation between seismic pattern and tectonic activity.

จุฬาลงกรณ์มหาวิทยาลัย
Chulalongkorn University

REFERENCES

Aki, K., 1981. A probabilistic synthesis of precursory phenomena. Earthquake Prediction: 566-574.

Asano, Y. et al., 2011. Spatial distribution and focal mechanisms of aftershocks of the 2011 off the Pacific coast of Tohoku Earthquake. Earth, planets and space, 63(7): 29.

Bayrak, Y. and Bayrak, E., 2012. Regional variations and correlations of Gutenberg–Richter parameters and fractal dimension for the different seismogenic zones in Western Anatolia. Journal of Asian Earth Sciences, 58: 98-107.

Bhattacharya, P.M. and Kayal, J., 2003. Mapping the b-value and its correlation with the fractal dimension in the northeast region of India. Geological Society of India, 62(6): 680-695.

Bhattacharya, P.M., Majumdar, R. and Kayal, J., 2002. Fractal dimension and b-value mapping in northeast India. Current Science: 1486-1491.

Cao, A. and Gao, S.S., 2002. Temporal variation of seismic b□values beneath northeastern Japan island arc. Geophysical research letters, 29(9).

DeMets, C., Gordon, R.G., Argus, D.F. and Stein, S., 1994. Effect of recent revisions to the geomagnetic reversal time scale on estimates of current plate motions. Geophysical research letters, 21(20): 2191-2194.

Duputel, Z. et al., 2012. The 2012 Sumatra great earthquake sequence. Earth and Planetary Science Letters, 351: 247-257.

Gardner, J. and Knopoff, L., 1974. Is the sequence of earthquakes in Southern California, with aftershocks removed, Poissonian? Bulletin of the Seismological Society of America, 64(5): 1363-1367.

Gutenberg, B. and Richter, C.F., 1944. Frequency of earthquakes in California. Bulletin of the Seismological Society of America, 34(4): 185-188.

Habermann, R.E., 1987. Man-made changes of seismicity rates. Bulletin of the Seismological Society of America, 77(1): 141-159.

Hirata, T., 1989. A correlation between the b value and the fractal dimension of earthquakes. Journal of Geophysical Research: Solid Earth, 94(B6): 7507-7514.

Huang, Q., 2004. Seismicity pattern changes prior to large earthquakes-An approach of the RTL algorithm. TERRESTRIAL ATMOSPHERIC AND OCEANIC SCIENCES, 15(3): 469-492.

Jaffe, B.E. et al., 2006. Northwest Sumatra and offshore islands field survey after the December 2004 Indian Ocean tsunami. Earthquake Spectra, 22(S3): 105-135.

Kumar, S., 2012. Seismicity in the NW Himalaya India: fractal dimension, b-value mapping and temporal variation for hazard evaluation. Geosci Res, 3(1): 83-87.

Lay, T. et al., 2005. The great Sumatra-Andaman earthquake of 26 december 2004. Science, 308(5725): 1127-1133.

Mogi, K., 1967. Earthquakes and fractures. Tectonophysics, 5(1): 35-55.

Nanjo, K., Rundle, J., Holliday, J. and Turcotte, D., 2006. Pattern informatics and its application for optimal forecasting of large earthquakes in Japan, Computational Earthquake Physics: Simulations, Analysis and Infrastructure, Part II. Springer, pp. 2417-2432.

Natawidjaja, D.H. et al., 2006. Source parameters of the great Sumatran megathrust earthquakes of 1797 and 1833 inferred from coral microatolls. Journal of Geophysical Research: Solid Earth, 111(B6).

Nuannin, P., Kulhanek, O. and Persson, L., 2005. Spatial and temporal b value anomalies preceding the devastating off coast of NW Sumatra earthquake of December 26, 2004. Geophysical research letters, 32(11).

Nuannin, P., Kulhánek, O. and Persson, L., 2012. Variations of b-values preceding large earthquakes in the Andaman–Sumatra subduction zone. Journal of Asian Earth Sciences, 61: 237-242.

Ozturk, S., 2012. Statistical correlation between b-value and fractal dimension regarding Turkish epicentre distribution. Earth Sciences Research Journal, 16(2): 103-108.

Pailoplee, S., Surakiatchai, P. and Charusiri, P., 2013. b-VALUE ANOMALIES ALONG THE NORTHERN SEGMENT OF THE SUMATRA–ANDAMAN SUBDUCTION

ZONE: IMPLICATIONS FOR UPCOMING EARTHQUAKES. Journal of Earthquake and Tsunami, 7(04): 1350030.

Rao, N.P., Kumar, P., Tsukuda, T. and Ramesh, D., 2006. The devastating Muzaffarabad earthquake of 8 October 2005: New insights into Himalayan seismicity and tectonics. Gondwana Research, 9(4): 365-378.

Roy, P. and Mondal, S., 2012. Identification of active seismicity by fractal analysis for understanding the recent geodynamics of central Himalaya. Journal of the Geological Society of India, 79(4): 353-360.

Scholz, C., 1968. The frequency-magnitude relation of microfracturing in rock and its relation to earthquakes. Bulletin of the Seismological Society of America, 58(1): 399-415.

Sukrungsri, S. and Pailoplee, S., 2017. Precursory seismic quiescence along the Sumatra-Andaman subduction zone: past and present. Journal of Seismology, 21(2): 305-315.

Waldhauser, F., Schaff, D.P., Diehl, T. and Engdahl, E.R., 2012. Splay faults imaged by fluid-driven aftershocks of the 2004 Mw 9.2 Sumatra-Andaman earthquake. Geology, 40(3): 243-246.

Wiemer, S. and Wyss, M., 1994. Seismic quiescence before the Landers (M= 7.5) and Big Bear (M= 6.5) 1992 earthquakes. Bulletin of the Seismological Society of America, 84(3): 900-916.

Yasui, Y., 1968. A study on the luminous phenomena accompanied with earthquakes (part 1). Mem. Kakioka Mag. Obs., 13: 25-61.

APPENDIX

จุฬาลงกรณ์มหาวิทยาลัย
Chulalongkorn University

VITA

Mr. Toatin Ketthong was born in Petchburi, Thailand on August 7th, 1990. In 2013 he received a Bachelor of Science degree in Applied Physics from Department of Physics, Faculty of Science, King Mongkut's University of Technology Thonburi. After graduation, he has entered the Earth Sciences program, Department of Geology, Faculty of Science, Chulalongkorn University with a focus on the focal mechanism and fractal dimension of earthquake for a Master of Science degree study.

จุฬาลงกรณ์มหาวิทยาลัย
Chulalongkorn University